Synthesis, characterization, wound healing study of green synthesized silver nanoparticle and stability study of bio-nano conjugate of grapheme

A thesis submitted towards partial fulfillment of the requirements for the degree of

MASTER OF ENGINEERING

IN

BIOMEDICAL ENGINEERING

Course affiliated to Faculty of Engineering and Technology (FET) and offered by Faculty of Interdisciplinary Studies, Law and Management (FISLM), Jadavpur University

Submitted by

ARKA JYOTI ROY

Examination Roll No.: M4BMD19005

Registration No.: 141088 of 2017-2018

Under the guidance of

DR. PIYALI BASAK

School of Bioscience and Engineering

Jadapur University

Kolkata-700032

Prof. Dr. Tapan Ganguly

School of Laser Science and Engineering

Jadavpur University

Kolkata-700032

DR. C.M.HOSSAIN

Bengal School of Technology

Sugandha, Delhi road

Hoogly-712102

2019

M.E. (Biomedical Engineering) course affiliated to
Faculty of Engineering and Technology
Jadavpur University
Kolkata-700032

CERTIFICATE OF RECOMMENDATION

We hereby recommend that the thesis entitled **"Synthesis, characterization, wound healing study of green synthesized silver nanoparticle and stability study of bio-nano conjugate of graphene"** carried out under mysupervision by Arka Jyoti Roy may be accepted in partial fulfilment of the requirement for awarding the Degree of Master in Biomedical Engineering of Jadavpur University. The project, in our opinion, is worthy for its acceptance.

Dr. Piyali Basak

(Thesis Advisor)
Assistant Professor
School of Bioscience and Engineering
Jadavpur University
Kolkata-700032

Prof. Dr. Tapan Ganguly

(Thesis Co-Advisor)
Emeritus fellow
School of Laser Science and Engineering
Jadavpur University
Kolkata-700032

DIRECTOR

School of Bioscience and Engineering
Jadavpur University
Kolkata-700032

Dr. C.M. Hossain

Bengal School of Technology
Sugandha, Delhi road
Hoogly-712102

Dean

Faculty Council of Interdisciplinary Studies, Law and Management
Jadavpur University
Kolkata – 700032

DECLARATION OF ORIGINALITY AND COMPLIANCE OF ACADEMIC ETHICS

I hereby declare that this thesis contains literature survey and original research work by the undersigned candidate, as part of his **Master of Engineering in Biomedical Engineering** studies during academic session 2018-2019.

All information in this document has been obtained and presented in accordance with academic rules and ethical conduct.

I also declare that, as required by this rules and conduct, I have fully cited and referred all material and results that are not original to this work.

NAME: ARKA JYOTI ROY

EXAM ROLL NUMBER: M4BMD19005

CLASS ROLL NUMBER: 001730201012

THESIS TITLE: *Synthesis, characterization, wound healing study of green synthesized silver nanoparticle and stability study of bio-nano conjugate of grapheme*

Signature: **Date:**

Certificate of Approval

The forgoing thesis is hereby approved as a creditable study of an engineering subject carried out and presented in a manner satisfactory to warrant its acceptance as a prerequisite to the degree for which it has been submitted. It is understood that by this approval the undersigned do not necessarily endorse or approve any statement made, opinion expressed or conclusion drawn therein but approve the thesis only for the purpose for which it is submitted.

Dr. Piyali Basak

(Thesis Advisor)
Assistant Professor
School of Bioscience and Engineering
Jadavpur University
Kolkata-700032

Prof. Dr. Tapan Ganguly

(Thesis Co-Advisor)
Emeritus fellow
School of Laser Science and Engineering
Jadavpur University
Kolkata-700032

Dr. C.M. Hossain

(Thesis Co-Advisor)
Bengal School of Technology
Sugandha, Delhi road
Hoogly-712102

Examiner

Acknowledgement

First of all, I would like to thank my supervisor Dr. Piyali Basak, Asst. Professor, School of Bioscience & Engineering, Jadavpur University for the opportunity to develop this project and for all the support, guidance and help. Furthermore, I would like to thank her for whatever she did to ensure all the necessary conditions for the development of this project.

I would like to thank my co-guide Prof. Dr. Tapan Ganguly for guiding me through this tough project and always helping me to develop myself.

I owe a deep sense of gratitude to Dr. C.M.Hossain, Principal of Bengal School of Technology for providing me the opportunity to work under his guidance and complete my animal study.

I would also like to express deep felt gratefulness to, Dr. Monisha Chakraborty, Associate Professor, School of Bioscience & Engineering, Jadavpur University for her kind support throughout this course.

I want to convey my heartiest gratitude to Mr. Sougata Mallic of Bengal School of Technology for helping me with the animal study.

I want to convey my heartiest gratitude to Dr. Somnath Paul, Dr. Madhurima Misra, Ms. IshaniMitra of School of Laser Science, Jadavpur University for inspiring, encouraging and helping me through the project.

I would like to forward my gratitude towards Biomaterials lab, School of bioscience and Engineering Jadavpur University. In addition, I would like to thank all my Classmates especially Ms. Priti Hazra, Mr. Imon Chakraborty and Mr. Tuhin Kahali for helping me during this work. Their friendship was really

important to overcome all the difficulties I faced. I would like to thank my seniors Mr. Pratik Das, Ms. Shreya Biswas, Mr. Samrat Pal for all the teaching and support during these last months. Without their support and help it would have been not that easy for me to complete the assigned task and work.

My thanks and gratitude to all my juniors especially Mr. Tamojit Santra who were a constant source of my delight during the work span of the thesis.

My heartiest thanks to my close friends Mr. Subha Nath, Mr. Saikat Biswas for their constant support and faith in me.

I want to convey my heartiest gratitude to Technical Education Quality Improvement Programme (TEQIP - III) for its support and help during this work.

Finally, special thanks and regards from the bottom of my heart to my parents and family who have been the constant source of my energy, inspiration and determination for going ahead with my academic pursuit. I thank you for all the education, the advices, the support and the love.

Date: *ARKA JYOTI ROY*

Dedicated to my
parents and friends

Contents

List of Figures:

List of Tables:

CHAPTER 1:

INTRODUCTION

1.1. **Drug delivery system**

1.2. **Nanoparticles**

1.3. **Factors effecting nanoparticle based drug delivery**

1.4. **Process of making nanoparticles**

1.5. **Types of Nanoparticles for Drug Delivery**

1. Introduction

The process of administering any natural or chemical product as a pharmaceutical product so that we can get a therapeutic activity to treat any particular illness in human and animals is called the drug delivery system.

1.1. Drug delivery systems

Scientists around the world are trying to find out new and improved ways of drug delivery. The introduction of nanoparticles had brought a new era in the field of modern day drug delivery systems. The nanoparticles are mostly used for the targeted drug delivery systems [1]. These nanoparticles ranging from 10-100 nm scale and can also be used for imaging purposes. There is a need of greater development in this field so that more effective, biosensing and biocompatible medicine and materials can be made [2]. There are a number of drug delivery routes. The most conventional routes of drug delivery are as follows:-

- Transdermal drug delivery
- Variable Release drug delivery system
- Carrier Based drug delivery system
- Nasal drug delivery system
- Implantable delivery system

1.2. Nanoparticles

Nanoparticles are very small sized particles if different metals and non metals whose size ranges between 10-1000nm. These nanoparticles also come in different shape and sizes i.e. nanotubes, nanowires, nanorods, quantumdots, nanosphers, nanocapsules and nanofilms. All these different changes in shapes of nanoparticles are achieved by changing the method of preparation [4]. Nanoparticles have found a wide spread use in different fields like textile, catalysis, biotechnology, coatings, healthcare, data storage, pharmaceutical and biomedical industries. Nanoparticles can be derived from different sources like metallic, carbon, metallic oxide-ceramic, composites, core-shells, polymers, alloy and biological components [5]. In case of medical studies mostly spherical nanoparticles are widely used. PEG or poly(ethylene glycol) a biodegradable polymer, its nanoparticles are now widely used for coating drugs because of their

hydrophilic nature. This PEG nanoparticle are used for targeted drug delivery to specific organs, used as carriers of DNA in gene therapy, deliver proteins, peptides and genes because they can circulate in the system for a long time. Such polymeric nanoparticles are being used extensively over conventional drug delivery systems using liposomes [6, 7].

- **The main reason behind using nanoparticles for drug delivery system over conventional drug delivery system are as follows:-**

I. The size and surface characteristics of nanoparticles can be easily modified even after being administered to the patient's body.

II. By choosing the matrix type and its constituent we can control the drug release rate and particle degradation rate.

III. Nanoparticles can deliver drugs to localized sites in a sustained and controlled way so as to achieve better drug efficiency and very low side effects.

IV. Drugs can be easily loaded on a nanoparticle without any chemical reaction and so it helps in retaining the drugs property.

V. Targeted drug delivery can be achieved by attaching targeting ligands to the nanoparticle surface or incorporating magnetic nanoparticles on the drug surface and then guide them to the specific target region by applying magnetic stimuli from outside.

VI. This nanoparticle mediated drug delivery can be incorporate in any type of drug delivery routes like oral, parenteral, nasal, intra ocular etc.

- **Drawbacks of nanoparticle to be used in drug delivery system:-**

I. In spite of having so many advantages of using nanoparticles in drug delivery systems there are certain drawbacks which should be considered and tested for before using them. These drawbacks are as follows:-

II. Nanoparticles are in general toxic in nature and so they cannot be directly administered to the patient.

III. Nanoparticles tend to have very short life span.

IV. Positively charged nanoparticles are found to have higher internalization by macrophages and dendritic cells in comparison to negatively charged or neutral particles.

1.3. Factors effecting nanoparticle based drug delivery

There are a lot of factors that affect the drug delivery systems by nanoparticles [8]. Some of these key features are discussed below:-

1.3.1 Size & shape

The shape and size of a nanoparticle based drug delivery system palys an important role. In most of the cases nano spheres are used for this purpose, as these nano spheres give good encapsulation of the drug leading to greater stability and longevity [9, 10]. The nano spheres are also called nanoshells. With the change in shape we can achieve better particle functions, enhanced biological processes like transportation through the blood vessels and targeted drug delivery to effected site [11].

The size of these nanodrugs should be large enough to prevent rapid leakage in blood capillaries and also should be small enough to escape the capture of macrophages in the reticuloendothelial system, such as the liver and spleen. It is found in different studies that the size of nanoparticles system required totally cell specific; particles having size less than 200 nm follows endocytic pathways where as particles above this size can be either engulfed through endocytosis or not internalized at all [12]. But for microsized particles they have to be internalized by phagocytic pathways.

1.3.2 Surface characteristics

As nanoparticles are toxic to human body so surface modifications are important before administering them. The nanoparticles must be conjugated or capped with biocompatible polymers, proteins or other functional groups that will partly depict its characteristics and will be easily accept by the body without any side effects. To make the nanoparticles more stable in the in-vivo and increase their life time they must be coated with biocompatible hydrophilic polymer molecules would improve their systemic circulation and resist their serum protein adsorption. For this purpose a number of variations of polyethylene glycol (PEG) had already been tested. Moreover surface charge can also affect nanoparticle stability depending on the cell type and the in-vivo environment.

1.4. Processes of making nanoparticles

1.4.1 Top-Down Approach

In this method of nanoparticle preparation the particles are made from bigger metallic salt granules. The metallic salts are mechanically or physically broken down gradually into fine powders that are having nano dimensions [13, 15].

1.4.2 Bottom-up approach

In this method the nanoparticles are made from smaller particles of the metallic salts. The metallic salts are dissolved in liquid solutions and reduced to desired size or shapes by different chemical approach [13, 16].

1.4.3 Vacuum Deposition and vaporization

In this process the vaporization source vaporizes materials by the thermal process. During this process the pressure is maintained at 0.1 Pa and vacuum levels are maintained between 0.1 to 10 MPa and 500^0 C. Research had shown that at 1.3 Pa the vaporization rate is optimum. The vapor is then passed through gas where cooling by nucleation and collision takes place. After deposition the particles are formed in the nano range (1-100 nm). It was found that better and longer clusters are formed from supersaturated vapor. This process is advantageous as it has high deposition rates and is economical. Mainly elements, compounds and alloys are deposited using this process [17, 31].

1.4.4 Chemical vapor condensation (CVC) and chemical vapor deposition (CVD) process

A CVD setup is comprised of a gas supply system, a deposition chamber and an exhaust system. In this process a solid is deposited my means of a chemical reaction on a heated surface from vapour phase. To activate this reaction process a temperature as high as 900^0 C is required. Nano composite powders of SiC/Si3N are made at 1400^0 C using CH4, H2, SiH4 and WF6 as the source [18].

In CVC process vapours of metal organic precursors are pyrolysed at a reduced atmospheric pressure. In this system the metalorganic precursors are sent in the hot reactor by means of a mass flow controller. It was developed in the year 1994 in Germany [19, 31].

1.4.5 Mechanical attrition

In this preparation method nanoparticles are produced by breaking the structural integrity of big precursors into fine grained structures because of plastic deformation. The techniques of rod milling and ball milling are used for mechanical alloy making and are mostly done at room temperature [20]. There are varieties of mechanical milling techniques as follows:-

I. Centrifugal type milling

II. High energy milling

III. Vibratory type milling

IV. Low energy type milling

V. Tumbling type milling

VI. Chemical precipitation

In this type of the nanoparticles are formed by precipitation technique. Oswald ripening and thermal coagulation are controlled by using non-aqueous solvents at low temperatures for synthesis which leads to controlled double layer repulsion of crystallites. The use of surfactants maintains separation between formed particles. The nanocrystals formed are collected by centrifugation and vacuum dried after washing. To obtain true quantum confinement the material is subjected to UV curing.

1.4.6 Sol-Gel techniques

The metal aloxysilanes and alkoxides are dispersed in gelatine and colloidal suspension (sol) to form continuous network in liquid phase (gel). Tetraethoxysilanes (TEOS) and tetramethoxysilane (TMOS) are two most widely used chemicals for silica gel formation [21, 31]. The organo metallic precursors of aluminium, zirconium, silica, titanium etc are made in sol gel process. As they are immiscible in water so mutual solvents like alcohol is used. A catalyst is then added to the sol gel to start reaction and conrol the pH. The sol gel formation takes place in a sequence following the four steps:-

I. Hydrolysis

II. Condensation

III. Growth of particles

IV. Agglomeration of particles

1.4.7 Electrodeposition

To prepare films which are uniform and mechanically strong this technique is used. This process is basically advancement in the field of DVD or CVD. It is mainly used synthesis, deposit nano particle and even coat materials [22, 31].

1.4.8 Emulsion solvent evaporation method

In this method the firstly the polymer is emulsified in an aqueous phase followed by evaporation. The polymer is found to form precipitate in the form of nanospheres. Then polymers are then washed by distilled water and then collected by centrifugation. The sample is then dried by lyophilization and stored for further use [3, 23].

1.4.9 Double emulsion and evaporation method

This method is used to encapsulate hydrophilic drugs. Aqueous soluble drugs are added to organic polymer solution and subjected to vigorous stirring resulting in the formation of w/o emulsion. The w/o emulsion is then added to another aqueous phase while stirring leading to formation of w/o/w emulsion. From this emulsion nanoparticles are removed by evaporation and centrifugation at high speed. The nanoparticles are than thoroughly washed and lyophilized before storing [3, 24].

1.4.10 Salting out method

In this method the drug or polymer is dissolved in a solvent and emulsified into an electrolyte and colloidal stabilizer (hydroxyethylcellulose or polyvinylpyrrolidone). The o/w is diluted with enough water to allow easy diffusion of solvent into aqueous solution and formation of nanosphere. As no heat is required for this process so heat sensitive substances can be used [3, 25].

1.4.11 Emulsion diffusion method

A partially water miscible solvent is used to dissolve the encapsulating polymer and saturated so that thermodynamic stability of both liquids is obtained. Than this saturated solvent is mixed with a solution containing stabilizer so that diffusion takes place and nanocapsules or

nanospheres are formed depending upon the oil-to-polymer ratio. Finally the solution is boiled and the nanoparticles are filtered out. The advantage of this process is that it has high encapsulation efficiencies (around 70%) [3, 26].

1.4.12 Solvent displacement/ precipitation method

The lipophilic surfactant, polymers and drugs are dissolved in water miscible semipolar solvent (ethanol or acetone). The solution is then mixed with a stabilizer solution and stirred continuously. This leads to instantaneous nanoparticle formation due to rapid solvent diffusion. Under reduced pressure the solvent is removed from suspension. The particle size can be changed by changing rate of organic phase addition to the aqueous phase. With the in mixing rate both drug entrapment rate and particle size reduction. So this process is very well suited for drugs that are poorly soluble [3, 27].

1.4.13 Green synthesis

Green chemistry is the process of developing new innovative ways of energy conservation, waste reduction and replace hazardous substances with combination of chemistry and natural products [1]. Scientists had always tried to mimic natural properties in the materials as natural products are easily absorbed by the body. In this method the nanoparticles are reduced form their metallic precursors by means of natural extract. Different plant sources have different combinations and concentrations of organic reducing agents that help in reducing the metals into metallic nanoparticles. In this method plant extracts are directly mixed with metallic salt solutions. The time taken for the formation of nanoparticles totally depends on the pH, concentration of extract, metal salt concentration, contact angle and temperature [28].

1.5. Types of Nanoparticles for Drug Delivery

I. Organic nanoparticles

Organic nanoparticles are basically nano sized particles of molecules that are bio compatible. The organic nanoparticles are basically template upon synthetic or natural organic molecules. Examples of organic nanoparticles are lipid bodies, protein aggregates, milk emulsions etc. The organic nanoparticles have found application in industrial products, cosmetics, biomedical science and pharmacy. Organic nanoparticles have found great applications in drug delivery system [13].

II. Metallic Nanoparticles

Scientists have always tried to find ways of utilizing the properties of different metals in improving human life and health. This attempt has lead to the application of nanoparticle in biomedical engineering. Research had led to development of metallic nanoparticle capped with different functional groups which allow them to easily conjugate with drugs, antibodies and ligands. With these new innovations we are able to achieve targeted drug delivery, gene delivery, imaging procedure to diagnose different diseases. For years metallic nanoparticles like silver, gold and iron are modified and used for diagnosis and treatment of several diseases [14].

Numerous different types of nanostructures exhibiting different physiochemical properties are employed to improve the efficiency of drug delivery to specific targets [6]. Few examples are given below:

(i) Solid lipid nanoparticles (SLNs)

SLNs mainly comprise lipids that are in solid phase at the room temperature and surfactants for emulsification, the mean diameters of which range from 50 nm to 1000 nm for colloid drug delivery applications. SLNs had unique properties such as very small size, large surface area and high drug loading. They are attractive as they have potential to improve performance of pharmaceuticals, improve the interaction of phases at the interfaces and other materials. Additionally, improved bioavailability, protection of sensitive drug molecules from the environment (water, light) and controlled and/or targeted drug release and improved stability of pharmaceuticals, feasibilities of carrying both lipophilic and hydrophilic drugs and most lipids being biodegradable SLNs possess a better stability and ease of upgradability to production scale as compared to liposomes [29].

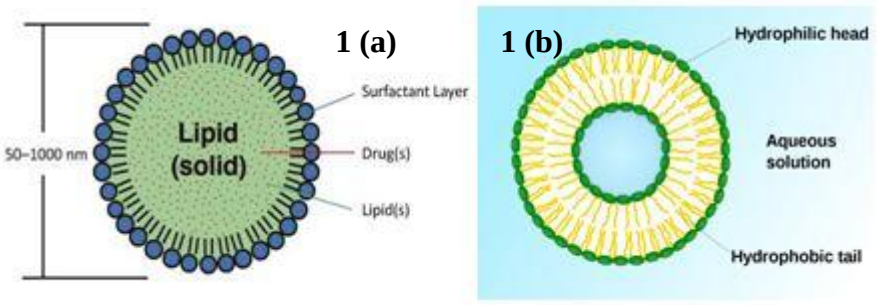

Fig. 1(a) Solid Lipid Nanoparticles, (b) Liposomes

(ii) Liposomes

Liposomes are mixture, perishable and spherical vesicles whose size varies from low micrometers vary to tens of micrometers [30].They have vesicular structures with an aqueous core surrounded by a hydrophobic lipid bilayer, created by the extrusion of phospholipids. Phospholipids are GRAS (generally recognized as safe) ingredients, therefore minimizing the potential for adverse effects. Certain drugs cannot pass through the hydrophobic bilayer. So the liposomes carry both hydrophobic and hydrophilic molecules. The lipid bilayer of liposomes can fuse with other bilayers such as the cell membrane, which promotes release of its contents, making them useful for drug delivery and cosmetic delivery applications [29]. Liposomes are made up of lipids or fat molecules are surrounded by water core. These types of liposomes are widely used for cancer treatment, infectious diseases and for vaccine preparation. The disadvantage of liposomes is leakage with poor controlled release and less encapsulation capacity [30].

(iii) Nanostructured lipid carriers (NLC)

Nanostructured Lipid Carriers are produced from blend of solid and liquid lipids, but particles are in solid state at body temperature. Lipids are versatile molecules that may form differently structured solid matrices, such as the nanostructured lipid carriers (NLC) and the lipid drug conjugate nanoparticles (LDC) that have been created to improve drug loading capacity. The NLC production is based on solidified emulsion (dispersed phase) technologies. NLC can present an insufficient loading capacity due to drug expulsion after polymorphic transition during storage, particularly if the lipid matrix consists of similar molecules. Drug release from lipid particles occurs by diffusion and simultaneously by lipid particle degradation in the body. Major application areas in pharmaceutics are topical drug delivery, oral and parenteral (subcutaneous or intramuscular and intravenous) route. LDC nanoparticles have proved particularly useful for targeting water-soluble drug administration. They also have applications in cosmetics, food and agricultural products. These have been utilized in the delivery of anti-inflammatory compounds, cosmetic preparation, topical corticotherapy and also increase bioavailability and drug loading capacity [29].

(iv) Fullerenes

A fullerene is any molecule composed entirely of carbon, in the form of a hollow sphere, ellipsoid, or tube. Spherical fullerenes are also called buck balls, and cylindrical ones are called carbon nanotubes or buck tubes. Fullerenes are similar in structure to the graphite, which is composed of stacked grapheme sheets of linked hexagonal rings, additionally they may also contain pentagonal (or sometimes heptagonal) rings to give potentially porous molecules. Buckyball clusters or buck balls composed of less than 300 carbon atoms are commonly known as endohedral fullerenes and include the most common fullerene, buckminsterfullerene, C60. Mega tubes are larger in diameter than nanotubes and prepared with walls of different thickness which is potentially used for the transport of a variety of molecules of different sizes Nano ions‘‘ are spherical particles based on multiple carbon layers surrounding a buck ball core which are proposed for lubricants. These properties of fullerenes hold great promise in health and personal care application [13,29].

(v) Nanoshells

Nanoshells are also notorious as core-shells, nanoshells are spherical cores of a particular compound (concentric particles) surrounded by a shell or outer coating of thin layer of another material, which is a few 1–20 nm nanometers thick. Nanoshell particles are highly functional materials show modified and improved properties than their single component counterparts or nanoparticles of the same size. The properties of nanoshells can be modified by changing the core-to-shell ratio. Nanoshell materials can be synthesized from semiconductors (dielectric materials such as silica and polystyrene), metals and insulators. Metal nanoshells are a novel type of composite spherical nanoparticles consisting of a dielectric core covered by a thin metallic shell which is typically gold. Nanoshells has favorable chemical and optical properties for their application in therapeutic and biomedical imaging. The main advantage of using nanoshells over conventional organic dyes is because of its reduced susceptibility to chemical/thermal denaturation and improved optical properties. In imaging applications, nanoshells can be tagged with specific antibodies for diseased tissues or tumors [11].

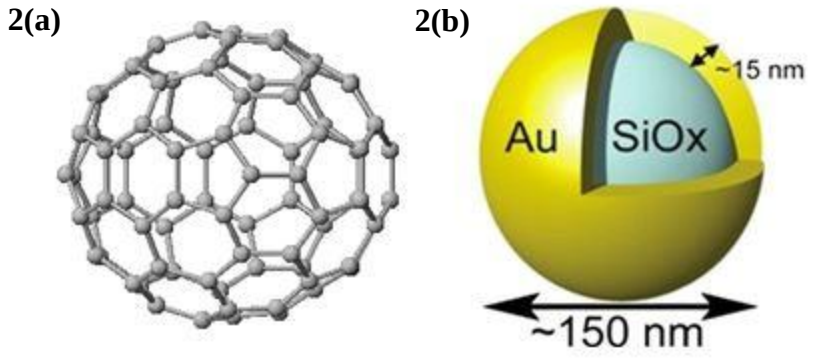

Fig. 2(a) Fullerenes, (b) Nanoshells

(vi) Quantum dots (QD)

Nanoparticles having a dimension between 2-20nm typically called as quantum dots. But according to many literatures the size of the QD must be strictly below 10nm. The dimension of the QD's depends on the base material from which they are made. A particle system is called QD because it experiences quantum confinement. This means the magnitude of radius of the nanoparticle is less than any one of the Bohr radius of the electron i.e. radius of electron (ae), radius of hole (ah), radius of excitation (aexc). Some particles have particle dimension greater than 10 or 20nm. So basically we can't surely distinguish nanoparticles based on dimension. QD's of metals (e.g Ag, Ni, Co, Pt) have been made already. But QD's of semiconductor material are mainly made. Researchers have also been able to make metalloid QD's such as silicon. Because of the quantum confinement the QD's have very different properties than that of bulk particles. The quantization effects in semiconductor structures can be divided into three groups depending on the no. of dimensions created by the arrangement of the charge carriers. One directional confinement creates two-dimensional (2D) structures, they are called quantum films or quantum wells. One-dimensional (1D) structure is created because of carrier confinement in two directions, such structures are called quantum wires. If the confinement is in three directions then zero-dimensional (0D) structures are formed. In these structures the electrons are mostly localized so quantum dots or quantum boxes are formed. Quantum dots are generally a cluster of few millions of atoms but only a few (<100) electrons are free. So depending on the electron confinement we can differentiate between the different structures i.e. vertical, planar and self-assembled. It is found that the electrostatic confinement gives a

dimension of around 100nm where as the structural confinement is found to be around 10nm. In self-assembled QD's the dimension comes around 10nm and shows structures like that of pyramidal or lens shape. Mostly pyramidal QD's are used for laser applications [3, 32].

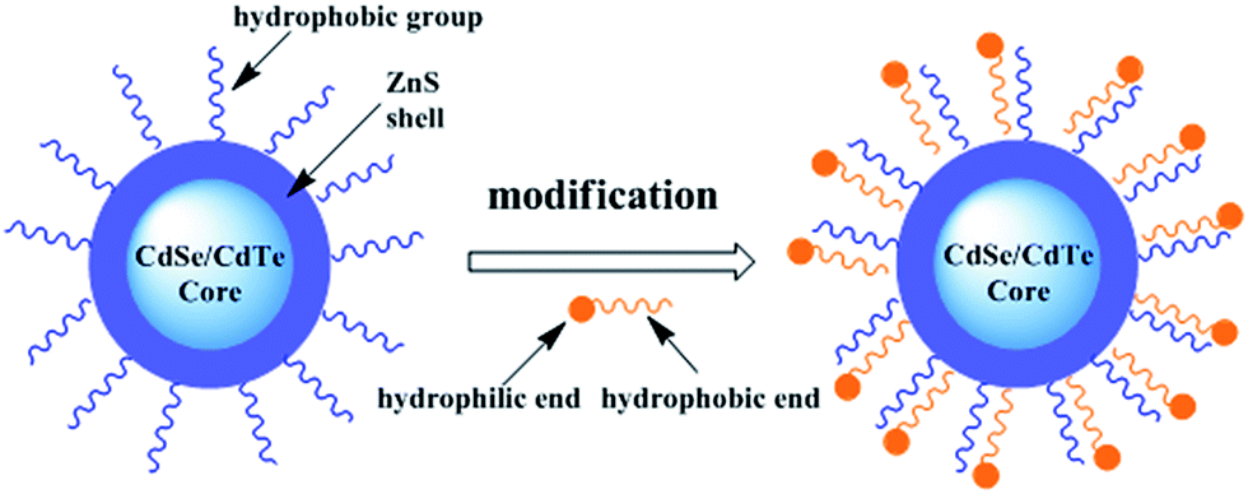

Fig. 3 Metal based Quantum Dots

(vii) Super paramagnetic nanoparticles

Super paramagnetic molecules are those that are attracted to a magnetic field but do not retain residual magnetism after the field is removed. The nanoparticles of iron oxide (5– 100 nm in diameter) have been used for the process of selective magnetic bioseparations. The technique mainly involve coating of the particles with antibodies for cell-specific antigens, this separates the nanoparticle from the surrounding matrix. The main advantages of super paramagnetic nanoparticles are that they can be visualized in magnetic resonance imaging (MRI) due to their paramagnetic properties; they can be guided to a location by the use of magnetic field and heated by magnetic field to trigger the drug release. Super paramagnetic nanoparticles based on their inducible magnetization, their magnetic properties allow them to be directed to a defined location or heated in the presence of an externally applied AC magnetic field. These characteristics make them attractive for many applications, ranging from various separation techniques and contrast enhancing agents for MRI to drug delivery systems, magnetic hyperthermia (local heat source in the case of tumor therapy), and magnetically assisted transfection of cells [29].

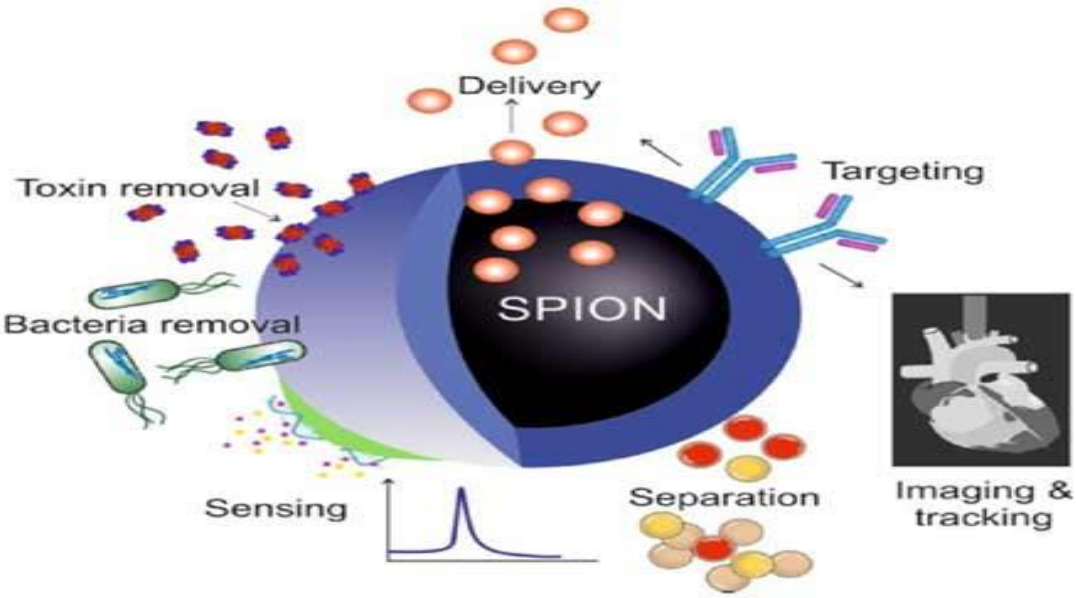

Fig. 4 Super paramagnetic nanoparticles

(viii) Polymersomes

Polymersome nanoparticles are synthetic amphiphilic blocks that are spherical vesicular bodies containing an aqueous solution. This unique copolymer is made of two components, a hydrophobic and hydrophilic subunits e.g. joined together. Polylactic/glycolic acid, Polyethylene glycol-block-polycaprolactone etc [33].

(ix) Nanocapsule

Are also known as liposomes which are a lecithin and stearate encapsulated structure with a lipid core where lecithin is sited in the inner part of the capsule. Polyethylene glycol could be employed to increase its half-life [13].

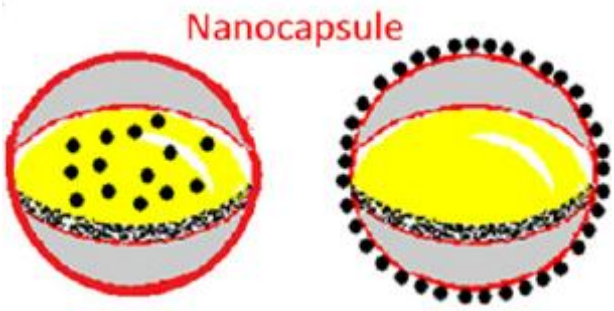

Fig. 5 Nanocapsule

(x) Silica nanoparticles

These are mesoporous nanoparticles with high specificity in terms of pore volume and surface area. To optimize the particle size differential surface enhancements are generally used. This directly influences the silica nanoparticles function. Silica nanoparticles are used extensively as imaging tools [33].

(xi) Amphiphilic nanoparticles

These dual nature nanoparticles consisted of hydrophobic and hydrophilic regions. Hydrophobic regions provide protection against the polar surroundings forming a micelle. In case of drug delivery it carries the drug and provides protection from the body‘s immune system to prevent its elimination e.g. polyethylene oxide-polyaspartic acid copolymers micelle carrying the drug doxorubicin[33].

(xii) Dendrimers

Repeatedly branching nanostructures with highly specific have large surface area making them target specific. It is mostly composed of polyamidoamines. For example telodendrimers made of polyethylene glycol and dendritic cholic acid subunits [13].

(xiii) Graphene

Graphene is a mother of all graphitic materials. It has two dimentional structures. Allotropic form of carbon has unique thermochemical properties and high tensile strength. Its unique hexagonal structure enables infrared radiation conversion in to heat. High surface area allows drug delivery in cancerous cell but is quite toxic in nature therefore requires surface shielding [33].

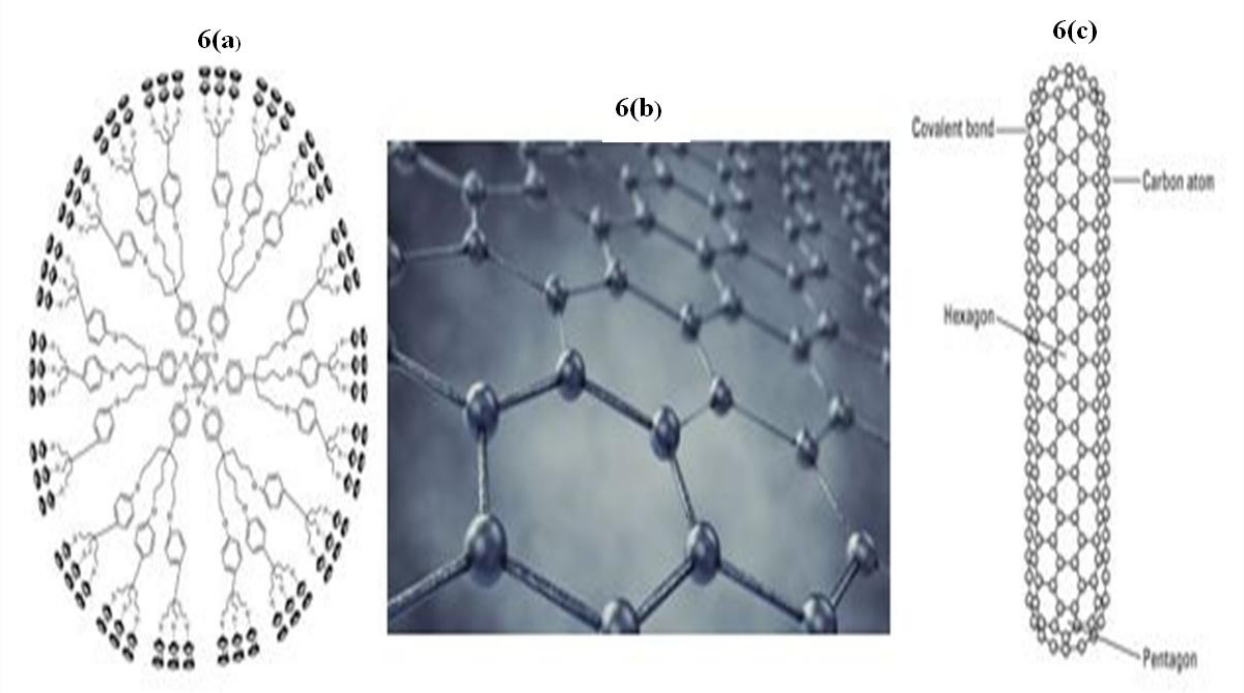

Fig. 6(a) Dendrimers (b) Graphene (c) Carbon nanotubes

(xiv) Carbon nanotubes

Carbon nanotubes are formed by rolling up graphite into cylinders. The hexagonal carbon network of atoms are having a diameter varying between 1-100 nm in length. Carbon nanotubes can be of two types multi-walled carbonnanotubes (MWCNTs) and single walled carbon nanotubes (SWCNTs). The nanotubes have exceptional mechanical, electrical and physical properties. Depending on the carbon leaf wound on itself they exhibit either semi conductive properties or metallic properties. Carbon nanotube is a superconductor as it can transport around one billion amperes of current per square meter. Carbon nanotubes have high mechanical strength around 60 times like that of a steel. The property of having great molecular absorportion and 3D configuration is of great importance. They are also chemically stable.

References

1. https://www.nibib.nih.gov/sites/default/files/Drug%20Delivery_English_508.pdf
2. Agnieszka Z. Wilczewska, KatarzynaNiemirowicz, Karolina H. Markiewicz, and Halina Car, *PR*,**2012**,64,1020-1037.
3. Pal, Sovan Lal, Utpal Jana, Prabal Kumar Manna, Guru Prasad Mohanta, and R. Manavalan. "Nanoparticle: An overview of preparation and characterization." *Journal of Applied Pharmaceutical Science* 1, no. 6 (2011): 228-234.
4. Mohanraj, V. J., and Y. Chen. "Nanoparticles-a review." Tropical journal of pharmaceutical research 5, no. 1 (2006): 561-573.
5. Drbohlavova, Jana, Vojtech Adam, Rene Kizek, and Jaromir Hubalek. "Quantum dots—characterization, preparation and usage in biological systems." International journal of molecular sciences 10, no. 2 (2009): 656-673.
6. Kumar, Challa SSR, ed. Nanomaterials for medical diagnosis and therapy. Vol. 10. John Wiley & Sons, 2007.
7. Nanoparticles – A Review,VJ Mohanraj1* and Y Chen2. Orchid Chemicals & Pharmaceuticals Limited, Chennai, India. School of Pharmacy, Curtin University of Technology, Perth, Australia.
8. SuwussaBamrungsap, ZilongZhao,Tao Chen, Lin Wang, Chunmei Li, Ting Fu and Weihong Tan ,*Nanomedicine* ,**2012**,7,1253–1271.
9. Zhuang, Jia, Chun-Hong Kuo, Lien-Yang Chou, De-Yu Liu, Eranthie Weerapana, and Chia-Kuang Tsung. "Optimized metal–organic-framework nanospheres for drug delivery: evaluation of small-molecule encapsulation." *ACS nano* 8, no. 3 (2014): 2812-2819.
10. Soppimath, Kumaresh S., Tejraj M. Aminabhavi, Anandrao R. Kulkarni, and Walter E. Rudzinski. "Biodegradable polymeric nanoparticles as drug delivery devices." *Journal of controlled release* 70, no. 1-2 (2001): 1-20.
11. Delcea, Mihaela, Helmuth Möhwald, and André G. Skirtach. "Stimuli-responsive LbL capsules and nanoshells for drug delivery." *Advanced drug delivery reviews* 63, no. 9 (2011): 730-747.
12. Sershen, S. R., S. L. Westcott, N. J. Halas, and J. L. West. "Temperature- sensitive polymer–nanoshell composites for photothermally modulated drug delivery." *Journal of*

Biomedical Materials Research: An Official Journal of The Society for Biomaterials, The Japanese Society for Biomaterials, and The Australian Society for Biomaterials and the Korean Society for Biomaterials 51, no. 3 (2000): 293-298.

13. Romero, Gabriela, and Sergio E. Moya. "Synthesis of organic nanoparticles." In *Frontiers of nanoscience*, vol. 4, pp. 115-141. Elsevier, 2012.
14. Pandey, Parijat, and Mandeep Dahiya. "A brief review on inorganic nanoparticles." *J Crit Rev* 3, no. 3 (2016): 18-26.
15. Kuykendall, Darrell W., and Steven C. Zimmerman. "Nanoparticles: a very versatile nanocapsule." *Nature nanotechnology* 2, no. 4 (2007): 201.
16. Pattekari, P., Z. Zheng, X. Zhang, T. Levchenko, V. Torchilin, and Y. Lvov. "Top-down and bottom-up approaches in production of aqueous nanocolloids of low solubility drug paclitaxel." *Physical Chemistry Chemical Physics* 13, no. 19 (2011): 9014-9019.
17. Yamada, Isao, and Toshinori Takagi. "Vaporized-metal cluster formation and ionized-cluster beam deposition and epitaxy." *Thin Solid Films* 80, no. 1-3 (1981): 105-115.
18. Nguyen, Tue, Lawrence J. Charneski, and Masato Kobayashi. "Enhanced CVD copper adhesion by two-step deposition process." U.S. Patent 5,948,467, issued September 7, 1999.
19. Kumbhar, A. S., D. M. Bhusari, and S. T. Kshirsagar. "Growth of clean amorphous silicon–carbon alloy films by hot- filament assisted chemical vapor deposition technique." *Applied physics letters* 66, no. 14 (1995): 1741-1743.
20. Lu, Ke, and Jian Lu. "Nanostructured surface layer on metallic materials induced by surface mechanical attrition treatment." *Materials Science and Engineering: A* 375 (2004): 38-45.
21. Larbot, A., J. P. Fabre, C. Guizard, and L. Cot. "Inorganic membranes obtained by sol-gel techniques." *Journal of membrane science* 39, no. 3 (1988): 203-212.
22. Pirota, K. R., D. Navas, M. Hernández-Vélez, K. Nielsch, and M. Vázquez. "Novel magnetic materials prepared by electrodeposition techniques: arrays of nanowires and multi-layered microwires." *Journal of alloys and compounds* 369, no. 1-2 (2004): 18-26.
23. O'Donnell, Patrick B., and James W. McGinity. "Preparation of microspheres by the solvent evaporation technique." *Advanced drug delivery reviews* 28, no. 1 (1997): 25-42.

24. Rosca, Iosif Daniel, Fumio Watari, and Motohiro Uo. "Microparticle formation and its mechanism in single and double emulsion solvent evaporation." *Journal of controlled release* 99, no. 2 (2004): 271-280.
25. Miller, S. A., D. D. Dykes, and H. F. R. N. Polesky. "A simple salting out procedure for extracting DNA from human nucleated cells." *Nucleic acids research* 16, no. 3 (1988): 1215.
26. Choi, Mi-Jung, Apinan Soottitantawat, Onanong Nuchuchua, Sang-Gi Min, and Uracha Ruktanonchai. "Physical and light oxidative properties of eugenol encapsulated by molecular inclusion and emulsion–diffusion method." *Food Research International* 42, no. 1 (2009): 148-156.
27. Mora-Huertas, C. E., H. Fessi, and A. Elaissari. "Influence of process and formulation parameters on the formation of submicron particles by solvent displacement and emulsification–diffusion methods: Critical comparison." *Advances in colloid and interface science* 163, no. 2 (2011): 90-122.
28. Makarov, V. V., A. J. Love, O. V. Sinitsyna, S. S. Makarova, I. V. Yaminsky, M. E. Taliansky, and N. O. Kalinina. "“Green” nanotechnologies: synthesis of metal nanoparticles using plants." *Acta Naturae (англоязычная версия)* 6, no. 1 (20) (2014).
29. Hnawate R.M, Deore P, Pharma Tutor; **2017**, 5,9-23.
30. S Suhasini and CH Ramesh Babu, *JPN* ,2016, 4,131-139.
31. Rajput, Namita. "Methods of preparation of nanoparticles-A review." *International Journal of Advances in Engineering & Technology* 7, no. 6 (2015): 1806.
32. Drbohlavova, Jana, Vojtech Adam, Rene Kizek, and Jaromir Hubalek. "Quantum dots—characterization, preparation and usage in biological systems." *International journal of molecular sciences* 10, no. 2 (2009): 656-673.
33. NidaTabassumKhan,*J Pharmacogenomics Pharmacoproteomics*,**2017**,8,1-3.

CHAPTER 2:

EXPERIMENT 1:- ALTERATION IN SPECTROSCOPIC PROPERTIES OF HUMAN HEMOGLOBIN IN PRESENCE OF GRAPHENE OXIDE AND ITS REDUCED FORM

2.1 Abstract

2.2 Literature Review

2.3 Materials and Methodology

2.4 Result and Discussion

2.5 Conclusion

Experiment 1.

Alteration in spectroscopic properties of Human Hemoglobin in presence of Graphene Oxide and its reduced form

2.1 Abstract

Recently, a tremendous amount of research activity is being directed towards the study of graphene oxide. This interest is driven by the novel properties that graphene possesses and its potential for use in a various fields that include but are not limited to: electronics, membrane technology, battery technology and advanced composites and especially in bio-sensing and drug-delivery system. In order to assess the potential application of graphene oxides in biological microenvironment, the nature of interactions between Human Hemoglobin (HHb) and GO and also RGO have been monitored spectroscopically. The observations reveal that GO and RGO interacted differently. From the absorption spectroscopic data, hyperchromicity for HHb-GO system and hypochromicity for HHb-RGO system is observed in the region of absorbance of tryptophan and tyrosine residues. Also there is an increase in Soret band intensity in presence of GO, but no change in this band upon interaction with RGO. Interestingly, steady-state fluorescence static quenching of HHb is noticed in presence of GO and enhancement of steady-state fluorescence is observed upon addition of RGO. The average fluorescence lifetime also appear to remain unchanged. Analysis of the thermodynamic parameters indicates that the formation of HHb-GO complex is spontaneous molecular interaction processes ($\Delta G < 0$) involving hydrogen bonding and van der Waals interactions to play a dominant role ($\Delta H < 0$, $\Delta S < 0$). Synchronous fluorescence quenching corresponding to microenvironment of tryptophan and tyrosine residues is observed in presence of GO whereas almost no change noticed upon interaction with RGO. Moreover FTIR spectroscopy reveal involvement of both amide I and amide II bond of HHb backbone through H-bonding interaction only in presence of GO. However the RLS spectra show opposite effects of increase in signal in presence of GO and a decrease in signal upon interaction with RGO. Surprisingly the CD spectra remain unaltered upon interaction with both GO and RGO thus supporting the potential application of GO in biological microenvironment. Therefore the above findings suggests that the alterations in spectroscopic properties upon interaction with GO is compromised upon its reduction to RGO.

Keywords: Graphene oxide; Reduced graphene oxide, Hemoglobin; Static quenching; Fluorescence enhancement; Native secondary structure.

2.2 Literature Review

Proteins are the most versatile macromolecules in living systems and several key properties enable proteins to serve fundamental functions to a large extent in all biological processes. They are known to bind to several ligands even in nano-dimensions. This may lead to the formation of protein-ligand bi-molecular or more complex interactions where a number of non-covalent interactions such as hydrophobic/ hydrophilic interactions, electrostatic interactions, van der Waals interactions produce conformational changes in the protein [1, 2, 6 and 18]. Thus, the primary understanding of the structural changes of protein in a protein-ligand system is essentially significant as this can precisely assist in the understanding of the role of protein in different realms like biochemistry, medicinal chemistry and nano-biotechnology.

One such important protein which is known to have immense biological significance is Human adult hemoglobin (HHb). HHb is not just a simple oxygen tank rather it is a sophisticated oxygen delivery system. It exists as a tetramer of globin chains, composed of two α and two β subunits, each of which has one redox iron heme as its prosthetic group, and the oxygen binding capacity of HHb is determined by the presence of heme, located in crevices at the exterior of the subunit. Also Hb has three Trp residues in each αβ dimer, for a total of six in the tetramer: two α14 Trp, two β15Trp, and β37Trp. Among three Trp residues, only β37 Trp is situated at the dimer-dimer interface, which is the region where structural differences between quaternary states are largest. HHb further possesses five Tyr residues in each dimer: αTyr 24, 42, 140 and βTyr 34, 144. Moreover the quaternary structure of Hb features strong interactions between unlike subunits. The $\alpha_1\beta_1$ interface (and its $\alpha_2\beta_2$ counterpart) involves more than 30 residues, and its interaction is sufficiently strong whereas the $\alpha_1\beta_2$ (and $\alpha_2\beta_1$) interface involves 19 residues [1, 2]. Hydrophobic interactions predominate at the interfaces, but there are also many hydrogen bonds and a few ion pairs existing as salt bridges. The binding of O_2 causes the heme to assume a more planar conformation, shifting the position of the proximal H is and the associated secondary structure. These changes lead to adjustments in the ion pairs at the $\alpha_1\beta_2$ interface. Furthermore it becomes apparent that the physiologically essential protein can also interact with medically important

ligands other than oxygen and such interactions may give insight in areas of nano-biotechnology, biomaterials, medicinal chemistry and many more [1, 2].

Thus HHb has not confined itself only as a major functional protein for reversible oxygen carrying and storage. It has appeared as a model protein which may undergo significant changes in conformation, function, and dynamic properties after binding of small molecules. Although the relationship between the structure and function of HHb is well studied but the research activity on its interaction with other molecules is limited to a small number of nano-molecules. Based on a systematic understanding of these interactions, one can possibly predict and even regulate the behavior of small molecules of nano-dimension at the nano–bio interface [1, 2, 6 and 18]. Vigorous research on these fields may considerably contribute to gain fruitful knowledge regarding their potential biomedical application especially as drug-delivery system [1, 2 and 6].

Nowadays, carbon nano-materials have been widely used in biological applications due to their unique and outstanding properties [3]. A novel two-dimensional (2D) carbon nanomaterial, graphene oxide (GO), has shown potential biotechnological applications in drug and gene delivery systems. Therefore, the understanding GO's influence on structure and activities of biomolecules are essential for before any biological applications of GO, especially for disease- and drug-related proteins, cellular bio-imaging and many more. However, so far very few studies on the biocompatibility of GO and its reduced form (RGO) with heme proteins, or on the toxic effects of GO/RGO on heme proteins at the spectroscopic level have been conducted.

In the present study, interaction of HHb with GO and RGO have been investigated by using various spectroscopic techniques. Comparative studies reveal that in almost all experiments the effect of GO in alteration of spectroscopic properties is compromised upon its reduction to RGO. Interestingly UV-vis spectra in the region of absorbance of tryptophan and tyrosine residues, steady-state fluorescence spectra and RLS spectra of HHb display opposite effect, for GO and RGO respectively. The observations not only give insight to the conformation behavior of HHb molecules upon interaction with GO but also creates a framework for analyzing the biosafety and potential application of GO/RGO in the biological microenvironment. In addition, these findings also shed light for utilization of GO/RGO as a drug-delivery system.

2.3 Materials and Methodology

2.3.1 Materials

Human Hemoglobin (HHb), purchased from Sigma Aldrich, is tested before use for the presence of any impurity in the region of wavelength studied. In all the experiments freshly prepared aqueous solutions of concentration ~ 5 x 10^{-6} M (0.645 mg/ml) have been used [1, 2].

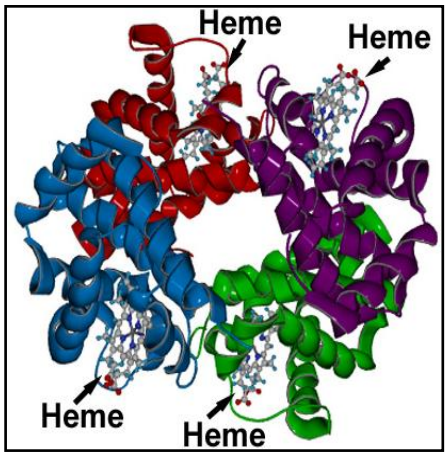

Fig 7: (Colour online) Molecular structure of HHb

2.3.2 Synthesis of GO and RGO

2 g of graphite powder is taken and mixed with 1 g of $NaNO_3$ by keeping it in an ice bath. Under constant stirring condition concentrated H_2SO_4 (130 ml) is carefully added to the mixture. Thereafter, 6 g of $KMnO_4$ is added slowly through vigorous stirring by maintaining the temperature of the reaction mixture at ~20 °C. The temperature of the reaction mixture is gradually elevated up to 40 °C for 6 h under stirring condition, when the color of the mixture is observed to change from dark grey to grayish green. Again additional 6 g of $KMnO_4$ is added to the mixture, under stirring conditions for further 6 h as a result of which the color of the reaction mixture turns grayish brown. Then 250 ml of triple distilled water is carefully and slowly added to the solution and stirred for 30 minutes during which the temperature of the solution rises to ~ 96 °C. Thereafter the solution is allowed to cool to room temperature. Furthermore additional 500 ml triple distilled water and 15 ml 30% H_2O_2 are added to the reaction mixture to terminate the process of oxidation and at this stage, the color of the solution turns yellow ochre thereby indicating high oxidation level of graphite. The yellow solution is then washed twice with 1M HCl solution and then repeated washing is carried out with triple distilled water to attain a solution of pH~ 5. Thorough washing is performed by centrifugation of the solution and

decantation of the supernatant. Vigorous washing and decantation is essentially required in order to exfoliate the graphene oxide layers and also removal of the unexfoliated graphene oxide layers. The resulting thick yellow brown gel is filtered and kept overnight for allowing it to dry to obtain a fine yellow graphene oxide (GO) powder. ~2 mg of GO is then taken in triple distilled water and ultrasonicated for 30 min to get a homogeneous solution.

In order to prepare RGO, hydrazine hydrate (2ml) is added to the solution. The reaction mixture is then heated to 100 °C for 6 h to obtain black RGO. Then the black solid is washed and the filtrate is dried at 80 °C to get reduced graphene oxide (RGO). To get a uniform dispersion ~ 2 mg of RGO is taken in triple distilled water and ultrasonicated for ~ 90 minutes [3, 4].

All the reagents are purchased from Sigma Aldrich and used in the expriments without any further process of purification. Water has been double distilled and then deionized using a Millipore Milli-Q system.

2.3.3 Spectroscopic Apparatus

Dilute solutions of the HHb (~10^{-6} M) are taken for the following spectroscopic techniqus are performed in absence and presence of GO and RGO at the ambient temperature - UV-vis absorption spectra, steady state fluorescence emission spectra, Resonance Light Scattering (RLS) spectra, synchronous fluorescence spectra, FTIR measurements and Circular dichroism (CD) spectroscopy measurements as described elsewhere [1, 2]. Briefly UV–vis absorption and steady state fluorescence emission spectra of dilute solutions of the samples are measured in absence and presence of GO and RGO in rectangular quartz cells of 1 cm path length at the ambient temperature. UV–vis absorption spectra are scanned by using JASCO UV–Vis absorption spectrometer (Model: V-630). Steady-state fluorescence emission spectra, RLS spectra and synchronous fluorescence spectra are monitored using JASCO Spectrofluorimeter (Model: 8200). For Benesi-Hildebrand plot, and fluorescence quenching analysis for evaluation of thermodynamic parameters the molecular weight of GO is considered as 2043.856.

Fluorescence lifetimes measurements of HHb in absence and presence of GO and RGO are carried out using a time correlated single-photon-counting (TCSPC) technique with the model FLUOROLOG TCSPC HORIBA JOBIN YVON using 280 nm (NanoLED 280) as impulse for excitation in Trp/Tyr region and an emission wavelength of 330 nm. The decay kinetics, the quality of fit with a plot of weighted residuals and other statistical parameters like reduced χ^2 and the Durbin–Watson (DW) parameters are checked for the entire decay along with the rising edge.

The Circular dichroism (CD) spectroscopy measurements are scanned using a PC driven JASCO CD spectropolarimeter (Model J-815) in the UV region (250–190 nm) at 25 °C in a rectangular quartz cell (1 mm).

The following observations are plotted and analyzed using Microcal Origin (version 8.5) software after taking original raw data directly from the instrument.

2.4 Result and Discussion

2.4.1 UV-vis absorption spectroscopy

As a first step to reveal the spectroscopic properties of HHb in presence of GO and RGO, UV-vis electronic absorption spectroscopy is performed. The UV-vis absorption spectra of HHb in Millipore water under physiological condition (pH~ 7.0) upon addition of increasing concentration of GO is shown in Fig. 8a. From Fig. 8a it is observed that the absorption spectra of HHb possess a broad absorption peak at ~270 nm which corresponds primarily due to the contribution of tryptophan and tyrosine. Upon addition of increasing concentration of GO to HHb solution, hyperchromicity of this peak without any noticeable spectral shift is noted.

Absorption spectroscopic measurements of HHb are also performed in presence of RGO. Here also the absorption spectra of HHb (Fig. 8b) show a broad absorption peak at around ~270 nm. Upon addition of increasing concentration of RGO the entire absorption spectra display a minor yet noticeable hypochromic effect without any noticeable spectral shift.

Moreover absorption spectra of GO displays a broad absorption maxima at 229 nm due to the π-π^* transition of aromatic C=C bonds and a shoulder at around ~301 nm due to the n-π^* transition of C=O bonds (Fig. 8c). Absorption spectra of RGO further reveal broad absorption maxima at 263 nm (Fig. 8d). Thus it appears that the λ_{max} has shifted from 229 nm for GO to 263 nm for RGO thus indicating the effective reduction of the GO by hydrazine hydrate [5]. The UV-vis absorption spectra of GO reveal that the highest concentrations of GO that is used in this study, show negligible absorbance below ~ 0.07 at around 270 nm (Fig. 8c). Likewise UV-vis absorption spectra of RGO reveal that the highest concentrations of RGO, display negligible absorbance below ~ 0.02 at around 270 nm (Fig. 8d). Since the absorbance of GO and RGO at the region of absorbance of tryptophan and tyrosine residues (270 nm) is much less so the corresponding emission spectra are not taken.

The absorption spectra of HHb also reveal an intense Soret band peak at around ~ 405 nm is attributed to the presence of porphyrin ring in HHb [2, 6, 7 and 8] (Fig. 8a and 8b). The Soret bands are known to occur due to electronic transitions (π-π^*) from ground state or S_0 to the second excited state S_2 within the hematoporphyrin that remain embedded in a hydrophobic pocket formed by three dimensional folding of the multi-subunit protein [8, 9 and 10]**.** Any alteration in the Soret band possibly indicates microenvironmental changes around heme moiety. The nature of Soret band as monitored by UV-Vis absorption spectroscopy display an increase in intensity upon gradual addition of GO. However the absorption band at ~ 360 nm (ε band) that occurs due to perturbation around the central Fe atom remains nearly unchanged [8, 9]. The increase of Soret band intensity usually indicates alteration in the microenvironment surrounding HHb perhaps due to perturbation around heme group [8, 9]. Moreover there can be possibilities of involvement of heme group during formation of ground-state complex in presence of GO [8, 9, 11 and 12]. Interestingly the Soret band intensity of HHb nearly remains unchanged in presence of RGO compared to GO. Thus it appears that the hyperchromic effect of the Soret band of HHb in presence of GO is compromised upon its reduction to RGO.

Although the above observations as obtained from UV-vis absorption spectroscopic studies demonstrate the hyperchromic effect for GO and the hypochromic effect for RGO in the region of absorbance of tryptophan and tyrosine residues however in spite of these interactions the overall spectral properties is not much affected. Also it appears the microenvironment of aromatic amino acid residues and heme group are involved in the formation of ground state complexes for HHb-GO system. The alterations in absorption spectral properties are observed to be even lesser in presence of RGO.

Accordingly the Benesi-Hildebrand (BH) plot is displayed using the following equation (1) [1, 13 and 14].

$$\frac{1}{(\varepsilon_c-\varepsilon_0)} = \frac{1}{(\varepsilon_b-\varepsilon_0)} + \frac{1}{K}.\frac{1}{(\varepsilon_b-\varepsilon_0)}.\frac{1}{C} \quad \text{…. (1)}$$

where ε_c denotes the molar extinction coefficient of the HHb at GO concentration "*C*", *K* indicates the equilibrium constant of formation of the ground state complex between HHb and GO. ε_o and ε_b signifies the molar extinction coefficients of the HHb without and with GO respectively.

The BH plot appear to be linear (Fig. 8e) thereby indicating the formation of 1:1 complex in the ground state for HHb upon interaction with GO. The association constant (K) of the HHb-GO complex as obtained from the BH plot is found out to be 0.19 x 10^6 M^{-1}.

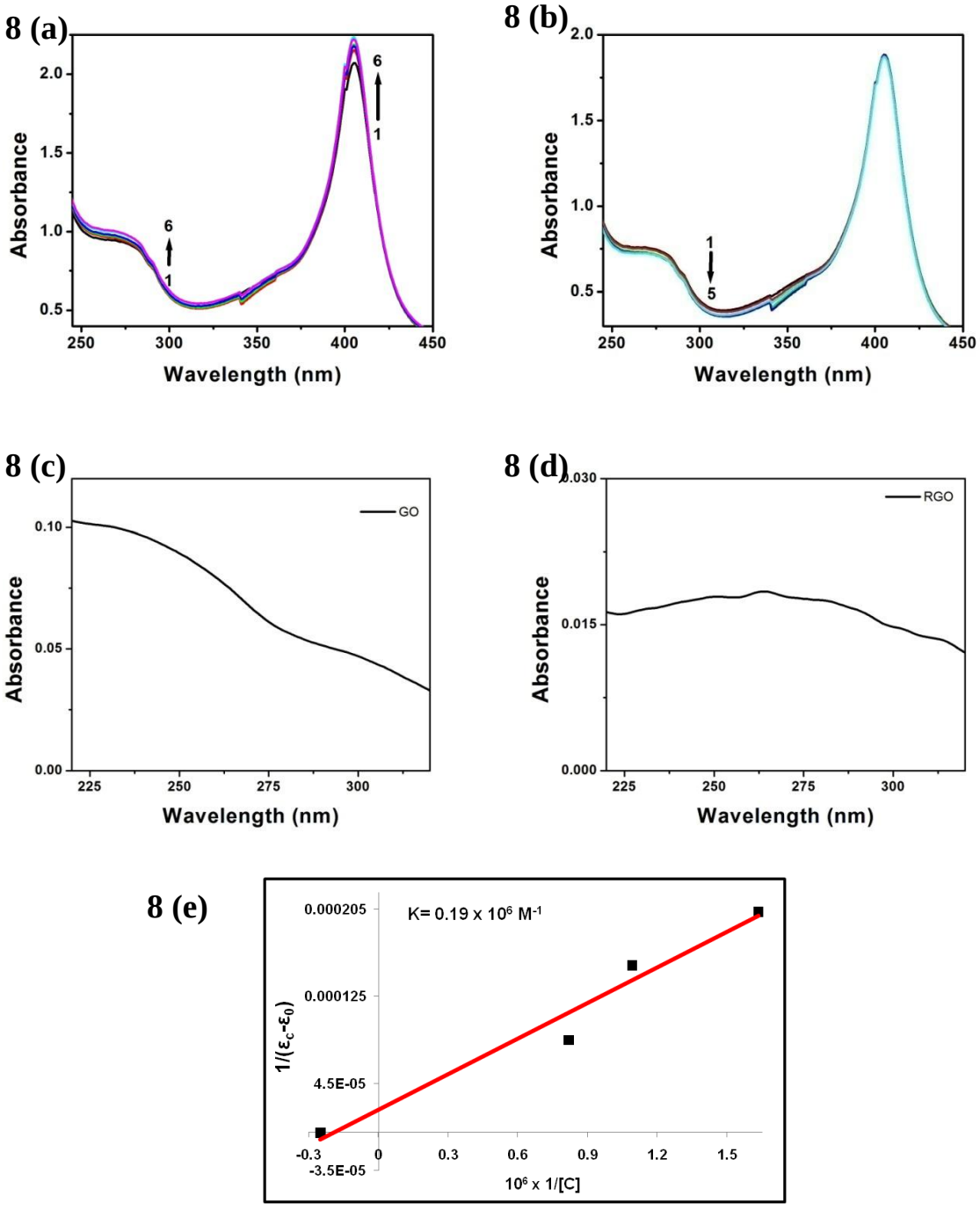

Fig. 8 (a) UV-vis absorption spectra of HHb upon addition of the following concentrations GO at ambient temperature - (1) 0, (2) 1 μg/ml, (3) 1.25 μg/ml, (4) 1.875 μg/ml, (5) 2 μg/ml, (6) 2.5

μg/ml. (**b**) UV-vis absorption spectra of HHb upon addition of the following concentrations RGO at ambient temperature - (1) 0, (2) 0.5 μg/ml, (3) 1 μg/ml, (4) 2 μg/ml, (5) 4.5 μg/ml. (c) Absorption spectra of GO of concentration 5 μg/ml. (d) Absorption spectra of RGO of concentration 5 μg/ml. (e) BH plot for the HHb-GO complex.

2.4.2 Steady-state fluorescence emission spectroscopy

It is already well known that a variety of molecular interactions like formation of ground-state complex can alter fluorescence properties of proteins. Since the fluorescence spectra of the protein (HHb) usually determine the microenvironment of the fluorescing aromatic residues (tryptophan and tyrosine residues) and thus any change in their neighboring environment will probably get revealed by monitoring the variations in the spectra. Thus to unravel the microenvironmental changes around tryptophan and tyrosine residues fluorescence spectral measurements are carried out in presence of GO and RGO. The steady state fluorescence emission spectra of HHb as shown in Fig. 9a reveal an emission maximum at ~331 nm when excited at ~ 270 nm. Fig. 9a shows that with increase in concentration of GO, the fluorescence maxima of HHb is observed to quench regularly without any noticeable spectral shift. Fluorescence quenching is also noticed at different temperatures: 288 K, 298 K, 308 K and 318 K [27].

The alteration in steady state fluorescence emission spectra of HHb in presence of RGO at the ambient temperature has been represented in the Fig. 9b. Here also emission maximum at ~331 nm when excited at ~ 270 nm has been observed. Interestingly Fig. 9b shows that upon addition of increasing concentration of RGO, there is no quenching of fluorescence. Instead of fluorescence quenching, enhancement of fluorescence without any spectral shift is noticed. Thus the quenching effect of GO is reversed upon its reduction to RGO which shows an enhancement effect. As such, the observations demonstrate fluorescence enhancement for HHb upon interaction with RGO, whereas interaction with GO shows fluorescence quenching. Such observations can be explained at least to some extent from the fact that fluorescence is the product of two processes: firstly it occurs due to excitation by the incident field influenced by the local environment, and secondly due to emission of radiation influenced by the balance of radiative and nonradiative decay. While the source of the first process is the external radiation field, in the second process it is the molecule itself which constitutes the source [15]. In the

present study the decrease and increase in fluorescence intensity may perhaps occur due to changes in microenvironment around tryptophan and tyrosine residues. Further investigations are needed in order to explore other possibilities. However it can be realized that in spite of the changes in the intensity of fluorescence upon interaction with GO and RGO the polarity around tryptophan and tyrosine residues are hardly affected probably due to absence of any spectral shift.

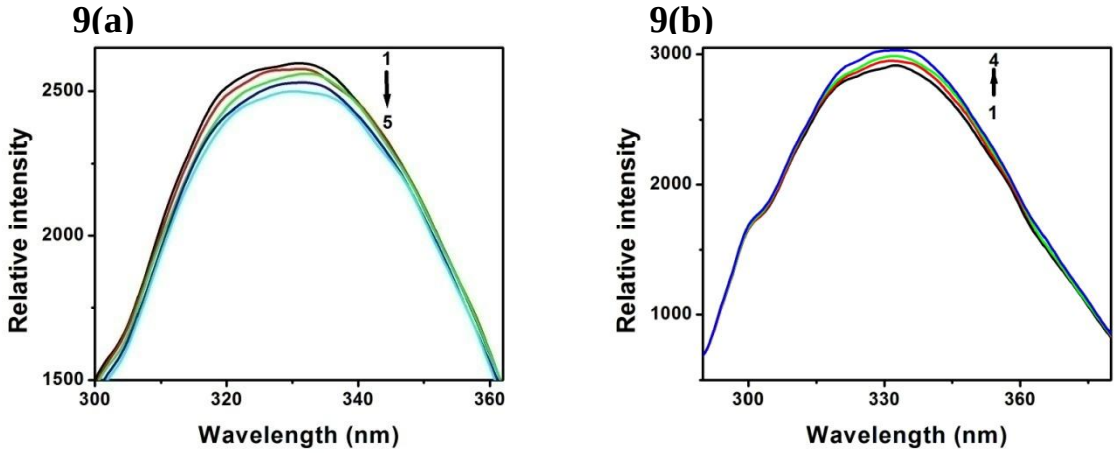

Fig. 9(a) Steady state fluorescence emission spectra of HHb in presence of GO at ambient temperature. The concentrations of GO are (1) 0, (2) 1 μg/ml, (3) 1.5 μg/ml, (4) 1.875 μg/ml, (5) 2.5 μg/ml. 9(b) Steady state fluorescence emission spectra of HHb in presence of RGO at ambient temperature. The concentrations of RGO are (1) 0, (2) 1 μg/ml, (3) 1.5 μg/ml, (4) 3 μg/ml (λ_{ex} = 270 nm)

The fluorescence intensity quenching in case of interaction with GO, are then studied using Stern-Volmer (SV) relation

$$\frac{F_0}{F} = 1 + K_{SV}[Q] \ldots. (2)$$

where F_0 and F indicates the fluorescence intensities of HHb in absence and presence of GO. K_{SV} refers to the Stern-Volmer (SV) constant and $[Q]$ denotes the concentrations of the GO used. The representative SV plot for the HHb-GO complex appears to be linear thus indicating that the quenching mode can either be of pure dynamic or of pure static in nature (Fig. 10a). In order to distinguish whether the type of quenching is static or dynamic in nature, temperature dependence of K_{SV} and fluorescence lifetime measurements are performed. It is already known that for static

quenching, the value of K_{SV} decreases whereas for dynamic quenching the value of K_{SV} increases with increase of temperature. This is because an increase of temperature would result in increasing rate of collision between the reacting species through diffusion mechanisms. Thus increase of effective collision number facilitates the energy transfer which is a dynamic process. In the present case, the value of K_{SV} appear to decrease with increase in temperature for HHb-GO interactions (Table 1). Thus the type of quenching of fluorescence of HHb by GO should primarily be of static in nature. The SV equation could not be applied for HHb-RGO system since there is no fluorescence quenching.

10(a) **10(b)**

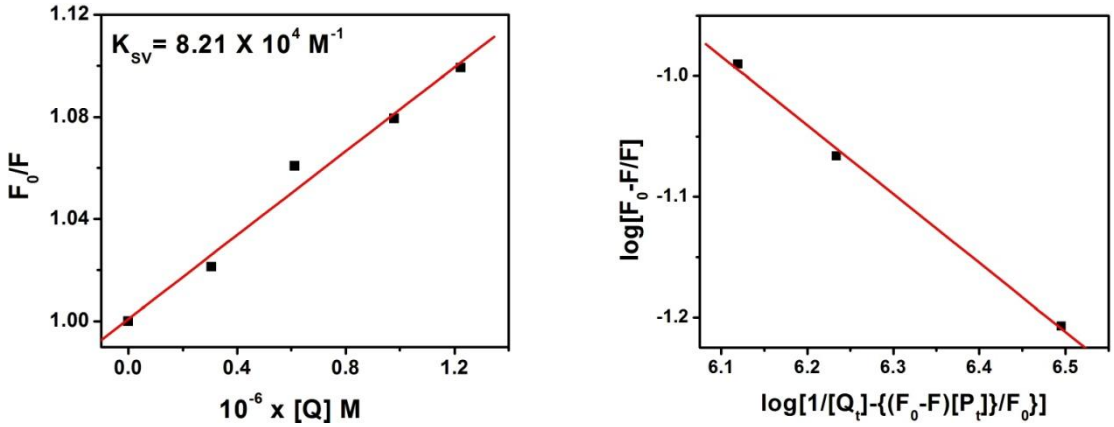

Fig. 10 (a) SV plot from steady-state fluorescence emission intensity measurements of HHb-GO complex at 298 K. (b) Plot using the general form $log\left(\frac{F_0-F}{F}\right) = nlogK_A - nlog\left(\frac{1}{[Q_t]-\frac{(F_0-F)[P_t]}{F_0}}\right)$ for HHb-GO complex at 298 K.

Temperature (K)	K_{SV} for GO (10^4 M^{-1})
288	11.8
298	8.21
318	6.8

Table 1: K_{SV} values for HHb-GO system at different temperatures.

To substantiate the occurrence of static quenching processes, time resolved spectroscopic measurements are performed to determine the fluorescence lifetimes by time correlated single photon counting (TCSPC) techniques (Fig. 11).

11(a)

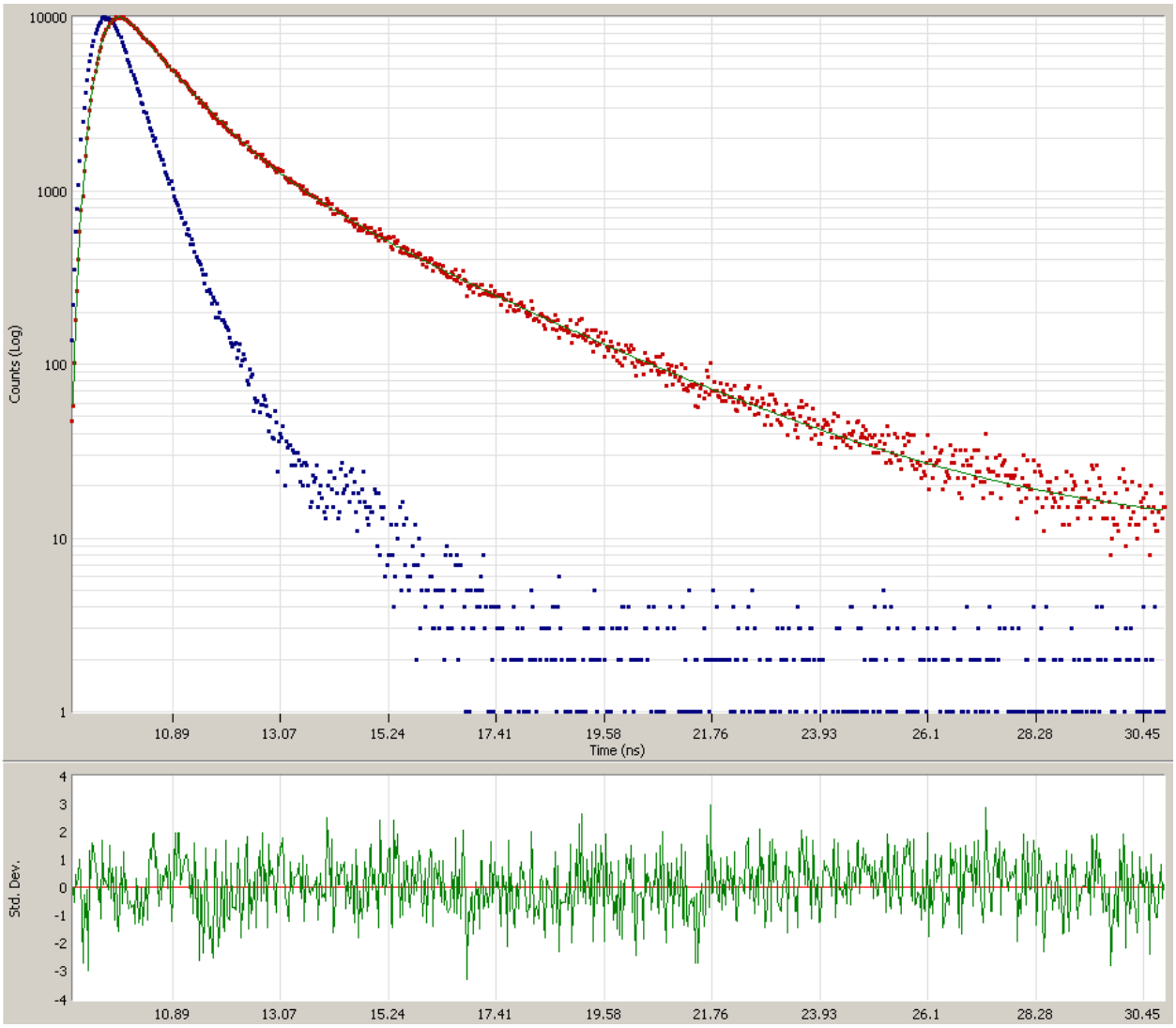

11(b)

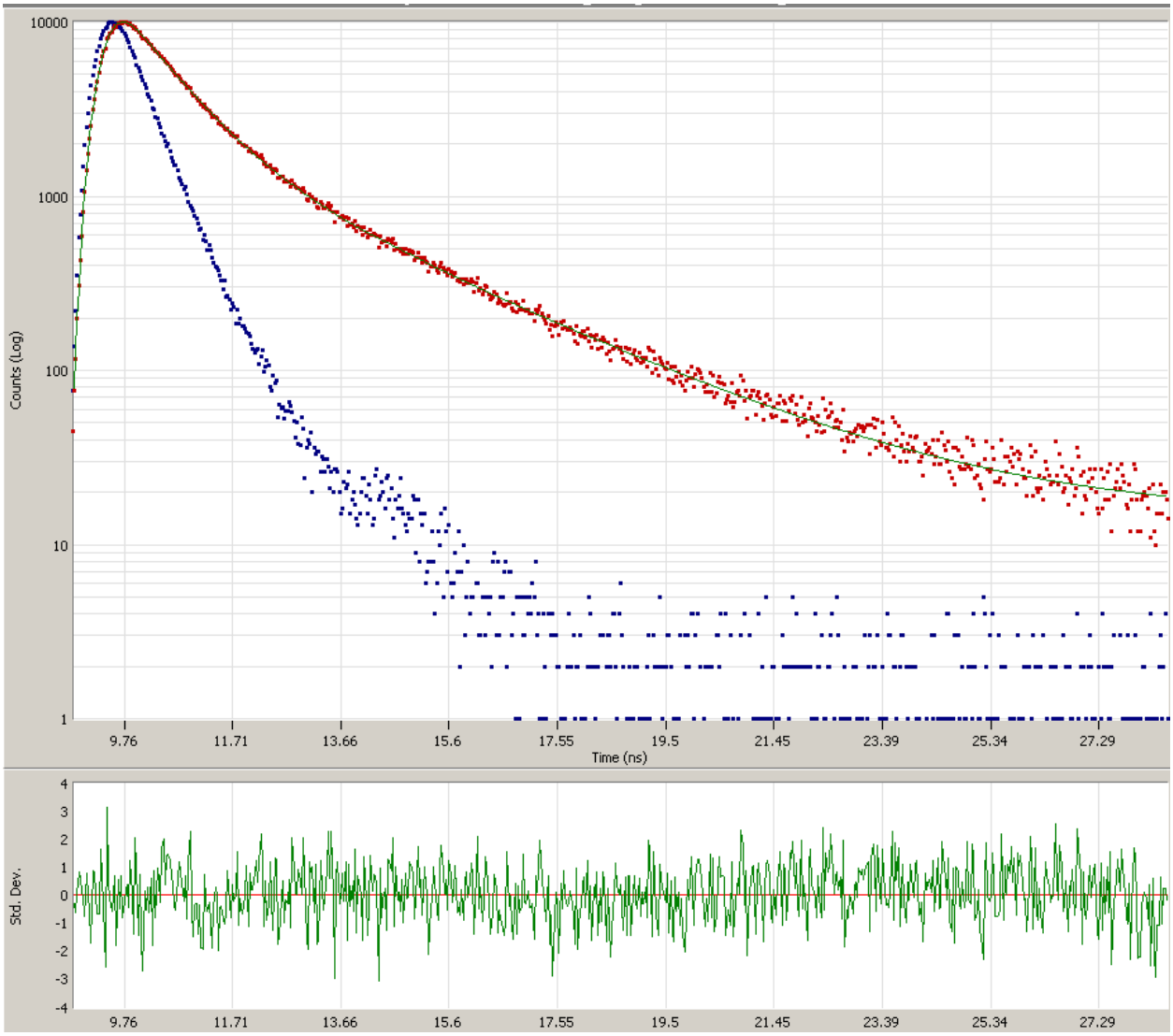
10000
1000
100
10
1
Counts (Log)
9.76
11.71
13.66
15.6
17.55
19.5
21.45
23.39
25.34
27.29
Time (ns)
4
3
2
1
0
-1
-2
-3
-4
Std. Dev.

11(c)

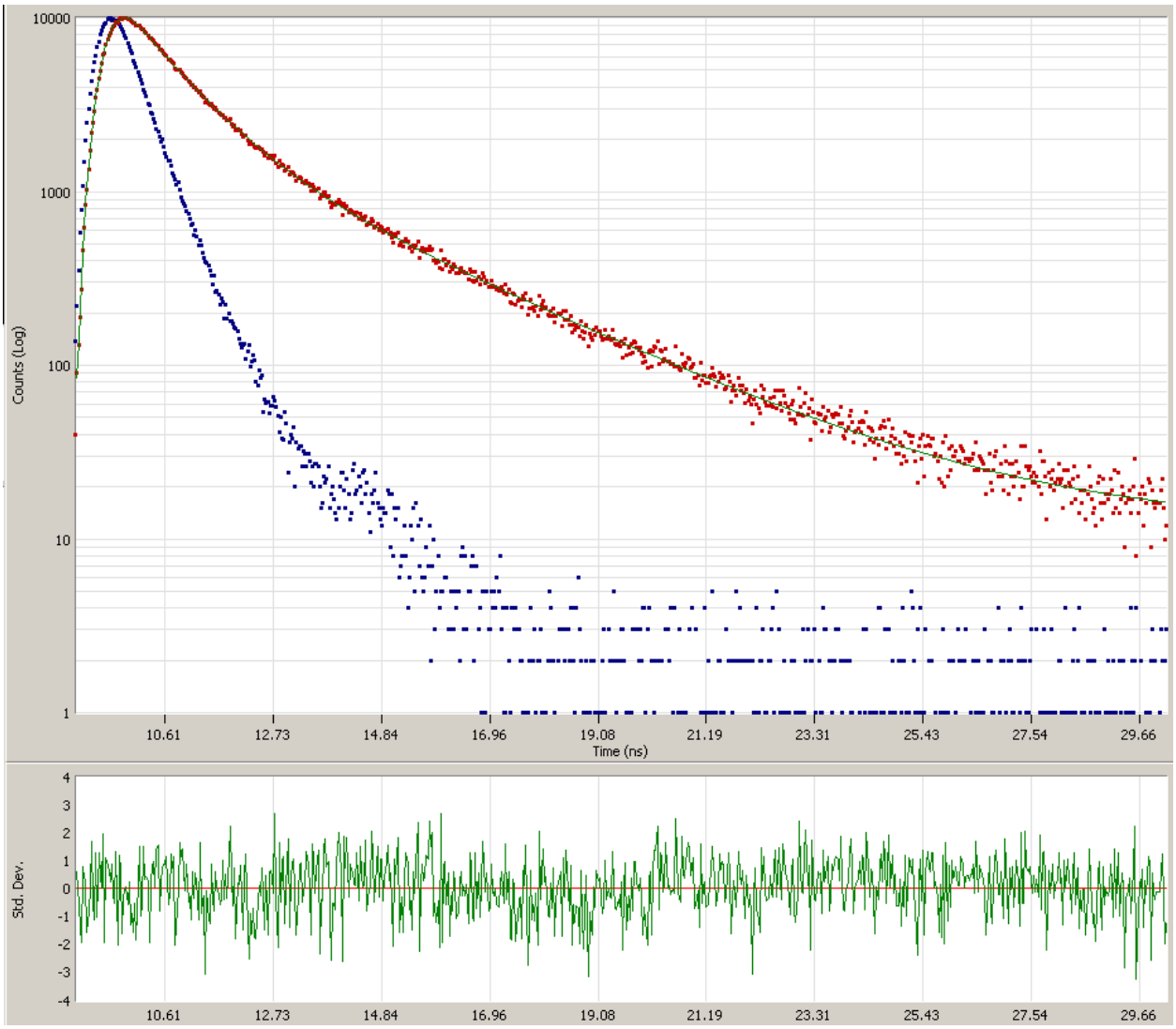

Fig. 11(a) Fluorescence decay of the HHb (red) along with the impulse response (faster component shown by the blue line). The residual is also shown. (χ^2 – 1.05). (b) Fluorescence decay of the HHb-GO complex (red) along with the impulse response (faster component shown by the blue line). The residual is also shown. (χ^2 – 1.095). Concentration of GO is ~ 2.5 µg/ml. (c) Fluorescence decay of the HHb-RGO complex (red) along with the impulse response (faster component shown by the blue line). The residual is also shown. (χ^2 – 1.08). Concentration of RGO is ~ 5 µg/ml.

As shown in Table 2, when excitation was made at 280 nm region the time-resolved fluorescence data showed three lifetimes 0.19 ns, 1.06 ns and 3.27 ns. The fractional contribution of each component is nearly same. The lifetime components are 0.11 ns, 0.79 ns and 2.97 ns in presence of GO and 0.18 ns, 0.95 ns and 3.19 ns in presence of RGO respectively. Here also the fractional contribution for each component remains nearly unchanged in presence of GO/RGO. Thus it is apparent that the lifetime of the individual components of HHb do not change significantly. For further understanding, the average emission lifetime, <τ>is calculated using the following equation

$$\langle \tau \rangle = \frac{\sum a_i {\tau_i}^2}{\sum a_i \tau_i} \quad \text{…. (3)}$$

where a_i and τ_i denote the normalized preexponential factor and the corresponding lifetime respectively [32, 37]. The average lifetimes $\langle \tau \rangle$ for HHb is 1.5 ns, for HHb-GO is 1.3 ns and for HHb-RGO is 1.5 ns. The magnitudes of the lifetimes of HHb do not alter significantly with addition of GO/RGO. The unperturbed values of the fluorescence lifetimes of HHb even in presence of GO/RGO further confirm that the quenching of fluorescence of HHb is probably of static in nature. Thus it corroborates the views made from the steady state measurements as discussed above.

Sample	**Conc. of GO/RGO**	**τ_1 ns**	**τ_2 ns**	**τ_3 ns**	**f_1**	**f_2**	**f_3**	**<τ> ns**
HHb	0	0.19	1.06	3.27	0.3	0.34	0.35	1.5
HHb-GO	2.5 μg/ml	0.11	0.79	2.97	0.34	0.32	0.32	1.3
HHb-RGO	5 μg/ml	0.18	0.95	3.19	0.29	0.33	0.36	1.5

Table 2: Fluorescence lifetimes (τ_1, τ_2, and τ_3), the corresponding fractional contributions (f_1, f_2, f_3) of the HHb in absence and presence of GO/RGO and the average emission life time <τ>, have been shown in the table.

2.4.3 Binding constant and number of binding sites of HHb-GO complex

In order to reveal the nature of interactions and to evaluate the binding constant (K_A) and number of binding sites (n) for HHb-GO complexes, the fluorescence spectroscopy data are used and the following generalized [6, 16] equation is applied:

$$log\left(\frac{F_0-F}{F}\right) = nlogK_A - nlog\left(\frac{1}{[Q_t]-\frac{(F_0-F)[P_t]}{F_0}}\right) \quad \text{…. (4)}$$

where F_0 and F are the fluorescence intensities before and after addition of GO; K_A is the apparent binding constant to a set of sites; and n is the average number of binding sites per HHb. $[Q_t]$ and $[P_t]$ are the total quencher concentrations and the total protein concentration, respectively. The plot of $log\left(\frac{F_0-F}{F}\right)$versus $log\left(\frac{1}{[Q_t]-\frac{(F_0-F)[P_t]}{F_0}}\right)$ at 298 K for HHb-GO complex has been represented in Fig. 4b. From the plots at different temperatures the binding constant K_A and n values are determined from intercept and slope, respectively and are shown in Table 3. As it is expected for static quenching phenomena, the values of $K_A$and n are found to decrease with increase of temperature. Also a significant decrease in K_A has been noticed at ~ 308 K which further gets decreased upon rise in temperature to 318 K. The decrease in K_A may suggest that the unstable ground state complex of HHb-GO system could be decomposed with rise of temperature.

Temperature (K)	n	K_A for GO (M^{-1})
288	0.698	2.68×10^4
298	0.570	2.37×10^4
308	0.128	0.4674
318	0.078	0.0147×10^{-4}

Table 3: Evaluation of binding constant and number of binding sites for HHb-GO

2.4.4 Thermodynamic Parameters and Nature of Binding Forces

To gain an idea about the forces involved in HHb-GO, thermodynamic parameters are estimated by using the following equations (equations 4 and 5) [17],

$$lnK_A = -\frac{\Delta H}{RT} + \frac{\Delta S}{R} \quad \text{…. (5)}$$

$$\Delta G = \Delta H - T\Delta S \quad \text{…. (6)}$$

Equations (5) and (6) are called van't Hoff equation and Gibbs–Helmholtz equation, respectively. The parameters ΔG, ΔH and ΔS represent standard changes in free energy, enthalpy and entropy respectively. From the plot of lnK_A versus $1/T$, the values of ΔH and ΔS are determined from the slope and the intercept respectively (Fig. 6). The values of ΔG are determined from Equation 6. The values of ΔH, ΔS and ΔG have been shown in Table 4.

From the Table 4, it is observed that ΔG is negative ($\Delta G < 0$) for HHb-GO complex which indicates the spontaneity of the binding of the HHb to GO at different temperatures.

Both ΔH and ΔS are found out to be negative and thus the predominant mode of interaction could be van der Waals interactions and hydrogen bonding (since $\Delta H < 0$ and $\Delta S < 0$) for HHb-GO interaction. Also relatively lower values of K_A and rapid lowering of this value with increase of temperature (Table 4) correspondingly suggest the presence of weaker binding forces such as van der Waals' interactions and hydrogen bonding for HHb-GO interaction.

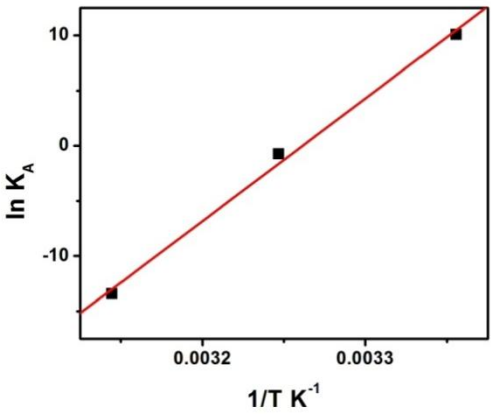

Fig. 12 Plot for lnK_A versus $1/T$ plot for HHb-GO complex have been shown.

T (K)	ΔH (KJmol^{-1})	ΔG (KJmol^{-1})	ΔS (KJmol^{-1}K^{-1})
288		-60.728	
298	-924.728	-30.7228	-3.0
308		-0.728	

Table 4. Thermodynamic parameters for HHb-GO complex at different temperatures have been shown in the table.

2.4.5 FT-IR studies

From the above observations the predominant interactions between HHb-GO appear to be hydrogen bonding and thus the pairing pattern of hydrogen bonds, is then checked by FT-IR spectroscopy. FT-IR bands are very sensitive to the conformational changes in the secondary structure of a protein and are related to the backbone conformation [2, 18]. FT-IR measurements of HHb are performed focusing on the effect on carbonyl (C=O) stretching mode in absence and in presence of GO/RGO. The most intense absorption band is the amide I band (1700-1600 cm^{-1}), associated with the C=O and C-N stretching vibrations of peptide linkages. Amide II region (1620–1500 cm^{-1}) comes from the in-plain N-H bending and C-N stretching. Positions and intensities of infrared absorption band of Amide I and Amide II could provide the information regarding conformational changes in HHb. From the Fig. 13a, it is apparent that the FT-IR spectra of HHb exhibit C=O stretching vibration (amide I) at 1650 cm^{-1}. The intensity of the amide I band decreases with broadening of the peak but spectral shift is not observed in presence of GO. The amide II band of HHb resides at 1546 cm^{-1} region. The amide II band becomes broadened and a decrease in the IR absorption intensity along with 1 nm red shift is noticed upon interaction with GO [42]. These changes in the IR absorption intensity of the C=O and N-H stretching vibration might suggest the participation of the C=O as well as NH group of the polypeptide chain in hydrogen bond formation with probably involvement of both the hydroxyl group present within tyrosine moiety as well as with indole N atom of tryptophan residues.

FT-IR measurements of HHb are also made focusing on the effect on C=O and N-H stretching mode in presence of RGO (Fig. 13b). As expected the amide I and amide II band of HHb nearly remain unchanged. The observations indicate that probably there is very less possibility of hydrogen bonding interaction involving C=O and N-H group of the polypeptide backbone.

The similar nature of the spectra of HHb in presence of GO and RGO suggest that HHb could preserve the essential features of its secondary structure even in the HHb-GO and HHb-RGO complexes. Here the possible interactions may also involve other weak non-covalent interactions like electrostatic interactions, hydrogen bonds, van der Waals interactions and hydrophilic interactions.

13(a) **13(b)**

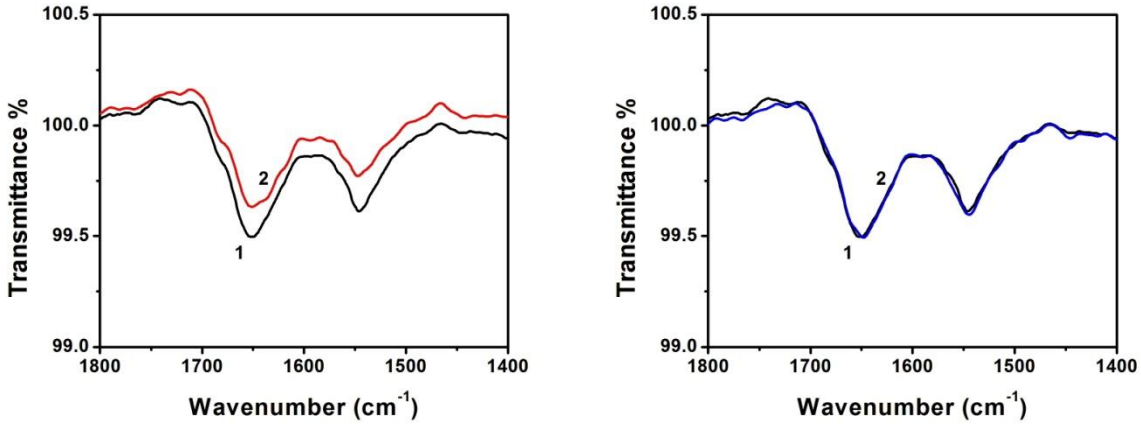

Fig. 13(a) FT-IR spectra of HHb and HHb-GO complex. Concentrations of GO are (1) 0, (2) 2.5 μg/ml. (b) FT-IR spectra of HHb and HHb-RGO complex. Concentrations of RGO are (1) 0, (2) 5 μg/ml.

2.4.6 Characteristic of the Resonance Light Scattering (RLS) spectra

It is apparent from the above discussion that ground state complex formations by hydrogen bonding interactions occur through preferably participation of C=O as well as N-H group of polypeptide linkage and hydroxyl group of tyrosine residue and indole N of tryptophan residues in the cases of both HHb-GO system. In order to check whether such interactions are having any effect of aggregation, resonance light scattering studies are performed. Since hydrogen bonding

interactions involving polypeptide backbone are not observed upon interaction with RGO and thus its effect on aggregation properties of HHb is also expected to get compromised.

RLS spectra of HHb, are recorded with the help of fluorescence spectrophotometer (see the experimental section) by using synchronously scanning mode from 250 to 650 nm, with $\Delta\lambda = 0$ nm (Fig. 14). Upon addition of GO to HHb solution, an increased RLS signal is noticed (Fig. 14a). The RLS intensity is dominated primarily by the particle dimension of the formed aggregate in solution [10, 18]. Considering these points, it is assumed that GO may interact with HHb in solution, forming a new HHb-GO complex that could be expected to promote aggregation thus suggesting increased light scattering signal occur under the given conditions.

Interestingly decrease in RLS signal of HHb is observed upon gradual addition of RGO. Since the RLS intensity is dominated primarily by the particle dimension of the formed aggregate in solution, the observations suggest that no such aggregation effect has occurred. This may be expected since hydrogen bond formation involving polypeptide backbone is observed to get compromised upon interaction with RGO.

14(a) **14(b)**

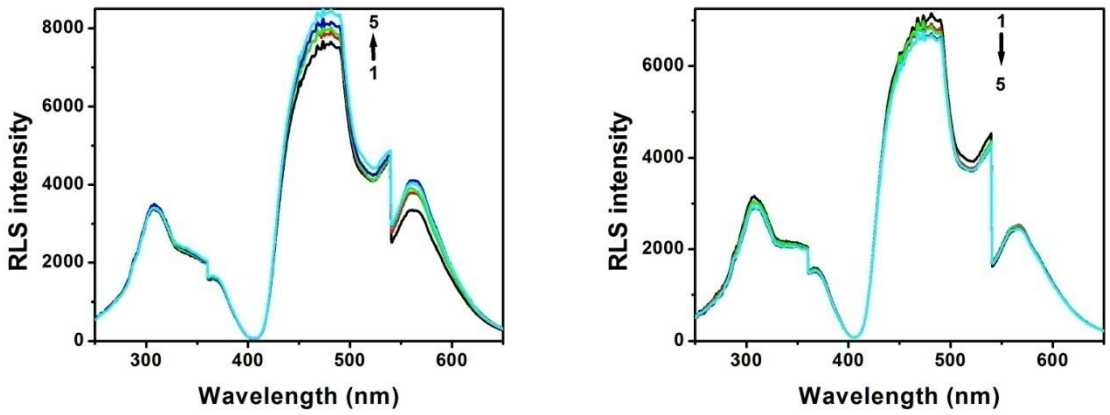

Fig. 14(a) RLS spectra of HHb and HHb –GO complex. Concentration of GNP are (1) 0, (2) ~ 2.5 μg/ml; (b) RLS spectra of HHb and HHb –RGO complex. Concentrations of GNS are (1) 0, (2) 5 μg/ml.

2.4.7 Synchronous Fluorescence Spectra

In order to check whether the interactions of HHb with RGO and especially GO could cause environmental alternations of aromatic residues (tryptophan and tyrosine) due to conformational change of HHb, synchronous fluorescence spectroscopy is performed. Synchronous fluorescence spectroscopy is a common method for the evaluation of protein conformational changes and it involves simultaneous scanning of the excitation and emission monochromators while maintaining a constant wavelength interval between them. The shift in the emission maximum reflects the changes of polarity around the chromophore molecule. When the $\Delta\lambda$ between excitation and emission wavelength is set at 15 nm and 60 nm, the synchronous fluorescence gives characteristic information of tyrosine and tryptophan residues respectively [19-23]. The synchronous fluorescence spectra at these two different wavelength intervals are presented in Fig. 15(a) and 15(b) for HHb in presence of increasing concentration of GO.

As the concentration of GO is gradually increased, the synchronous fluorescence intensity gradually decreases for the tyrosine ($\Delta\lambda$=15 nm) peak. The emission maximum of tyrosine residues is observed at 306 nm with no reproducible spectral shift upon addition of GO (Fig. 15a and 15c). Although a decrease in synchronous fluorescence intensity ($\Delta\lambda$=15 nm) indicate alterations around microenvironment of tyrosine residues probably due to hydrogen bonding interaction however the polarity around the tyrosine residues remains more or less unperturbed in presence of GO. The synchronous fluorescence intensity of HHb also gradually decreases for the tryptophan ($\Delta\lambda$=60 nm) peaks with no spectral shift in presence of GO (emission maxima at ~ 338 nm). Here also decrease in synchronous fluorescence intensity ($\Delta\lambda$=60 nm) indicate alterations around microenvironment of tryptophan residues probably due to hydrogen bonding interaction involving its indole N. But the polarity around the tryptophan residues is observed to remain nearly unchanged in presence of GO (Fig. 15c).

As expected in case of addition of RGO the synchronous fluorescence intensity of HHb does not exhibit any significant change for both tyrosine (emission maxima at 306 nm) (Fig. 15b) and tryptophan residues (emission maxima at 338 nm) (Fig. 15d). Thus the observations suggest the microenvironment of both the tyrosine and tryptophan residues nearly remains unaffected with no spectral shift in presence of RGO.

Thus it appears that upon interaction with GO the weak non-covalent forces are formed involving hydroxyl group of tyrosine and indole group of tryptophan residues. Such interactions are also affecting the hydrogen bonding pattern of polypeptide backbone as evident in the FTIR spectra (Fig 13a). Intriguingly such interactions are not promoting any change in the polarity around the microenvironment of tryptophan and tyrosine residues of HHb. All together both GO and RGO have not induced any significant structural modification that might affect the physiological function of HHb.

15(a) **15(b)**

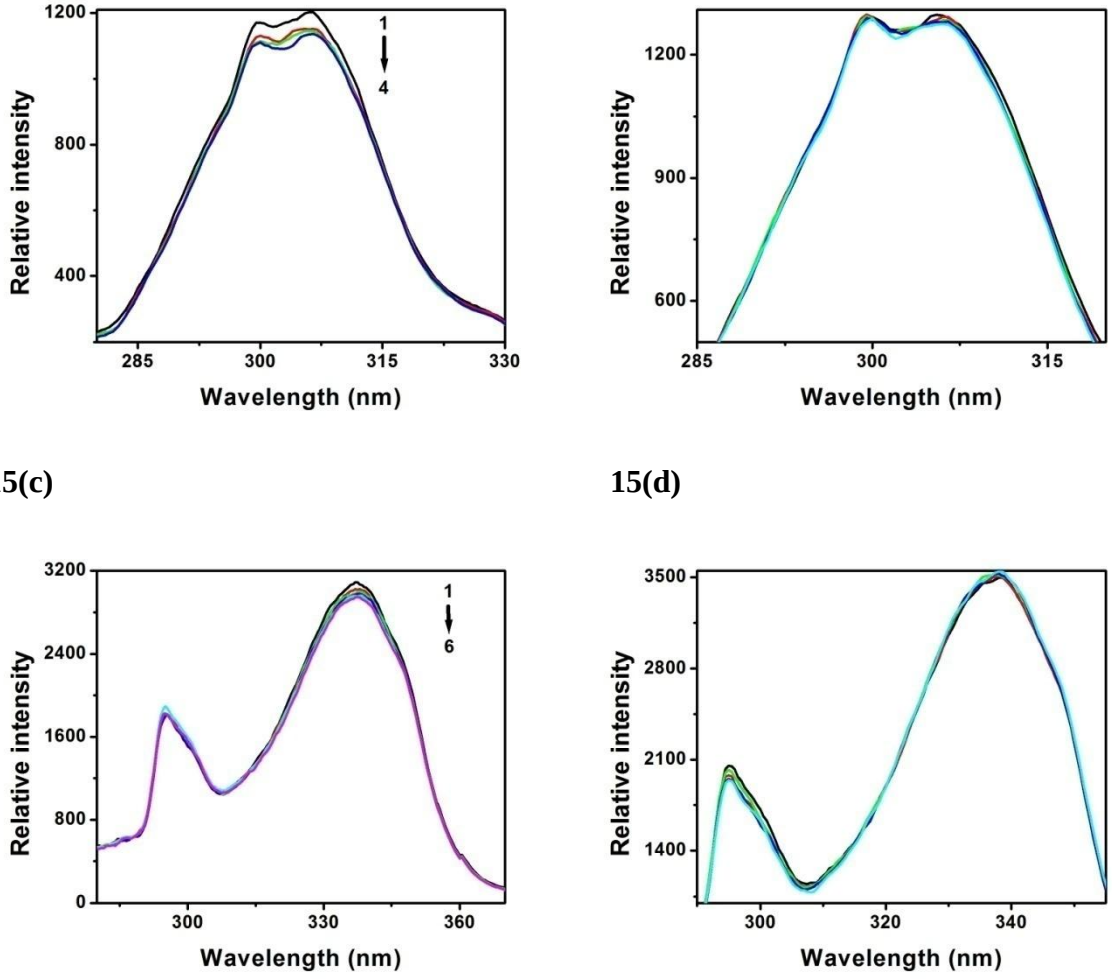

15(c) **15(d)**

Fig. 15(a) The synchronous fluorescence spectra of the HHb in presence of GO, where Δλ= 15 nm. The concentrations of GO are (1) 0, (2) 1 μg/ml, (3) 2 μg/ml, (4) 2.5 μg/ml. (b) The synchronous fluorescence spectra of the HHb in presence of RGO, where Δλ= 15 nm. The concentrations of RGO are (1) 0, (2) 1.5 μg/ml, (3) 3 μg/ml, (4) 4 μg/ml (5) 5 μg/ml. (c) The

synchronous fluorescence spectra of the HHb in presence of GO, where Δλ= 60 nm. The concentrations of GO are (1) 0, (2) 0.625 μg/ml, (3) 1 μg/ml, (4) 1.25 μg/ml, (5) 1.875 μg/ml, (6) 2.5 μg/ml. (d) The synchronous fluorescence spectra of the HHb in presence of RGO, where Δλ= 60 nm. The concentrations of RGO are (1) 0, (2) 1.5 μg/ml, (3) 3 μg/ml, (4) 4 μg/ml, (5) 5 μg/ml.

2.4.8 CD Spectra and the Secondary Structural Changes

To get further information regarding conformational change of the protein in presence of GO and RGO, CD measurements are performed. CD spectroscopy is a quantitative technique to investigate the conformation of proteins in aqueous solution [24-27]. From Fig. 10a and 10b**,** negative bands at about 209 and 220 nm are observed which were characteristic of α-helical content of HHb. Thus from far-UV CD data in the wavelength range from 190 to 240 nm a deep insight to the secondary structures of HHb is obtained. The intensities of the negative bands at 209 nm although increases slightly upon addition of GO but the band at 220 nm remains almost unchanged. However in presence of RGO, the intensities of the negative bands at 209 and 220 nm decrease marginally. For further clarification, the CD results are then expressed in terms of mean residue ellipticity (MRE) in degree cm^2 mol^{-1} according to the following equation

$$[\theta_\lambda] = \frac{\theta}{10nlc} \qquad \text{…. (7)}$$

where c is the concentration of protein in g/ml, θ is observed rotation in degree, l is the path length in cm, and n is the number of amino acid residues of HHb (574 amino acid residues). Quantitative assessment of the percentage of α-helix in HHb in presence of GO is estimated by the following equation

$$\%\ of\ \alpha - Helix = \frac{-[\theta]_{208} - 4000}{33000 - 4000} \qquad \text{…. (8)}$$

$$\%\ of\ \alpha - Helix = \frac{[\theta]_{222} + 2340}{-30300} \qquad \text{…. (9)}$$

According to Equation 8, the percentage of α-helix content of HHb has been calculated and % α-helicity is observed to decrease by only 1.4 % at 209 nm in presence of GO. Likewise according to equation 9, the % of α–helicity decrease by only 0.5 % at 220 nm upon interaction with GO. However, the percentage of α-helicity of HHb as calculated from equation 8 appears to increase by only 1.1 % 209 nm upon addition of RGO. Similarly according to equation 9, the % of α–

helix content increase by only 0.55 % at 220 nm in presence of GO. Thus upon addition of GO and RGO, the spectral shape of HHb remains more or less unaltered though very little change in the values of mean residue ellipticity (MRE), θ, is observed. This observation demonstrates that although extremely small changes have occurred in the secondary structure as observed upon binding of GO/RGO but the overall secondary structure of HHb is mostly retained and its identity is maintained even after complex formation with GO or RGO. Thus upon interaction of GO and RGO with biomolecules like HHb, no significant distortion in the secondary structural pattern of the latter occurs. All the above observations indicate that both GO and RGO should have potential applications in biological microenvironment especially as a drug delivery system.

16(a) **16(b)**

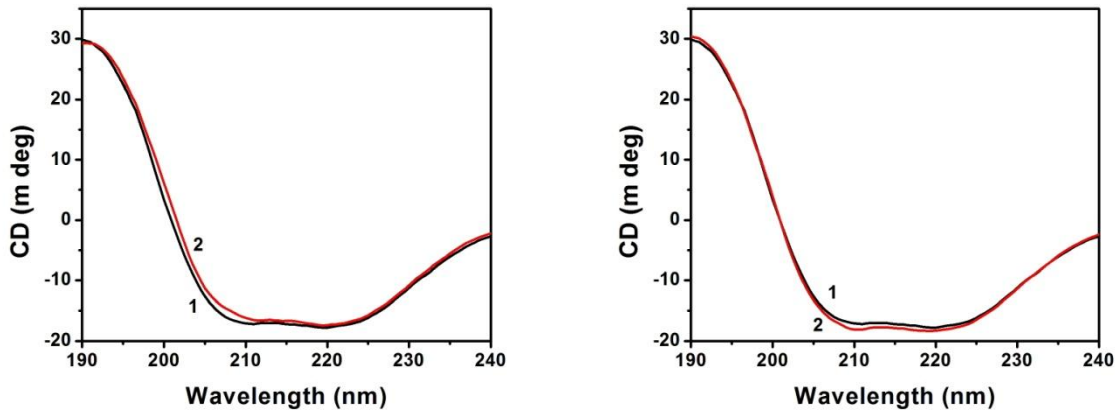

Fig. 16. (a) CD spectra of HHb in presence of GO. The concentrations of GO are (1) 0, (2) 2.5 μg/ml. (b) CD spectra of HHb in presence of RGO. The concentrations of RGO are (1) 0, (2) 5 μg/ml.

2.5 Conclusions

The present spectroscopic investigations reveal the nature of interactions of biologically significant protein HHb with the member of carbon family- GO/RGO. UV-vis absorption data reveal hyperchromic effect at 270 nm due to absorbance by tryptophan and tyrosine indicating the possibility of formation of ground state complex in presence of GO, whereas hypochromicity at this region is observed, in presence of RGO. Moreover steady-state fluorescence static

quenching with no spectral shift is observed in presence of GO and fluorescence enhancement with no spectral shift is noticed upon interaction with RGO. Although a change in the fluorescence intensity is noted in both the cases, but the alterations in the microenvironment is not accompanied by changes in polarity around tryptophan and tyrosine residues. Also the amide I and II bands in the FTIR spectra are decreased in presence of GO but those bands remain almost unchanged in presence of RGO. Surprisingly GO is observed to promote the aggregation effect in HHb by showing an increased RLS signal. But in case of RGO decrease in RLS signal is observed. Moreover although the alterations in microenvironment of HHb in presence of GO and RGO appear to occur in different manner, but still the overall secondary structure of the HHb is retained as revealed in CD spectral analysis in both the cases. The present investigation hints that in spite of such interactions between HHb and GO/RGO, the safety of the protein environment retains. Above all the investigation also reveal that the effect of GO on the spectroscopic properties of HHb are being compromised upon its reduction to RGO.

Largely the systematic efforts determine the interaction of HHb with GO and RGO and suggest the potential applications of GO/RGO in biological microenvironment especially as drug delivery systems in human as well. Also the underlying role of HHb as a model protein in bimolecular interaction has been highlighted in the next chapter.

References

[1] M. Chakraborty, S. Paul, I. Mitra, M. Bardhan, M. Bose, A. Saha, T. Ganguly, Journal of Photochemistry & Photobiology, B: Biology.178 (2018) 355–366.

[2] M. Chakraborty, I. Mitra, K. Sarkar, M. Bardhan, S. Paul, S. Basu, A. Goswami, A. Saha, B. Show, T. Ganguly. Spectrochimica Acta Part A: Molecular and Biomolecular Spectroscopy 215 (2019) 313–326.

[3] A. Mallick, A. S. Mahapatra, A. Mitra, J. M. Greneche, R. S. Ningthoujam and P. K. Chakrabarti. JOURNAL OF APPLIED PHYSICS 123, 055103 (2018)

[4] D.C. Marcano, D.V. Kosynkin, J.M. Berlin, A. Sinitskii, Z. Sun, A. Slesarev, L.B. Alemany, W. Lu and J.M. TourACS NANO VOL. 4, NO. 8, 4806–4814, 201

[5] C.S.R. Vusa, S. Berchmans and S. Alwarappan, RSC Adv., 2014, 4, 22470.

[6] P. Mandal, T. Ganguly, J. Phys. Chem. B 113 (2009**)** 14904–14913

[7] A. K. Bhunia, T. Kamilya,S .Saha, Nano Convergence. 4:28 (2017).

[8] M. Mahato, P. Pal, T.Kamilya, R. Sarkar, A. Chaudhuri, G.B.Talapatra, J. Phys. Chem. B. 114(2010**)** 7062–7070.

[9] M. Mahato, P. Pal, B.Tah, M. Ghosh, G. B.Talapatra, *Colloids and Surfaces B: Biointerfaces*. 88 (2011) 141– 149.

[10] M. Uttamlal, A. S. Holmes-Smith, The excitation wavelength dependent fluorescence of porphyrins, Chem Phys Letts 454 (2008) 223–228.

[11] M. Akram, S. Anwar, I. A. Bhat, K. -ud-Din. *Colloids and Surfaces A*. 527 (2017) 145–157.

[12] E. Karnaukhova, S. Rutardottir, M. Rajabi, L. W. Rosenlöf, A. I. Alayash and B. Åkerström, Characterization of heme binding to recombinant **α**1-microglobulin, (2014) Volume 5 Article 465

[13] H. Benesi, J. Hildebrand, A spectrophotometric investigation of the interaction of iodine with aromatic hydrocarbons, J. Am. Chem. Soc. 71 (1949) 2703–2707.

[14] T. Ganguly, S.B. Banerjee, Effect of hydrogen bonding on the electronic absorption spectra of xylenols, Spectrochim. Acta 34A (1977) 617–623.

[15] P. Anger, P. Bharadwaj, and L. Novotny, Enhancement and Quenching of Single-Molecule Fluorescence, PRL **96,** 113002 (2006)

[16] Y.Q. Wang, H.M. Zhang, G.C. Zhang, S.X. Liu, Q.H. Zhou, Z.H. Fei, Int. J. Biol. Macromol. 41(2007) 243–250.

[17] P. Atkins, J.D. Paula, 10th ed., W. H. Freeman & Company, 978-0-19-969740-3, 2014, p. 256.

[18] G. Mandal, S. Bhattacharya, T. Ganguly, J. Appl. Phys. 110 (2011) 024701–024708.

[19] J.Q. Xi, R. Guo, Int. J. Biol. Macromol. 40 (2007) 305–311.

[20] X.J. Yang, J. Chou, G.Q. Sun, H. Yang, T.H. Lu, Microchem. J. 60 (1998) 210–216.

[21] B. Klajnert, M. Bryszewska, Bioelectrochemistry 55 (2002) 33–35

[22] J. R. Lakowicz, (1999**)** 2nd ed.; Plenum Press: New York.

[23] J.B.F. Lloyd, Nature 231 (1971) 64–65.

[24] N. Sreerama, R.W. Woody, Anal. Biochem. 287 (2000) 252–260.

[25] Y.H. Chen, J.T. Yang, H.M. Martinez, Biochemistry 11 (1972) 4120–4131.

[26] Z.X. Lu, T. Cui, Q.L. Shi, first ed., Science Press, 1987.

[27] P. Mandal, M. Bardhan, T. Ganguly, J. Photochem. Photobiol. B Biol. 99 (2010) 78–86.

CHAPTER 3:

SPECTROSCOPIC PROPERTIES OF HUMAN HEMOGLOBIN ALTER DIFFERENTLY IN PRESENCE OF TWO MEMBERS OF CARBON NANOFAMILY: COMPARATIVE SPECTROSCOPIC APPROACH UPON INTERACTION WITH CARBON QUANTUM DOT AND GRAPHENE OXIDE

Experiment 1.

Spectroscopic properties of Human Hemoglobin alter differently in presence of two members of carbon nanofamily: Comparative spectroscopic approach upon interaction with carbon quantum dot and graphene oxide

3.1 Abstract

In our previous work we observed the nature of interactions of HHb with carbon quantum dots (CQD). With respect to this, a brief discussion regarding the interaction of HHb with different nanoparticles examined has been outlined in this chapter. The aim is to discuss the role of HHb as a model protein upon interaction with two different nanoparticles of a single carbon family (GO/RGO/CQD). Also a detailed insight regarding, nature of interaction of the same model protein with different nanomaterials of same family can be obtained. Although the nanostructures belong to similar family yet they have different physicochemical and electronic properties based on their unique structural properties. Thus if proper knowledge is gathered, these nanostructures can be utilized in wide-range of applications. Their potential in the biological realm however cannot be fundamentally realized unless their interaction whether stable or unstable is assessed with biological macromolecules of immense physiological significance like HHb. Thus it appears that the interaction of HHb with different nanostructures if understood properly at the nano-biointerface, it will definitely give some hints regarding their particular field of application. Keeping all these in mind the following comparative analysis has been performed regarding interaction of HHb with members of carbon family (GO/RGO and CQD). Interestingly it appears that upon interaction with CQD and GO/RGO, the overall secondary structure of HHb is mostly retained thus highlighting the potential application of CQD and GO/RGO as a drug-delivery system.

Keywords: Graphene oxide; Carbon Quantum Dots, Human Hemoglobin; Model protein; Native Secondary structure; Drug-delivery system

3.2 Literature Review

In recent years probing molecular structure and conformational dynamics of the biomolecules by developing innovative fluorescence- based tools are subjects of great interest in biophysical

chemistry. Hemoglobin (Hb) is an iron-based complex which physiologically plays the crucial role in binding molecular oxygen, but the study of hemoglobin has gone beyond the interest in its physiological role as an oxygen carrier because it can be considered from all points of view an ideal model for investigating the properties of proteins in general, and enzymes in particular [1–9]. Nonetheless, Hb serves biochemical roles involving electron transfer, oxygen transfer and storage, and metabolism. Hb is a globular protein made up of four sub-units. Each subunit has a polypeptide chain attached to an iron-containing component called heme. Each heme group contains one iron atom and each iron atom can bind one O_2 molecule. The polypeptide chains of hemoglobin are referred to as the globin portion of the molecule. Normal adult hemoglobin (hemoglobin A) has four sub-units build up of two alpha (α) and two beta (β) polypeptide chains. In the normal adult HHb each α-chain contains 141 amino acid residues and each β-chain contains 146 amino acid residues. There are three intrinsic fluorophores in HHb: (i) tryptophan, (ii) tyrosine, and (iii) phenylalanine. Tetrameric hemoglobin contains six tryptophan residues: two Trpα14, two Trpβ15, and Trpβ37 [10-12]. Among three Trp residues only β37Trp is situated at the dimer–dimer interface. This is the region where structural differences between quaternary states are largest [12]. Moreover, Hb contains five Tyr residues in each dimer: Tyrα24, 42, 140 and Tyr β34, 144 [13-17].

Although the relationship between the structure and function of HHb has been thoroughlystudied, however the research on its interaction with other molecules is limited to a few small molecules. Interaction of HHb as one of the most important physiologically active protein with small molecules of clinical interest can give knowledge regarding HHb-mediated drug targeting. Such bimolecular interactions between proteins like HHb and small molecules might have immense biological significance since HHb serves numerous biochemical roles in electron transfer, oxygen transfer and storage and in metabolic pathways. In this respect, binding of small molecules of medical importance to HHb can cause significant changes in conformation, which may further provide interesting information regarding structure, function, and dynamic properties of HHb.

Moreover miniaturization of structures in the form of nanoscale materials and their small sizes, have well-defined characteristics compared to the bulk form of the same material[18]. Nanoparticles provide large surfaces for reactions involving biomolecules thus suggesting a meaningful pathway to combine biomolecular functionality with unique electronic and optical

attributes of nanoparticles. As such,perception regarding the role of nanoparticles as drug or drug delivery system can be obtained, if interactions between nanoparticles and biomolecules are investigated. Thorough idea of protein-nanoparticle interactions will thus be essential to realizehow nanoparticles will function in biological milieuespecially as drug delivery systems and consequentlyproviding information to whether the nanoparticles are causing any significant changes in the structure and function of biomolecules in its biological surroundings.

In this respect the small molecules of nano-dimension that are chosen for investigation are thought to be carbon quantum dots. This may be well imagined since CQDs have gained noble attention as a member of carbon nanomaterial family due to their extensive physical and chemical properties [19-26]. CQDs are nanomaterials with size less than ~10 nm, first obtained in 2004 during purification of single-walled carbon-nanotubes. Since then CQDs have been used in a wide range of applications due to their low cost of preparation and favorable properties such as chemical inertness, biocompatibility, non-toxicity and solubility in aqueous medium**.** These notable properties of carbon-based quantum dots, enable them with potential applications in numerous fields of research like bio-imaging**,** biosensor**,** photo-physics and drug-delivery systems. However the application of CQDs in drug-delivery system has not gained much attention. It may happen that the study of protein-quantum dot interactions may open new areas and highlight the understanding of how nanoparticles function in biological environment especially in the fields of drug-delivery systems.

Moreover a novel single-atom-thick and two-dimensional (2D) carbon nanomaterial, graphene oxide (GO), belonging to an oxidized derivative of graphene, has attracted significant attention recently due to its remarkable structural, chemical, mechanicaland electronic properties, and has shown great promise for different applications in many fields [27–29]. Lately, the application of GO has been extending to biological systems, including biodevices, microbial detection, disease diagnosis, and drug delivery systems, due to its considerably large specific surface area (two accessible sides), its rich oxygen-containing surface functionalities like epoxide, hydroxyl and carboxylic groups, and its high water solubility [30, 31]. However, a key issue that needs to be addressed before the large-scale implementation of GO in a wide range of biological applications isits less-studied biosafety and biocompatibility properties, especially when its facts such as high accumulation, long term retention and relative long blood circulation time in organisms are under consideration [32].

In this section it has been observed that the spectroscopic properties of HHb alter in different manner upon interaction with either CQD, GO and RGO. Strikingly in spite of the alterations observed in the microenvironment of HHb, upon its interaction with CQD, GO and RGO, the overall secondary structure of HHb as revealed by CD spectroscopy, is however more or less retained. Thus interactions of CQD, GO and RGO at the nano bio-interface can be widely utilized in wide-range of fields.

3.3 Materials and Methodology

Materials

Human Hemoglobin (HHb), purchased from Sigma Aldrich, is tested before use for the presence of any impurity in the region of wavelength studied. In all the experiments freshly prepared aqueous solutions of concentration ~ 5 x 10^{-6} M (0.645 mg/ml) have been used [1, 2].

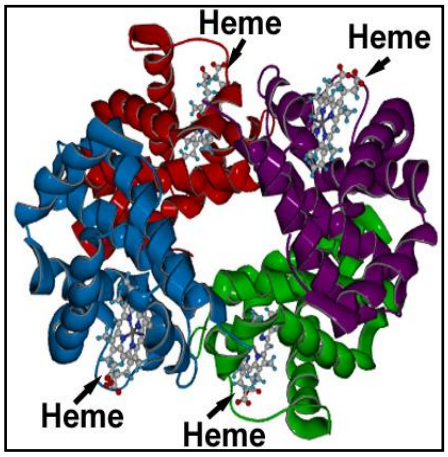

Fig 7: (Colour online) Molecular structure of HHb

Synthesis of Carbon Quantum Dots

CQDs are synthesized from citric acid by microwave-assisted method. Briefly, 1 g of citric acid is dissolved in 10 mL of water. The citric acid solution is then heated in a domestic microwave oven (Whirlpool) at 1200 W power for ~ 7-8 min and in the course of which the solution color is changed from colorless to pale yellowish brown thereby denoting the formation of CQD. The obtained product after dispersing in Millipore water is centrifuged at 10 000 rpm for 1 hour.

Finally the supernatant collected carefully and purified as mentioned elsewhere and pure CQD obtained are used for experimental studies [2]. The average diameter is observed to be ~ 2-5 nm.

All the reagents are purchased from Sigma Aldrich and used in the experiments without any further process of purification. Water has been double distilled and then deionized using a Millipore Milli-Q system.

Spectroscopic Apparatus

Dilute solutions of the HHb (~10^{-6} M) are taken for the following spectroscopic techniqus are performed in absence and presence of GO and RGO at the ambient temperature - UV-vis absorption spectra, steady state fluorescence emission spectra, Resonance Light Scattering (RLS) spectra, synchronous fluorescence spectra, FTIR measurements and Circular dichroism (CD) spectroscopy measurements as described elsewhere [1, 2]. Briefly UV–vis absorption and steady state fluorescence emission spectra of dilute solutions of the samples are measured in absence and presence of GO and RGO in rectangular quartz cells of 1 cm path length at the ambient temperature. UV–vis absorption spectra are scanned by using JASCO UV–Vis absorption spectrometer (Model: V-630). Steady-state fluorescence emission spectra, RLS spectra and synchronous fluorescence spectra are monitored using JASCO Spectrofluorimeter (Model: 8200). For Benesi-Hildebrand plot, and fluorescence quenching analysis for evaluation of thermodynamic parameters the molecular weight of GO is considered as 2043.856.

Fluorescence lifetimes measurements of HHb in absence and presence of GO and RGO are carried out using a time correlated single-photon-counting (TCSPC) technique with the model FLUOROLOG TCSPC HORIBA JOBIN YVON using 280 nm (NanoLED 280) as impulse for excitation in Trp/Tyr region and an emission wavelength of 330 nm. The decay kinetics, the quality of fit with a plot of weighted residuals and other statistical parameters like reduced χ^2 and the Durbin–Watson (DW) parameters are checked for the entire decay along with the rising edge.

The Circular dichroism (CD) spectroscopy measurements are scanned using a PC driven JASCO CD spectropolarimeter (Model J-815) in the UV region (250–190 nm) at 25 °C in a rectangular quartz cell (1 mm).

The following observations are plotted and analyzed using Microcal Origin (version 8.5) software after taking original raw data directly from the instrument.

3.4 Result and Discussion

Comparative spectroscopic approach for CQD and GO

3.4.1 UV-vis absorption study

UV-vis electronic absorption spectra of HHb reveal a prominent hyperchromic effect with no spectral shift for both CQD and GO. The observations suggest the formation of ground-state complex upon interaction with CQD and GO and the change in the regions of absorbance of tryptophan and tyrosine residues is comparable. Thus CQD and GO upon interaction with HHb are altering the microenvironment of the fluorescing aromatic residues tryptophan and tyrosine in a similar manner.

3.4.2 Steady-state fluorescence spectroscopic study

In case of steady state fluorescence emission spectra of HHb the in presence of CQD, fluorescence enhancement with significant ~ 10 nm red shift is observed. This red shift indicates exposure of tryptophan and tyrosine residues to a more hydrophilic environment. Steady-state static type quenching is also noticed for HHb upon interaction with GO but with no spectral shift. Unlike the observations for UV-vis absorption spectra where the observations are comparable showing hyperchromicity, the steady state fluorescence emission spectral analysis reveals different observations pointing fluorescence enhancement and static quenching respectively.

3.4.3 Time-resolved fluorescence study

Moreover the magnitudes of the τ of HHb remain nearly similar in presence of GO. However the magnitude of τ of HHb, increases significantly (~ 1.7 times) upon addition of CQD.

3.4.4 Synchronous fluorescence spectroscopy

As expected there is an increase in synchronous fluorescence intensity in presence of both CQD. Surprisingly the tyrosine peak shows an intense blue shift of ~ 7 nm while the tryptophan peak displays red shift of ~ 2 nm. Thus the possible interaction of HHb with CQD is probably exposing tryptophan residues to a more hydrophilic environment and tyrosine residues to a more hydrophobic environment.

In case of GO, synchronous fluorescence intensity of HHb gradually decreases without any spectral shifts for the tyrosine residues ($\Delta\lambda$=15 nm). Likewise synchronous fluorescence intensity of HHb gradually decreases without any spectral shifts for the tryptophan residues ($\Delta\lambda$=60 nm). Different nanostructures (GO and CQD) after interacting with the same model protein (HHb) are altering the microenvironment of HHb differently such that the tryptophan and tyrosine residues are getting exposed to either a hydrophilic or hydrophobic environment. These observations may be expected since CQD and GO vary in size, shape, physicochemical and photo-physical properties from each other.

3.4.5 FTIR spectroscopy study

In case of FTIR study, the intensity of the amide I bandupon interaction with CQD is decreased but with no spectral shift.This band is also observed todecreases with broadening of the peak but with no spectral shift upon interaction with GO.

3.4.6 RLS intensity

In presence of CQD, increase in RLS intensity is noticed. Since an increase in RLS intensity corresponds to increase in particle dimension of the formed aggregate in solution thus it appears that interaction with CQD may promote aggregation of HHb.

Moreover it is observed that GO may interact with HHb in solution, forming a new HHb-GO complex that could be expected to promote aggregation thus suggesting increased light scattering signal to occur under the given conditions.

Thus the interactions of CQD and GO are facilitating stable interaction of individual HHb to enhance protein aggregation.

3.4.7 Secondary structural analysis

Strikingly in spite of the alterations observed in the microenvironment of HHb, upon its interaction with CQD and GO, the overall secondary structure of HHb as revealed by CD spectroscopy, is however more or less retained.

The observations are represented in a tabular form (Table 1).

Table 1:HHb as model protein for interaction with CQD and GO

Properties	CQD	GO
UV-vis absorption	Hyperchromicity ↑	Hyperchromicity↑
Steady-state fluorescence emission	Fluorescence enhancement ↑	Static quenching ↓
	10 nm red shift	No spectral shift
τ	1.7 times increment	No change
Synchronous fluorescence		
	Δλ=15 nm Fluorescence enhancement	**Δλ=15 nm** Fluorescence quenching
	7 nm blue shift	No spectral shift
	Δλ=60 nm Fluorescence enhancement	**Δλ=60 nm** Fluorescence quenching
	2 nm red spectral shift	No spectral shift
Microenvironment of Tryptophan residues	Exposed to a more hydrophilic environment	No change in polarity
Microenvironment of Tyrosine residues	Exposed to a more hydrophobic environment	No change in polarity
CD spectra	Overall secondary structure retained	Overall secondary structure retained
RLS signal	Increased	Increased

Comparative spectroscopic approach for CQD and RGO

3.4.8 UV-vis absorption study

UV-vis electronic absorption spectra of HHb reveal a prominent hyperchromic effect with no spectral shift for CQD. However the UV-vis electronic absorption spectra of HHb reveal a weak yet noticeable hypochromic effect for RGO. The observations suggest the formation of ground-state complex upon interaction with CQD and RGObut the change in the regions of absorbance of tryptophan and tyrosine residues is different. Thus CQD and RGO upon interaction with HHb

are altering the microenvironment of the fluorescing aromatic residues tryptophan and tyrosine in a different manner.

3.4.9 Steady-state fluorescence spectroscopic study

In case of steady state fluorescence analysis of HHb in presence of CQD, fluorescence enhancement with significant ~ 10 nm red shift is observed. This red shift indicates exposure of tryptophan and tyrosine residues to a more hydrophilic environment. Surprisingly steady-state fluorescence enhancement is also noted for HHb upon interaction with RGO. Here also the changes in steady-state fluorescence intensity occur in a similar pattern of fluorescence enhancement. The observations are interesting since comparison for CQD and GO shows different pattern of fluorescence enhancement and static type of quenching respectively, whereas for CQD and RGO the observations reveal fluorescence enhancement.

3.4.10 Time-resolved fluorescence study

Although the magnitude of the τ of HHb remains nearly unchanged in presence of RGO, but τ, increases significantly (~ 1.7 times) upon addition of CQD. .

3.4.11 Synchronous fluorescence spectroscopy

As expected there is an increase in synchronous fluorescence intensity in presence of both CQD. Surprisingly the tyrosine peak shows an intense blue shift of ~ 7 nm while the tryptophan peak displays red shift of ~ 2 nm. Thus the possible interaction of HHb with CQD is probably exposing tryptophan residues to a more hydrophilic environment and tyrosine residues to a more hydrophobic environment.

In case of RGO, synchronous fluorescence intensity of HHbdo not show any significant change for both tyrosine residues ($\Delta\lambda$=15 nm) and tryptophan residues ($\Delta\lambda$=60 nm) thus indicating no change in microenvironment and polarity around tryptophan and tyrosine residues.

Thus CQD and RGO in spite of being the member of the same carbon nano family, are interacting with the same model protein (HHb) in a dissimilar manner. These observations can be expected by considering the fact thatCQD and RGO vary in size, shape, physicochemical and photo-physical properties from each other.

3.4.12 FTIR spectroscopy study

In case of FTIR study, the intensity of the amide I band upon interaction with CQD is decreased but with no spectral shift. However this FTIR band nearly remains unchanged upon interaction with RGO.

3.4.13 RLS intensity

In presence of CQD, increase in RLS intensity is noticed. Since an increase in RLS intensity corresponds to increase in particle dimension of the formed aggregate in solution thus it appears that interaction with CQD may promote aggregation of HHb.

Interestingly decrease in RLS signal of HHb is observed upon gradual addition of RGO. Since the RLS intensity is dominated primarily by the particle dimension of the formed aggregate in solution, the observations suggest that no such aggregation effect has occurred. This may be expected since hydrogen bond formation involving polypeptide backbone is observed to get compromised upon interaction with RGO.

Thus the interactions with CQD are facilitating stable interaction of individual HHb to enhance protein aggregation. However there is no such aggregation effect the in presence of RGO.

3.4.14 Secondary structural analysis

Strikingly in spite of the alterations observed in the microenvironment of HHb, upon its interaction with CQD and RGO, the overall secondary structure of HHb as revealed by CD spectroscopy, is however more or less retained.

The observations are represented in a tabular form (Table 2).

Table 2:HHb as model protein for interaction with CQD and RGO

Properties	CQD	RGO
UV-vis absorption	Hyperchromicity ↑	Hypochromicity ↓
Steady-state fluorescence emission	Fluorescence enhancement ↑	Fluorescence enhancement ↑
	10 nm red shift	No spectral shift
τ	1.7 times increment	No change
Synchronous fluorescence		
	Δλ=15 nm Fluorescence enhancement	**Δλ=15 nm** No change
	7 nm blue shift	No spectral shift
	Δλ=60 nm Fluorescence enhancement	**Δλ=60 nm** No change
	2 nm red spectral shift	No spectral shift
Microenvironment of Tryptophan residues	Exposed to a more hydrophilic environment	No change in polarity
Microenvironment of Tyrosine residues	Exposed to a more hydrophobic environment	No change in polarity
CD spectra	Overall secondary structure retained	Overall secondary structure retained
RLS signal	Increased	Decreased

3.5 Conclusion

Thus interactions of these biocompatible particles at the nano bio-interface can be widely utilized in wide-range of fields. Whether the CQD and GO/RGOcan be used as an efficient drug-delivery system, biosensor or bioimaging and other biological fields will then depend on their properties and their nature of interactions. Moreover the observations further indicate that in spite of being the members of the same family-CQD and GO/RGO interact with HHb in comparatively different manner.Thus it becomes apparent that different nanostructures can affect the spectroscopic properties of the same biomolecule HHb in their own way. All in all the systematic efforts have revealed the role of HHb as a model protein in bimolecular interaction (Table 1 and Table 2) suggesting the potential application of HHb as a model protein.

Reference

2. [1] M.Chakraborty, S.Paul, I.Mitra, M.Bardhan, M. Bose, A. Saha, T. Ganguly, Journal of Photochemistry & Photobiology, B: Biology.178 (2018) 355–366.
3. [2] M. Chakraborty, I. Mitra, K. Sarkar,M.Bardhan, S. Paul, S.Basu,A.Goswami, A.Saha, B. Show, T.Ganguly. SpectrochimicaActa Part A: Molecular and Biomolecular Spectroscopy 215 (2019) 313–326.
4. [3] A.K. Bordbar, A.A. Mooasavi-Movahedi, Bull. Chem.Soc. Jpn. 69 (8) (1996) 2231–2234.
5. [4] A.K. Bordbar, A. Nasehzadeh, D. Ajloo, K. Omidiyan, H. Naghibi, M. Mehrabi, H.Khajehpour, M. Rezaei-Tavirani, A.A. Moosavi-Movahedi, Bull.Kor. Chem. Soc. 23 (8) (2002) 1073–1077.
6. [5] C.W. Liu, A. L Bo, G.J. Cheng, X.Q. Lin, S.J. Dong, Biochim. Biophys.Acta 1385 (1998) 53–60.
7. [6] S. De, A. Girigoswami, J. Colloid Interf. Sci. 296(2006) 324–331.
8. [7] Y. Cheng, H.K. Lin, D.P. Xue, R.C. Li, K. Wang, Biochim. Biophys.Acta 1535 (1) (2001) 200–216.
9. [8] S. Sil, M. Kar, A.S. Chakraborti, J. Photochem.Photobiol. B Biol. 41 (1997) 67–72.
10. [9] X.-C. Shen, X.-Y.Liou, L.-P.Ye, H. Liang, Z.-Y. Wang, J. ColloidInterf. Sci. 311 (2007) 400–406.
11. [10] S. Venkateshrao, P.T. Manoharan, *Spectrochim. Acta Part A*60 (2004) 2523–2526.
12. [11] R.A. Goldbeck, R.M. Esquerra, D.S. Kliger, *J. Am. Chem. Soc*.124 (2002) 7646–7647.
13. [12] T.C. Mueser, P.H. Rogers, A. Arnone, *Biochemistry* 39(2000) 15353–15364.

14. [13] M.F. Perutz, A.J. Wilkinson, M. Paoli, and G.G. Dodson,*Annu. Rev. Biophys. Biomol.Struct.*27(1998) 1-34.
15. [14] G.K. Ackers,*Adv. Protein Chem.*51(1998) 185-253.
16. [15] G.K. Ackers, M.L. Doyle, D. Myers, and M.A. Daugherty, *Science*255 (1992) 54-63.
17. [16] G. Fermi, M.F. Perutz, B. Shaanan, and R. Fourme,*J. Mol. Biol.* 175 (1984) 159-174.
18. [17] J.V. Kilmartin and L. Rossi-Bernardi*Physiol. Rev.* 53 (1973) 836-890.
19. [18] W. Shang, J. H. Nuffer, V. A. Muniz-Papandrea, W. Colon, R. W. Siegel,and J. S. Dordick, *Small*5(2009) 470-476.
20. [19] Y.Wang, A. Hu, J. Mater. Chem. *C.* 2 (2014) 6921-6939.
21. [20] R. Wang, K. Q. Lu, Z. R. Tang, Y. J. Xu,. J. Mater. Chem. A. 5 (2017) 3717-3734
22. [21] Z. L. Wu, Z. X. Liu, Y. H. Yuan, J. Mater. Chem. B5 (2017) 3794-3809.
23. [22] X. Xu,R. Ray, Y. Gu, H. J. Ploehn, L.Gearheart, K.Raker, W. A. Scrivens, J. Am. Chem. Soc 126 (2004) 12736–12737.
24. [23] H. Ding, L. W. Cheng, Y. Y. Ma, J. L. Kong, H. M. Xiong, New J. Chem.37 (2013) 2515-2520.
25. [24] X. He, L. Gao, N. Ma, Sci Rep. 3 (2013**)** 2825.
26. [25] T. T. Bui, S. Y. Park, *Green Chem*. 18 (2016) 4245-4253.
27. [26] P. Lv, Y. Yao, H. Zhou, J. Zhang, Z. Pang, K.Ao, Y.Cai, Q. Wei, Nanotechnology. 28 (2017**)** 165502-165512.
28. [27] Y. Zhu, S. Murali, W. Cai, X. Li, J.W. Suk, J.R. Potts, et al. Adv Mater 2010;22(35):3906–24.
29. [28] O.C. Compton, S.T. Nguyen, Small 2010;6(6):711–23.

30. [29] C.N.R. Rao, A.K. Sood, K.S. Subrahmanyam, A. Govindaraj,AngewChemInt Ed 2009;48(42):7752–77.
31. [30] X. Sun, Z. Liu, K. Welsher, J. Robinson, A. Goodwin, S. Zaric, et al.Nano Res 2008;1(3):203–12.
32. [31] Y.Wang, Z. Li, J.Wang, J.Li, Y.Lin. biotechnology. Trends Biotechnol 2011;29(5):205–12.
33. [32] X.Zhang, J.Yin, C.Peng, W.Hu, Z .Zhu, W.Li, et al. Carbon 2011;49(3):986–95.
34. [33] A. Mallick, A. S. Mahapatra, A. Mitra, J. M. Greneche, R. S. Ningthoujamand P. K. Chakrabarti. JOURNAL OF APPLIED PHYSICS 123, 055103 (2018)
35. [34] D.C. Marcano, D.V. Kosynkin, J.M. Berlin, A. Sinitskii, Z. Sun, A. Slesarev, L.B. Alemany, W. Lu and J.M. TourACS NANO VOL. 4, NO. 8, 4806–4814, 201
36. [35] S.Singha, G.Dutta (Pal),P.P. Bose, S. Das, M.Bardhan,B. P. Chatterjee and T.Ganguly, J NanosciNanotechnol 15,(2015) 1–11.
37. [36] G. Pal, A. Paul, S. Yadav, M. Bardhan, A. De, J. Chowdhury,A. Jana, and T. Ganguly,*J. Nanosci. Nanotechnol.*15, (2015)5775-5784.

CHAPTER 4:

ROLE OF HUMAN HEMOGLOBIN AS A MODEL PROTEIN IN STUDYING BIMOLECULAR INTERACTIONS: COMPARATIVE SPECTROSCOPIC APPROACH

Experiment 1.

ROLE OF HUMAN HEMOGLOBIN AS A MODEL PROTEIN IN STUDYING BIMOLECULAR INTERACTIONS: COMPARATIVE SPECTROSCOPIC APPROACH

4.1 Abstract

In our previous work we observed the nature of interactions of HHb with gold nanoparticles (GNP). With respect to this, a brief discussion regarding the interaction of HHb with different nanoparticles examined has been outlined in this chapter. The aim is to discuss the role of HHb as a model protein upon interaction with two different nanoparticles of two different families- gold (GNP) and carbon family (GO/RGO). Also a detailed insight regarding, nature of interaction of the same model protein with different nanomaterials can be obtained. This is because different nanomaterials have different physicochemical and electronic properties based on their structure; as such the GNP and GO/RGO are known to have varied unique properties. Thus if proper knowledge is gathered, thesematerials can be utilized in wide-range of applications. Their potential in the biological realm however cannot be fundamentally realized unless their interaction whether stable or unstable is assessed with biological macromolecules of immense physiological significance like HHb. Thus it appears that the interaction of HHb with different nanomaterials if understood properly at the nano-biointerface, it will definitely give some hints regarding their particular field of application. Keeping all these in mind the following analysis has been performed regarding interaction of HHb with members of gold nano family (GNP) and carbon family (GO). Interestingly it appears that upon interaction with GNP and GO/RGO, the overall secondary structure of HHb is mostly retained thus highlighting the potential application of GNP and GO/RGO as a drug-delivery system.

Keywords: Graphene oxide; Gold Nanoparticle, Human Hemoglobin; Model protein; Native Secondary structure; Drug-delivery system

4.2 Literature Review

Human adult hemoglobin (HHb) is an important protein of vertebrate erythrocytes. The capacity of Hb to bind oxygen is determined by the presence of a bound prosthetic group called heme and this group is responsible for the typical red color of blood. The heme group consists of a central

iron atom and an organic component, called protoporphyrin, which is composed of four pyrrole rings linked by methene bridges to form a tetrapyrrole ring. Four methyl groups, two vinyl groups, and two propionate side chains are also attached. Human Hb, present in adults, consists of four subunits: two α subunits and two β subunits. The three-dimensional structure of hemoglobin is best described as a pair of identical αβ dimers ($\alpha_1\beta_1$and $\alpha_2\beta_2$) that associate to form the hemoglobin tetramer. These αβ dimers are linked by an extensive interface, which includes, among other regions, the carboxyl terminus of each chain. The heme groups are well-separated in the tetramer with iron-iron distances ranging from 24 to 40 Å[1-9].Also, HHb with high α-helical content has three Tryptophan (Trp) residues in each αβdimer, for a total of six in the tetramer: two α14 Trp, two β15Trp, and β37Trp[10, 11].Moreover, Hb contains five Tyrosine (Tyr) residues in each dimer: αTyr 24, 42, 140 and βTyr 34, 144 [12]. HHb is not only an iron-based complex which physiologically plays extremely crucial role in binding molecular oxygen,but investigation on hemoglobin has gone beyond the interest in its physiological role as an oxygen carrier since it has been considered from all points of view an ideal model protein for investigating the properties of proteins and enzymes in general. Furthermore the binding of the oxygen molecule at the sixth coordination site of the iron ion rearranges the electrons within the iron so that the ion turns out to be smaller, permitting it to step into the plane of the porphyrin. Thus binding of small molecules to HHb may produce considerable changes in quaternary structure of the protein [13-17].

Although the relationship between the structure and function of HHb has been thoroughly studied, however the research on its interaction with other molecules is limited to a few small molecules. Interaction of HHb as one of the most important physiologically active protein with small molecules of clinical interest can give knowledge regarding HHb-mediated drug targeting. Such bimolecular interactions between proteins like HHb and small molecules might have immense biological significance since HHb serves numerous biochemical roles in electron transfer, oxygen transfer and storage and in metabolic pathways. In this respect, binding of small molecules of medical importance to HHb can cause significant changes in conformation, which may further provide interesting information regarding structure, function, and dynamic properties of HHb.

Furthermore miniaturization of structures in the form of nanoscale materials has produced a so-called nanoplatform for applied biomedical research in evolving innovative and upgraded diagnostics. Nanoparticles provide large surfaces for reactions involving biomolecules thus

suggesting a meaningful pathway to combine biomolecular functionality with unique electronic and optical attributes of nanoparticles. Small molecules like nanoparticles have also emerged as a promising strategy for the efficient delivery of drugs used in the treatment of different types of diseases because of its many advantages over classical delivery matrices. The important technological advantages of nanoparticles used as drug carriers are its high stability, high carrier capacity, feasibility of incorporation of both hydrophilic and hydrophobic substances, and feasibility of variable routes of administration, including oral application and inhalation. Nanoparticles, because of their small sizes, have well-defined characteristics compared to the bulk form of the same material[18]. It must be mentioned here that understanding the role of nanoparticles as drug or drug delivery system can be simplified, if interactions between nanoparticles and biomolecules are investigated. Knowledge of protein-nanoparticle interactions will thus be essential to comprehend how nanoparticles will function in biological environment as drug delivery systems. Such studies may also provide information to whether the nanoparticles are causing any significant changes in the structure and function of biomolecules in its biological surroundings.

Lately biomolecules like proteins conjugated with gold nanoparticles as efficient drug-delivery system have received much attention because spherical gold nanoparticles (GNP) are generally nontoxic, biosafe and biocompatible [19-23]. Moreover, in recent years detection and treatment of cancer cells with the help of GNPs has become interesting field of research [24, 25]. Furthermore, popular herbal medicine Swarnabhasma has been found to contain only micrometer and nanometer sized gold particles without any impurities [26]. The adsorption of biomolecules on nanoparticles and its outcomes on the structure and function are intensely related to the size and shape of the nanoparticles. Thus from the above information it is apparent that interactions of HHb with gold nanoparticles of different morphologies will have enormous physiological significance which can further provide innovative advancements in the developments of biosensors and biomedicines in the field of bio-nanotechnology.

Moreover a novel single-atom-thick and two-dimensional (2D) carbonnanomaterial, graphene oxide (GO), belonging to an oxidizedderivative of graphene, has attracted significant attention recentlydue to its remarkable structural, chemical, mechanicaland electronic properties, and has shown great promise fordifferent applications in many fields [27–29]. Lately, the applicationof GO has been extending to biological systems, includingbiodevices, microbial detection, disease diagnosis, anddrug delivery systems, due to its considerably large specificsurface area (two

accessible sides), its rich oxygen-containingsurface functionalities like epoxide, hydroxyl and carboxylicgroups, and its high water solubility [30, 31]. However, a key issuethat needs to be addressed before the large-scale implementationof GO in a wide range of biological applications isits less-studied biosafety and biocompatibility properties,especially when its facts such as high accumulation, longterm retention and relative long blood circulation time inorganisms are under consideration [32].

In this section it has been observed that the spectroscopic properties of HHb alter in definite manner upon interaction with either GNP, GO and RGO. Strikingly in spite of the alterations observed in the microenvironment of HHb, upon its interaction with GNP, GO and RGO, the overall secondary structure of HHb as revealed by CD spectroscopy, is however more or less retained. Thus interactions of biocompatible GNP, GO and RGO at the nano bio-interface can be widely utilized in wide-range of fields.

4.3 Materials and Methodology

4.3.1Materials

Human Hemoglobin (HHb), purchased from Sigma Aldrich, is tested before use for the presence of any impurity in the region of wavelength studied. In all the experiments freshly prepared aqueous solutions of concentration ~ 5 x 10^{-6} M (0.645 mg/ml) have been used [1, 2].

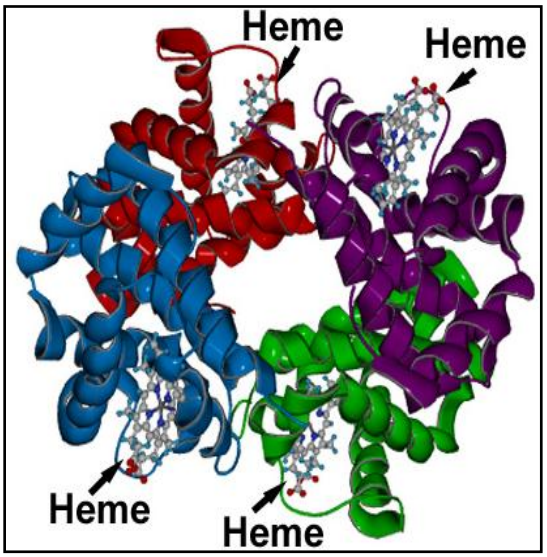

Fig 7: (Colour online) Molecular structure of HHb

4.3.2 Synthesis of GNP

10 ml of 1 mMAurium tetrachloride tri hydrate ($HAuCl_4 \cdot 3H_2O$) was prepared in deionized water and mixed with 10 ml of 1% SDS followed by the addition of 10 ml of 0.5 mM PEG. The mixture was then stirred vigorously and was heated to 90 °C. After attaining 90°C,10 ml of 38.8 mM tri-sodium citrate was quickly added to form a burgundy colored nanosphere sol. Heating with stirring was continued for another 30 minutes. Then the gold nanosphere (GNP) solution was cooled down at room temperature and stored until further use. The sizes of the GNP were estimated from high resolution Transmission Electron Micrograph (HRTEM). The sizes of GNP are of the order of 18–20 nm [1, 35 and 36].

All the reagents are purchased from Sigma Aldrich and used in the experiments without any further process of purification. Water has been double distilled and then deionized using a Millipore Milli-Q system.

4.3.3 Spectroscopic Apparatus

Dilute solutions of the HHb ($\sim 10^{-6}$ M) are taken for the following spectroscopic techniqus are performed in absence and presence of GO and RGO at the ambient temperature - UV-vis absorption spectra, steady state fluorescence emission spectra, Resonance Light Scattering (RLS) spectra, synchronous fluorescence spectra, FTIR measurements and Circular dichroism (CD) spectroscopy measurements as described elsewhere [1, 2]. Briefly UV–vis absorption and steady state fluorescence emission spectra of dilute solutions of the samples are measured in absence and presence of GO and RGO in rectangular quartz cells of 1 cm path length at the ambient temperature. UV–vis absorption spectra are scanned by using JASCO UV–Vis absorption spectrometer (Model: V-630). Steady-state fluorescence emission spectra, RLS spectra and synchronous fluorescence spectra are monitored using JASCO Spectrofluorimeter (Model: 8200). For Benesi-Hildebrand plot, and fluorescence quenching analysis for evaluation of thermodynamic parameters the molecular weight of GO is considered as 2043.856.

Fluorescence lifetimes measurements of HHb in absence and presence of GO and RGO are carried out using a time correlated single-photon-counting (TCSPC) technique with the model FLUOROLOG TCSPC HORIBA JOBIN YVON using 280 nm (NanoLED 280) as impulse for excitation in Trp/Tyr region and an emission wavelength of 330 nm. The decay kinetics, the

quality of fit with a plot of weighted residuals and other statistical parameters like reduced χ^2 and the Durbin–Watson (DW) parameters are checked for the entire decay along with the rising edge.

The Circular dichroism (CD) spectroscopy measurements are scanned using a PC driven JASCO CD spectropolarimeter (Model J-815) in the UV region (250–190 nm) at 25 °C in a rectangular quartz cell (1 mm).

The following observations are plotted and analyzed using Microcal Origin (version 8.5) software after taking original raw data directly from the instrument.

4.4 Result and Discussion

Comparative spectroscopic approach for GNP and GO

4.4.1 UV-vis absorption study

UV-vis electronic absorption spectra of HHb reveal a prominent hyperchromic effect with no spectral shift for both GNP and GO. The observations suggest the formation of ground-state complex upon interaction with GNP and GOand the change in the regions of absorbance of tryptophan and tyrosine residues is comparable. Thus GNP and GO upon interaction with HHb are altering the microenvironment of the fluorescing aromatic residues tryptophan and tyrosine in a similar manner.

4.4.2 Steady-state fluorescence spectroscopic study

In case of steady state fluorescence emission spectra of HHb the noble nanometal gold (GNP), fluorescence quenching of static type without any spectral shift is observed. Steady-state static type quenching is also noticed for HHb upon interaction with GO.

4.4.3 Time-resolved fluorescence study

Moreover the magnitudes of the τ of HHb remain nearly similar in presence of GNP and GO.

Although the structural properties of GNP and GO are quiet different yet the spectroscopic properties of HHb are not observed to alter much.

4.4.4 Speculation of thermodynamic parameters to reveal the nature of interactions between HHb-GNP and HHb-GO complex

Both ΔH and ΔS are found out to be negative and thus the predominant mode of interaction could be van der Waals interactions and hydrogen bonding (since $\Delta H < 0$ and $\Delta S < 0$) for HHb-GNP interaction. The values for ΔH and ΔS are also noticed to be negative for HHB-GO system and thus the interacting forces for HHb-GO complex could be van der Waals interactions and hydrogen bonds.

Also and rapid lowering of values of K_A with increase of temperature correspondingly suggest the presence of weaker binding forces such as van derWaals' interactions and hydrogen bonding for HHb-GO system compared to HHb-GNP.

4.4.5 Synchronous fluorescence spectroscopy

Moreover synchronous fluorescence intensity of HHb shows a decrease for the tyrosine (Δλ=15 nm) peaks with weak red shift (from 304 to 305 nm) in presence of GNP. The red shift is perhaps indicating exposure of tyrosine residues to a more hydrophilic environment in presence of GNP. However the synchronous fluorescence intensity of HHb gradually decreases without any spectral shifts for the tryptophan residues (Δλ=60 nm) upon addition of both GNP. In case of GO, synchronous fluorescence intensity of HHb gradually decreases without any spectral shifts for the tyrosine residues (Δλ=15 nm). Likewise synchronous fluorescence intensity of HHb gradually decreases without any spectral shifts for the tryptophan residues (Δλ=60 nm).

Thus GNP and GO after interacting with the same model protein (HHb) are altering the microenvironment of HHb slight differently such that the tyrosine residues are getting exposed to a more hydrophilic environment only in presence of GNP. Although the microenvironment of tryptophan and tyrosine residues are being affected in presence of GO but the polarity around the fluorescing aromatic residues are nearly remaining unaffected. These observations may be expected since GNP and GO vary in size, shape, physicochemical and photo-physical properties from each other.

4.4.6 FTIR spectroscopy study

In case of FTIR study, the intensity of the amide I band becomes broadened and a decrease in the IR absorption intensity is observed with negligible spectral shift in presence of GNP. This band is also observed to decreases with broadening of the peak but spectral shift is not observed upon interaction with GO.

4.4.7 RLS intensity

In presence of GNP, increase in RLS intensity is noticed (Fig. 10a). Since an increase in RLS intensity corresponds to increase in particle dimension of the formed aggregate in solution thus it appears that interaction with GNP may promote aggregation of HHb.

Moreover it is observed that GO may interact with HHb in solution, forming a new HHb-GO complex that could be expected to promote aggregation thus suggesting increased light scattering signal to occur under the given conditions.

Thus the interactions of GNP and GO are facilitating stable interaction of individual HHb to enhance protein aggregation.

4.4.7 Secondary structural analysis

Strikingly in spite of the alterations observed in the microenvironment of HHb, upon its interaction with GNP and GO, the overall secondary structure of HHb as revealed by CD spectroscopy, is however more or less retained.

The observations are represented in a tabular form (Table 1).

Table 1:HHb as model protein for interaction with GNP and GO

Properties	GNP	GO
UV-vis absorption	Hyperchromicity ↑	Hyperchromicity↑
Steady-state fluorescence emission	Static quenching ↓	Static quenching ↓
	No spectral shift	No spectral shift
τ	No change	No change
Synchronous fluorescence		
	Δλ=15 nm Fluorescence quenching	**Δλ=15 nm** Fluorescence quenching
	1 nm red shift	No spectral shift
	Δλ=60 nm Fluorescence quenching	**Δλ=60 nm** Fluorescence quenching
	No spectral shift	No spectral shift
Microenvironment of Tryptophan residues	No change in polarity	No change in polarity
Microenvironment of Tyrosine residues	Exposed to a more hydrophilic environment	No change in polarity
CD spectra	Overall secondary structure retained	Overall secondary structure retained
RLS signal	Increased	Increased

Comparative spectroscopic approach for GNP and RGO

4.4.8 UV-vis absorption study

UV-vis electronic absorption spectra of HHb reveal a prominent hyperchromic effect for GNP. However the UV-vis electronic absorption spectra of HHb reveal a weak yet noticeable hypochromic effect for RGO. The observations suggest the formation of ground-state complex

upon interaction with both GNP and RGO. Thus GNP and RGO upon interaction with HHb are altering the microenvironment of the fluorescing aromatic residues tryptophan and tyrosine in a different manner.

4.4.9 Steady-state fluorescence spectroscopic study

In case of steady state fluorescence emission spectra of HHb the noble nanometal gold (GNP), fluorescence quenching of static type without any spectral shift is observed. Surprisingly steady-state fluorescence enhancement is noted for HHb upon interaction with RGO. Here also the changes in steady-state fluorescence intensity occur differently. The observations are interesting since comparison for GNP and GO shows similar pattern of static type of quenching whereas for GNP and RGO the observations reveal static type quenching and fluorescence enhancement.

4.4.10 Time-resolved fluorescence study

However the magnitudes of the τ of HHb remain nearly similar in presence of GNP and RGO.

4.4.11 Synchronous fluorescence spectroscopy

Moreover synchronous fluorescence intensity of HHb shows a decrease for the tyrosine ($\Delta\lambda$=15 nm) peaks with weak red shift (from 304 to 305 nm) in presence of GNP. The red shift is perhaps indicating exposure of tyrosine residues to a more hydrophilic environment in presence of GNP. However the synchronous fluorescence intensity of HHb gradually decreases without any spectral shifts for the tryptophan residues ($\Delta\lambda$=60 nm) upon addition of both GNP. In case of RGO, synchronous fluorescence intensity of HHb do not show any significant change for both tyrosine residues ($\Delta\lambda$=15 nm) andtryptophan residues ($\Delta\lambda$=60 nm).

Thus GNP and RGO after interacting with the same model protein (HHb) are altering the microenvironment of HHb differently such that the tyrosine residues are getting exposed to a more hydrophilic environment only in presence of GNP. However the microenvironment of tryptophan and tyrosine residues nearly remain affected in presence of RGO. These observations may be expected since GNP and RGO vary in size, shape, physicochemical and photo-physical properties from each other.

4.4.12 FTIR spectroscopy study

In case of FTIR study, the intensity of the amide I band becomes broadened and a decrease in the IR absorption intensity is observed with negligible spectral shift in presence of GNP. However this band nearly remains unchanged upon interaction with RGO.

4.4.13 RLS intensity

In presence of GNP, increase in RLS intensity is noticed (Fig. 10a). Since an increase in RLS intensity corresponds to increase in particle dimension of the formed aggregate in solution thus it appears that interaction with GNP may promote aggregation of HHb.

Interestingly decrease in RLS signal of HHb is observed upon gradual addition of RGO. Since the RLS intensity is dominated primarily by the particle dimension of the formed aggregate in solution, the observations suggest that no such aggregation effect has occurred. This may be expected since hydrogen bond formation involving polypeptide backbone is observed to get compromised upon interaction with RGO.

Thus the interactions with GNP are facilitating stable interaction of individual HHb to enhance protein aggregation. However there is no such aggregation effect the in presence of RGO.

4.4.14 Secondary structural analysis

Strikingly in spite of the alterations observed in the microenvironment of HHb, upon its interaction with GNP and RGO, the overall secondary structure of HHb as revealed by CD spectroscopy, is however more or less retained.

The observations are represented in a tabular form (Table 2).

Table 2:HHb as model protein for interaction with GNP and RGO

Properties	GNP	RGO
UV-vis absorption	Hyperchromicity ↑	Hypochromicity ↓
Steady-state fluorescence emission	Static quenching ↓	Fluorescence enhancement ↑
	No spectral shift	No spectral shift
τ	No change	No change
Synchronous fluorescence		
	Δλ=15 nm Fluorescence quenching	**Δλ=15 nm** No change
	1 nm red shift	No spectral shift
	Δλ=60 nm Fluorescence quenching	**Δλ=60 nm** No change
	No spectral shift	No spectral shift
Microenvironment of Tryptophan residues	No change in polarity	No change in polarity
Microenvironment of Tyrosine residues	Exposed to a more hydrophilic environment	No change in polarity
CD spectra	Overall secondary structure retained	Overall secondary structure retained
RLS signal	Increased	Decreased

4.5 Conclusion

Thus interactions of these biocompatible particles at the nano bio-interface can be widely utilized in wide-range of fields. Whether the GNP and GO can be used as an efficient drug-delivery system, biosensor or bioimaging and other biological fields will then depend on their properties and their nature of interactions. Moreover the observations further indicate that although GNP and GO being from distinct family interact with HHb in comparatively similar manner, however RGO interacts with HHb in a different manner compared to GNP. Thus it becomes apparent that different nanomaterials can affect the spectroscopic properties of the same biomolecule HHb in their own way. All in all the systematic efforts have revealed the role of HHb as a model protein in bimolecular interaction (Table 1 and Table 2) suggesting the potential application of HHb as a model protein. Knowledge regarding the potential applications of different nanomaterials can be obtained by monitoring the nature of interactions between them.

Reference

[1] M.Chakraborty, S.Paul, I.Mitra, M.Bardhan, M. Bose, A. Saha, T. Ganguly, Journal of Photochemistry & Photobiology, B: Biology.178 (2018) 355–366.

[2] M. Chakraborty, I. Mitra, K. Sarkar,M.Bardhan, S. Paul, S.Basu,A.Goswami, A.Saha, B. Show, T.Ganguly. SpectrochimicaActa Part A: Molecular and Biomolecular Spectroscopy 215 (2019) 313–326.

[3] A.K. Bordbar, A.A. Mooasavi-Movahedi, Bull. Chem.Soc. Jpn. 69 (8) (1996) 2231–2234.

[4] A.K. Bordbar, A. Nasehzadeh, D. Ajloo, K. Omidiyan, H. Naghibi, M. Mehrabi, H.Khajehpour, M. Rezaei-Tavirani, A.A. Moosavi-Movahedi, Bull.Kor. Chem. Soc. 23 (8) (2002) 1073–1077.

[5] C.W. Liu, A. L Bo, G.J. Cheng, X.Q. Lin, S.J. Dong, Biochim. Biophys.Acta 1385 (1998) 53–60.

[6] S. De, A. Girigoswami, J. Colloid Interf. Sci. 296(2006) 324–331.

[7] Y. Cheng, H.K. Lin, D.P. Xue, R.C. Li, K. Wang, Biochim. Biophys.Acta 1535 (1) (2001) 200–216.

[8] S. Sil, M. Kar, A.S. Chakraborti, J. Photochem.Photobiol. B Biol. 41 (1997) 67–72.

[9] X.-C. Shen, X.-Y.Liou, L.-P.Ye, H. Liang, Z.-Y. Wang, J. ColloidInterf. Sci. 311 (2007) 400–406.

[10] S. Venkateshrao, P.T. Manoharan, *Spectrochim. Acta Part A*60 (2004) 2523–2526.

[11] R.A. Goldbeck, R.M. Esquerra, D.S. Kliger, *J. Am. Chem. Soc*.124 (2002) 7646–7647.

[12] T.C. Mueser, P.H. Rogers, A. Arnone, *Biochemistry* 39(2000) 15353–15364.

[13] M.F. Perutz, A.J. Wilkinson, M. Paoli, and G.G. Dodson,*Annu. Rev. Biophys. Biomol.Struct.*27(1998) 1-34.

[14] G.K. Ackers,*Adv. Protein Chem.*51(1998) 185-253.

[15] G.K. Ackers, M.L. Doyle, D. Myers, and M.A. Daugherty, *Science*255 (1992) 54-63.

[16] G. Fermi, M.F. Perutz, B. Shaanan, and R. Fourme,*J. Mol. Biol.* 175 (1984) 159-174.

[17] J.V. Kilmartin and L. Rossi-Bernardi*Physiol. Rev.* 53 (1973) 836-890.

[18] W. Shang, J. H. Nuffer, V. A. Muniz-Papandrea, W. Colon, R. W. Siegel,and J. S. Dordick, *Small*5(2009) 470-476.

[19] G. Pal, A. Paul, S.Yadav, M.Bardhan, A. De, J.Chowdhury, A. Jana, T.Ganguly,*J NanosciNanotechnol*. 15 (2015) 5775-5784

[20] S. Eustis and M. A. El-Sayed,*Chem. Soc. Rev.* 35 (2006) 209-217

[21] C. M. Cobley, J. Chen, E. C. Cho, L. V. Wang, and Y. Xia,*Chem.Soc. Rev.* 40 (2011) 44-56

[22] T. Ming, X. S. Kou, H. J. Chen, T. Wang, H. L. Tam, K. W. Cheah,J. Y. Chen, and J. F. Wang,*Angew Chem. Int Ed.* 47 (2008) 9685-90

[23] C. Li, F. Fan, B. Yin, L. Chen, T. Ganguly, and Z. Q. Tian,*NanoResearch*6(2013) 29-37.

[24] K. S. Soppimath and G. Betageri, John Wiley &SonsInc, New York (2008).

[25] Y. Pellequer and A. Lamprecht, Pan Stanford PublishingPte. Ltd., Singapore, (2009), p. 93.

[26] U. K. Sur, G. Mandal, and T. Ganguly, *Nanosci. Nanotechnol. An Indian Jour.* 6 (2012) 104-107

[27] Y. Zhu, S. Murali, W. Cai, X. Li, J.W. Suk, J.R. Potts, et al. Adv Mater 2010;22(35):3906–24.

[28] O.C. Compton, S.T. Nguyen, Small 2010;6(6):711–23.

[29] C.N.R. Rao, A.K. Sood, K.S. Subrahmanyam, A. Govindaraj,AngewChemInt Ed 2009;48(42):7752–77.

[30] X. Sun, Z. Liu, K. Welsher, J. Robinson, A. Goodwin, S. Zaric, et al.Nano Res 2008;1(3):203–12.

[31] Y.Wang, Z. Li, J.Wang, J.Li, Y.Lin. biotechnology. Trends Biotechnol 2011;29(5):205–12.

[32] X.Zhang, J.Yin, C.Peng, W.Hu, Z .Zhu, W.Li, et al. Carbon 2011;49(3):986–95.

[33] A. Mallick, A. S. Mahapatra, A. Mitra, J. M. Greneche, R. S. Ningthoujamand P. K. Chakrabarti. JOURNAL OF APPLIED PHYSICS 123, 055103 (2018)

[34] D.C. Marcano, D.V. Kosynkin, J.M. Berlin, A. Sinitskii, Z. Sun, A. Slesarev, L.B. Alemany, W. Lu and J.M. TourACS NANO VOL. 4, NO. 8, 4806–4814, 201

[35] S.Singha, G.Dutta (Pal),P.P. Bose, S. Das, M.Bardhan,B. P. Chatterjee and T.Ganguly, J NanosciNanotechnol 15,(2015) 1–11.

[36] G. Pal, A. Paul, S. Yadav, M. Bardhan, A. De, J. Chowdhury,A. Jana, and T. Ganguly,*J. Nanosci. Nanotechnol.*15, (2015)5775-5784

CHAPTER 5:

Experiment 2- Synthesis, characterization, wound healing study of green synthesized silver nanoparticle

5.1 Literature Review

5.2 Proposed plan of Work

5.3 Sample collection

5.4 Extract preparation

5.5 Phytochemical Analysis

5.6 Characterisation of green synthesized silver nanoparticles

5.7 Ointment preparation

5.8 Wound creation and treatment protocol

5.9 Result and Discussion

5.1 Literature Review

Durva Grass or *Cynodondactylon*

The "durva"or *Cynodondactylon* is a perennial grass member of the family Poaceae or Graminae (the largest of the Angiosperms). This grass, also known as the "Bermuda grass" is presumed to have its origin at the Africa. It has a world-wide distribution and grows almost ubiquitously in the Indian peninsula. Warm climates in this region promotes rapid and robust growth of the grass and generally reproduces by both sexual and asexual means. Propagation by rhizomes are also very common [1].

The scientific classification is being provided below:

Kingdom:	Plantae
***Clade*:**	Angiosperms
***Clade*:**	Monocots
***Clade*:**	Commelinids
Order:	Poales
Family:	Poaceae
Genus:	*Cynodon*
Species:	*C. dactylon*

Table 1:- Details of *Cynodondactylon*(L.) Pers.

Fig. 17: Picture of *Cynodondactylon*(L.) Pers.

The complete binomial nomenclature is: ***Cynodondactylon*(L.) Pers.**

Apart from its cultural uses in India, the durva grass has an array of medicinal utilities and has been used in Ayurvedic medicine since time immemorial. Till today, fresh durva is used to heal minor cuts and wounds or warts in the tradition Indian system of medicine. It has also been used to ameliorate gastro-intestinal irritation, nausea, common cold etc.

Several research articles report the presence of important plant metabolites like beta-sitosterol, alkaloids, flavonoids etc. in considerable amounts which indicates its medicinal potential.

5.2 Proposed plan of Work

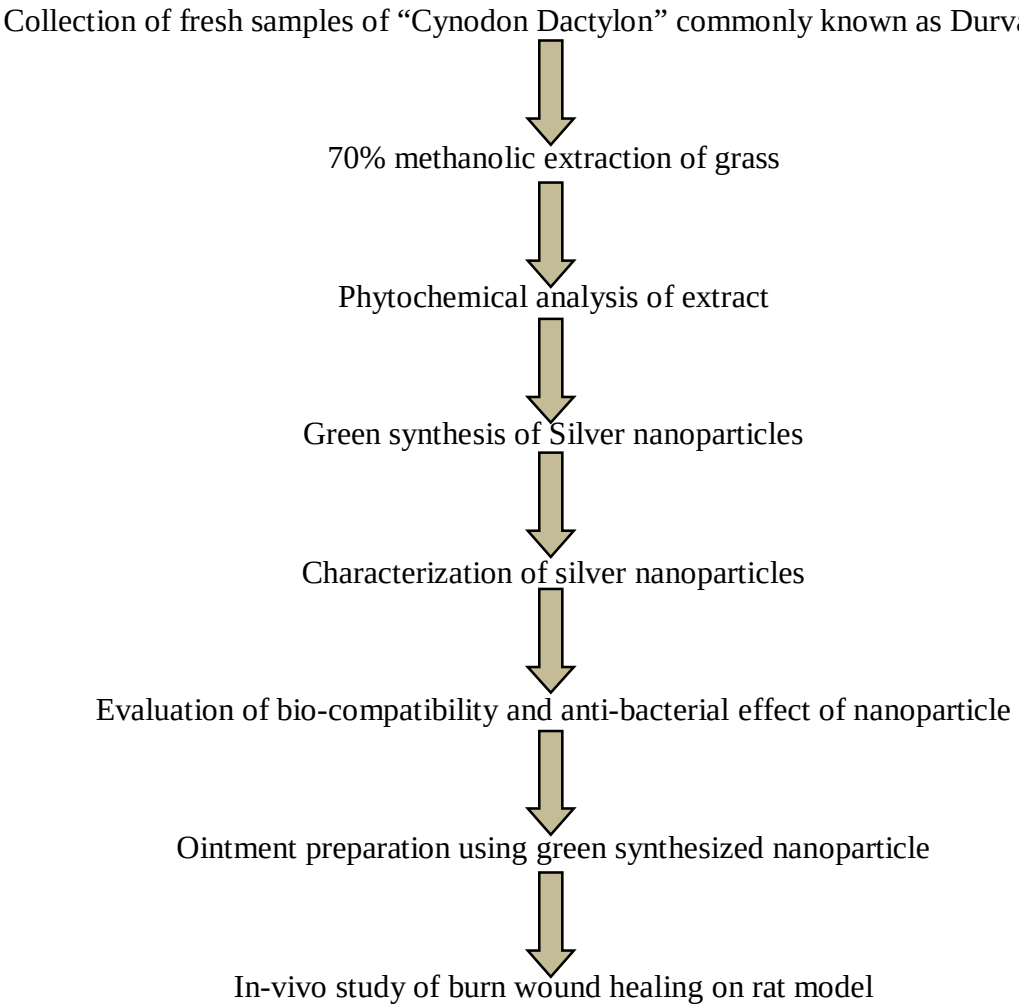

Grass Extract Preparation and investigating its different Biological activity.

5.3 Sample collection:

Fresh green sample of grass was collected from the field of Jadavpur University and washed thoroughly with distilled water. Unwanted impurities were removed by hand picking. Washed samples were shade dried for 24 hours.

5.4 Extract Preparation:

Shade dried sample if grass was taken and 15gm of it was weighed in balance. It was then added to 100 ml (70% ethanol) solution and was kept in an undisturbed place for 3-4 days for maceration. After 4 days the sample was filtered using a glass funnel and filter paper to obtain the final extract solution [2].

- **Nanoparticle preparation method**

The Silver Nitrate ($AgNO_3$) was purchased from Merck (Mumbai, India) and a 20mM stock was made from it in 50mL distilled water. Different concentrations of 0.5, 1, 2.5, 5, 7.5 mM concentration was made and mixed with extract of Cynodon dactylon to make 10ml mixture. The mixtures were then heated and mixed on a magnetic stirrer until the desired redish brown colour is obtained. Similar concentrations were made and exposed to bright sunlight for 5 minutes. Similarly time dependent studies were done at 2.5 mM concentrations of silver nitrate and extract mixture. The mixtures were exposed to bright sun light for 1, 2, 3, 4 and 5 minutes.

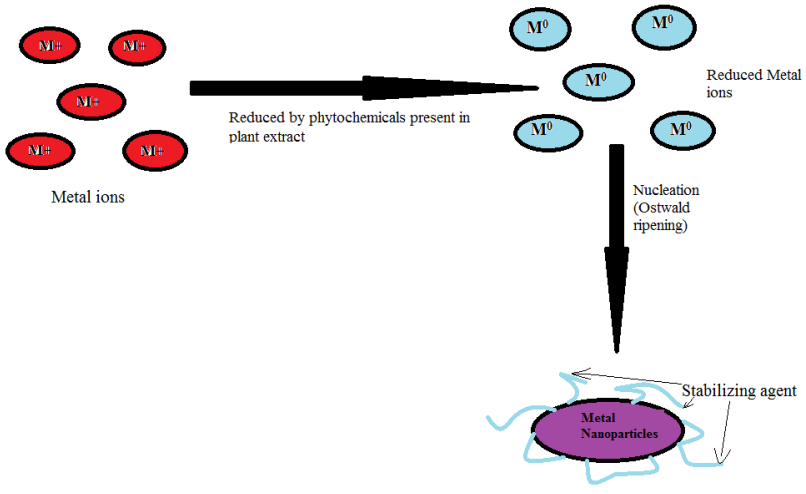

Fig. 18: Diagram to represent Nanoparticle formation by green synthesis method.

5.5 Phytochemical Analysis:

Phytochemical analysis was performed to determine the presence of Phenols, Tannin, Falvonoids, Saponin, Phlobatannins, Alkaloids, Reducing sugars were done following standard protocols [2].

- **Qualitative Analysis of Phytochemicals**

Phenols

A few drops of 5% ferric chloride (FeCl3) solution was added to 2ml of plant extract. The presence of phenols is confirmed by appearance of blue, greenish blue, green or violet color [3].

Flavonoids

In 1ml plant extract 1.5 ml of dilute ammonia was added, followed by addition of 0.5ml concentrated Sulphuric acid (H2SO4). Yellow coloration in the extract confirms the presence of flavonoids [3].

Tannins

A few drops of 10% ferric chloride (FeCl3) solution was added to the extract resulting in blue or green colour, thus indicating the presence of tannins [4].

Phlobatannins

Red precipitate formation confirms presence of phlobatannins when the plant extract was boiled with 1% aqueous hydrochloric acid (HCl) [5].

Saponin

The plant extract was boiled and then filtered. 5ml of the filtrate was then added to 10ml of distilled water in a test tube. The mixture was then shaken well for 30 seconds and observer for frothing, thus confirming presence of saponins [6].

Alkaloids

2ml of hexane was added to 0.1gm of plant sample and shaken well followed by filtration. The filtrate was then mixed with 2ml 2% hydrochloric acid (HCl). This solution was then heated for

some time and filtered. A few drops of picric acid was added to the filtrate solution to form yellow precipitate. This indicates the presence of alkaloids [6, 7].

Reducing Sugar

1ml of Fehling's A and Fehling's B was taken in a test tube and boiled. The boiled mixture was then added to the plant extract and change in colour was noticed. This confirms the fresence of reducing sugars [8].

5.6 Characterisation of green synthesised silver nanoparticle

- **UV-Vis spectra study:**

UV visible spectrum study (Carry 60 UV-Vis, Agilent Technologies) was carried out for the reaction mixture against distilled water as a blank. The spectrum analysis was performed at a resolution from 200 nm to 800 nm.

- **FTIR study:**

The sample was prepared with KBr (Purchased from Merck, Mumbai, India). Thin pellet of sample was made by hydraulic Pellet Press and proceed to FTIR study (PerkinElmer spectrometer, with range of 4000-400 cm-1 at a resolution of 4cm-1).

- **SEM study:**

FE scanning electron microscope (FE-SEM) study was done using JEOL JSM 6700-F machine. Very little amount of sample dropped on a carbon coated copper grid and the extra solution was removed. Thin film of the sample was dried and subjected to analysis.

- **Hemocompatibility test:**

Fresh human blood was used for Hemolysis study of the nanoparticle and estimates its Hemocompatibility. 2mL of fresh human blood was collected in a EDTA tube and was diluted using 2.5mL normal saline solution. A standard sample was made using 10ml normal saline and kept in an incubator for 30 minutes at 37□C. Then 0.2mL of diluted blood was added to that incubated saline water and mixed well gently and again incubated for 60 minutes. For making positive control 0.2mL of diluted blood was taken in 10mLof 0.1% sodium carbonate solution. Similarly for negative control 0.2mL of blood was diluted in 10mL of normal saline solution and

incubated at 37□C for 60 minutes. The nanoparticle sample was also incubated at 37□C for 60 minutes. After 60 minutes of incubation the test tubes were centrifuged at 4000 rpm for 5 minutes. The supernatant was carefully removed and its optical density was measured at 545nm wavelength and percentage hemolysis was calculated [9].

Percentage hemolysis is a calculation based on the average of three replicates.

$$\%Hemolysis = \frac{OD\ test - OD\ negative\ control}{OD\ positive\ control - OD\ negative\ control} \times 100$$

1. Highly hemocompatible (<5% hemolysis)

2. Hemocompatible (within 10% hemolysis)

3. Non Hemocompatible (>20% hemolysis)

- **Antimicrobial Activity**

The nanoparticle was tested for antimicrobial activity by well diffusion method using S. aureus (gram positive) and E. coli (Gram negative) strains.

For well diffusion method a few drops of bacteria culture was mixed with the semi cold liquid agar solution and casted in petri dishes. After the agar solution has cooled down and solidified then 4 wells are made on each of these petri dishes. In each of these plates one well is filled by 70% methanol, another with an antibiotic (streptomycin) and the rest two wells are filled with different concentrations of nanoparticles. After this the plates were incubated at 37□C overnight and the inhibition zones were measured the next day.

5.7 Ointment preparation:

Materials required: Beeswax (Loba Chemie Pvt. Ltd., CAS number: 8012-89-3), Edible olive oil certified by FSSAI.

The beeswax was used as the base material for the ointment. The beeswax was collected in glass beaker and placed in water bath at 65□C until the wax melts. After the wax has melted olive oil was added to it in 1:2 ratio by weight and mixed well. After the mixture was made 0.2% by weight of silver nanoparticle was added to the mixture [10].

Skin irritation test:

Two groups of 3 Healthy Wistar female rats were grouped in 2 separate cages and marked A and B respectively. The dorsal hair was removed from both sides of the back and ointment was applied on one side, while the other side was kept clean as control. Group A was given the ointment base and group B was given the silver nanoparticle mixed ointment. Ointments were applied daily for 5 days and dermal toxicity was checked. Observation was done to check for occurrence of any edema or erythema because of the application of the ointments.

Wound healing activity:

Experimental animals: Healthy Wistar female rats weighing between 120-150 gm were used for this study. Acclimatization of the animals was done to the laboratory conditions for3-4 days before starting the experiment. The rats were housed in cages made of polypropylene and wielded in standard laboratory conditions of 12 hrs of light–dark cycle and 20-24□C temperature. Standard diet was provided with water and ad-libitum throughout the tenure of the experiment.

5.8 Wound creation and treatment protocol:

Materials required: Ketamine, formaldehyde, diethyl ether, surgical tape.

Instruments required: Surgical blade No. 10, forceps, scissors, steel plate.

The dorsal hair of rat was removed and the area is cleaned with 70% ethanol. The animals were divided into 4 groups comprising of 3 rats in each group and named A, B, C and D respectively. Group A is the control where no wound is done on the animals. Group B is the challenged group where burn wound is created and left for self recovery. Group D is treated with sample ointment made in our laboratory. Group C is treated with Silverex Ointment [11].

Burn wound model: A heated steel plate was touched with the skin of the rat and hold there for 5 sec creating 1st degree burn wound on the back of the rat. After that the test ointment was applied on group D rats and silverex ointment was applied on group C rats. The ointments were applied continiusly on the rats for the next 5 days.

On the 7th day the tissue from the burnt area was collected and fixed in formalin. Histopathological test was done using H and E staining to determine the healing property of the synthesised nanoparticle.

5.9 Result and discussion:

- **Phytochemical Analysis:**

The result of phytochemical analysis of the extract of Cynodon Dactylon is given by the following table. In the results it was found that there is major presence of phytochemicals including flavonoids, tannins, saponins and phenolic compounds.

Serial no.	Phytochemicals	Results
1	Flavonoids	+
2	Saponins	+
3	Phenolic compounds	+
4	Tannins	+
5	Probatanins	-
6	Reducing Sugars	+
7	Alkaloids	+

Table 2:- Details of Phytochemical study

- **Visual examination:**

Leaf extract of Cynodon Dactylon was mixed with Silver Nitrate solution. Then the initial greenish yellow color changed to dark brown color within 15 minutes. The visual colour change indicated the green synthesis of silver nanoparticles (Figure1).

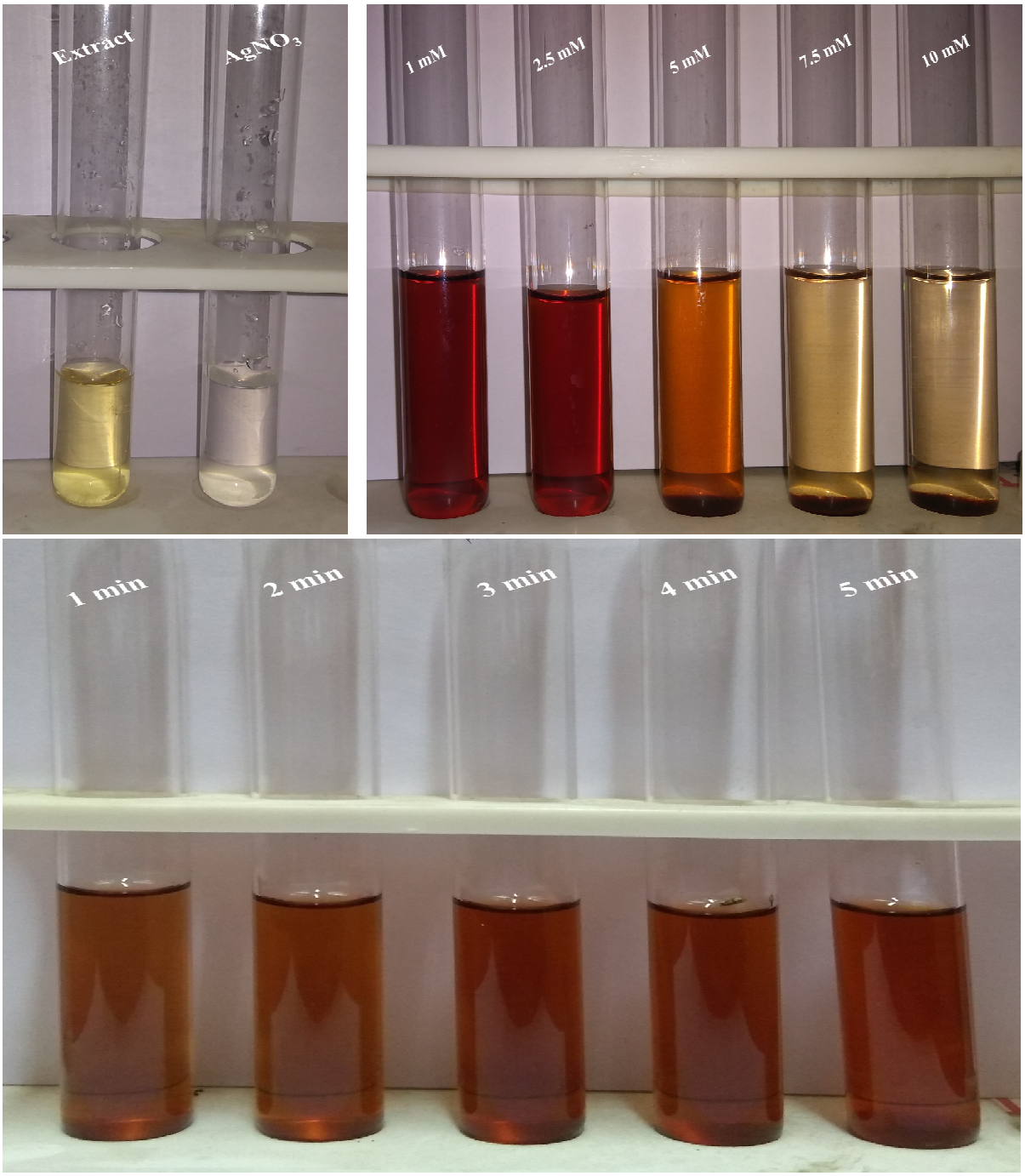

Fig. 19: Visual observation of colour change before (A) and after (B) the reduction process of silver ions to silver nanoparticles using green synthesizing method

❖ **UV-Vis spectrum analysis:**

Reduction of silver ions was ensured by UV Vis spectrum analysis and characteristics absorption peak was seen at 434 nm. The spectrum of synthesized silver nanoparticles was given in Figure 2.

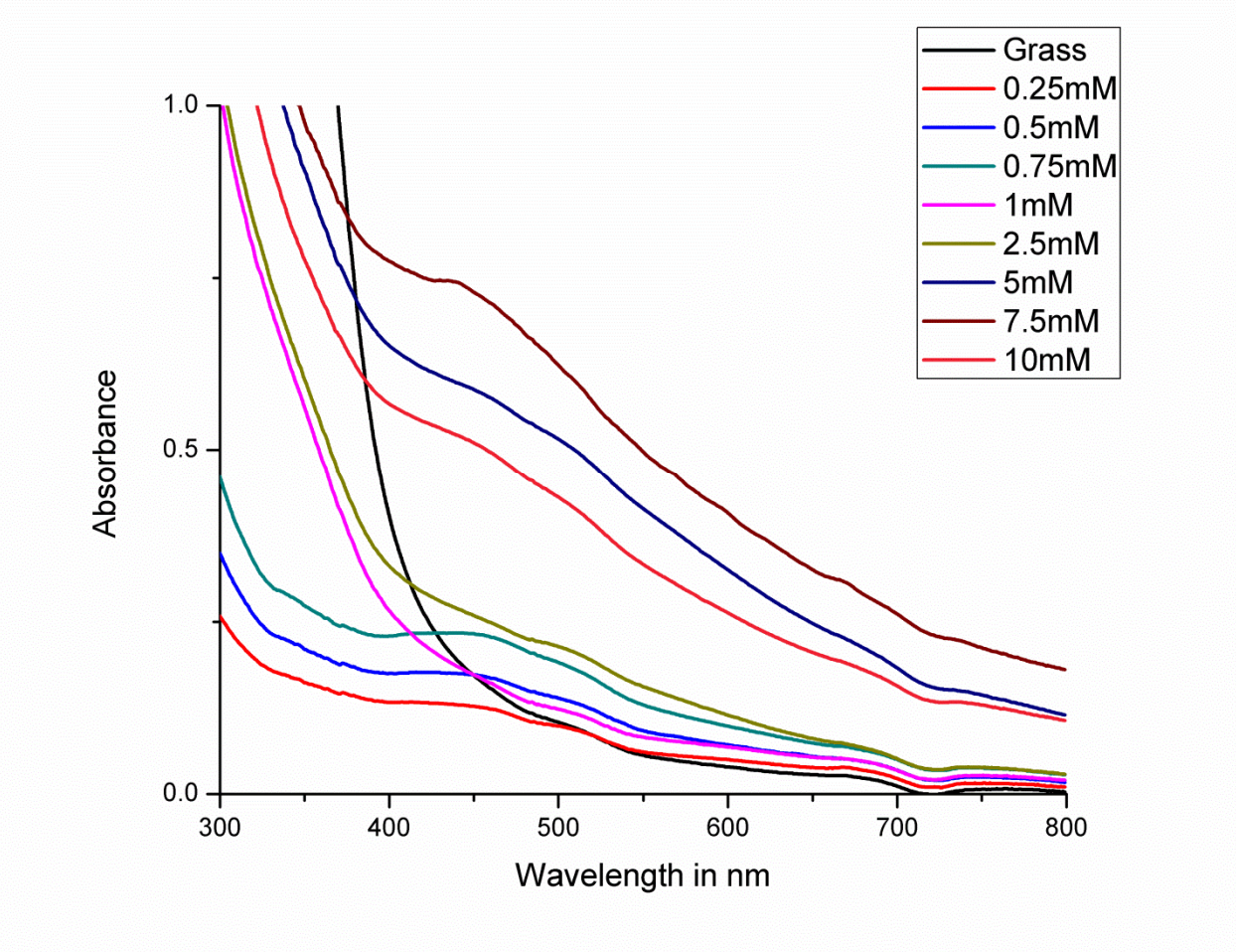

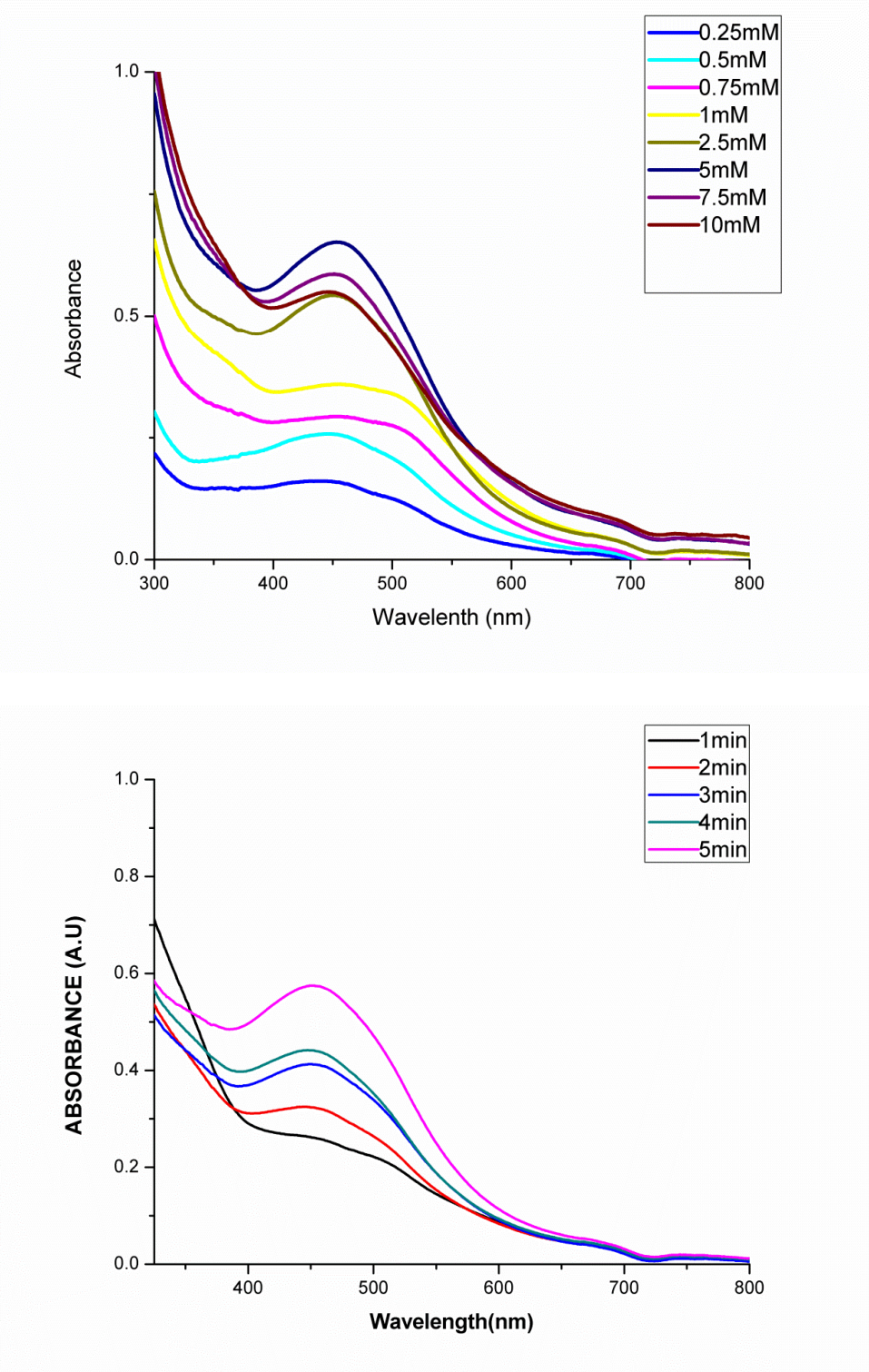

Fig. 20: Absorption spectra of UV Vis spectrophotometric analysis of silver nanoparticle synthesization from top A)based on heat prepared, B) Sunlight synthesized, C) Sunlight synthesized based on concentration.

❖ **FTIR Analysis:**

The FTIR analysis shows bands were found at 3600, 3089, 2368, 1655, 1542, 1124 and 1036 cm^{-1} . This indicates the presence of phenols, alkanes, nitro compounds, carboxylic acid groups, esters and alcohols. Thus the FTIR analysis confirmed that bioreduction of silver ions (Ag^{+}) to silver nanoparticles (Ag^{0}) reduction are caused by the above mentioned capping material present in the plant extract.

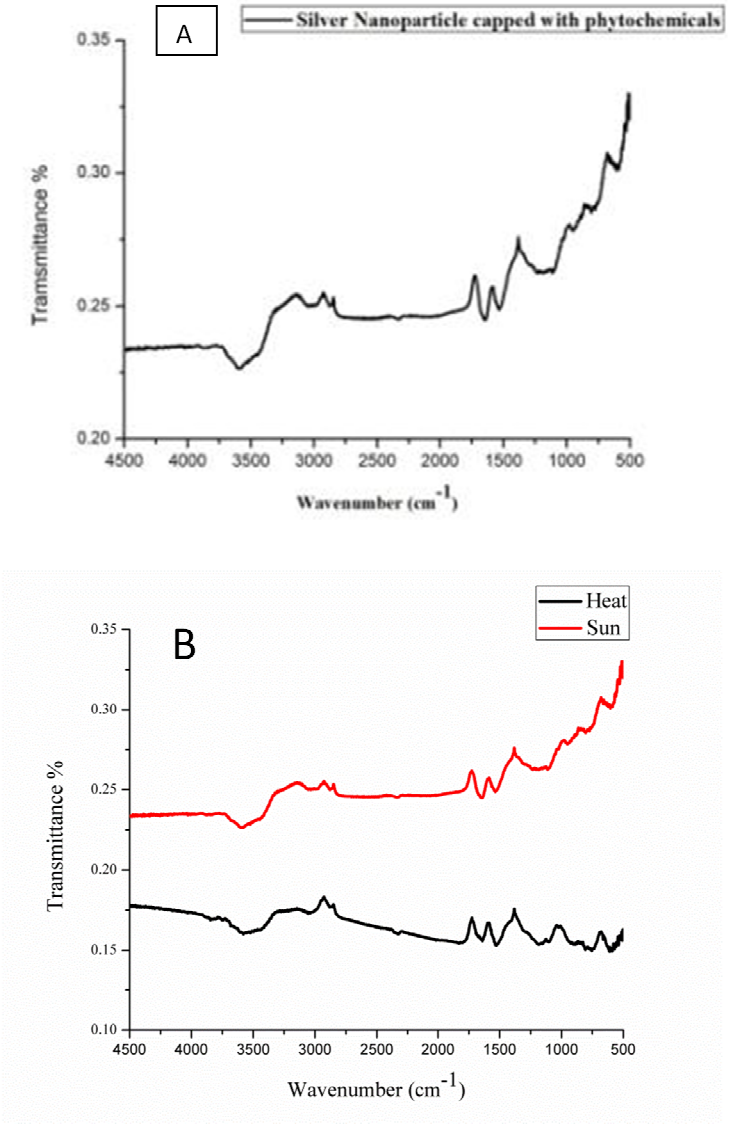

Fig. 21: FTIR spectra of A)Green synthesized silver nanoparticle using Cynodon Dactylon leaf extract. B) Represents FTIR of Green synthesized silver nanoparticle prepared by two means, application of heat and Sunlight.

❖ **SEM Analysis:**

The Scanning Electron Microscope image analysis provides information regarding morphological phenomena of the synthesized nanoparticles. SEM images of green synthesized silver nanoparticle were shown in Figure4. The SEM image of silver nanoparticle was aggregated with diameter range 30-70 nm. SEM images confirmed the almost spherical shape of the nanoparticles.

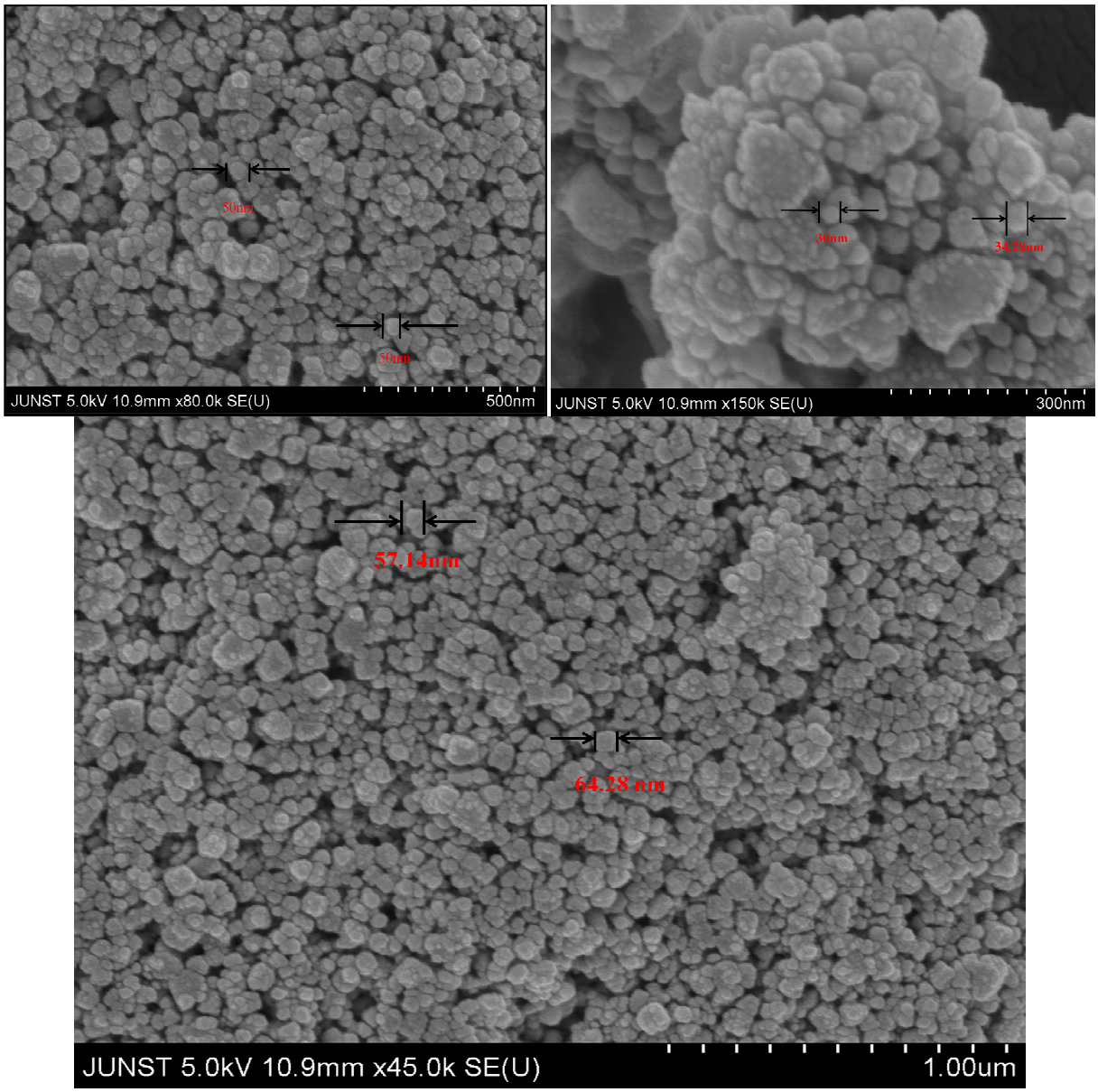

Figure 22: Scanning electron microscopic image of synthesized silver nanoparticle in colloidal condition at different nanometer scale

❖ **Antimicrobial activity analysis:**

Green synthesis silver nanoparticles were subjected to exhibit antimicrobial properties against clinical pathogenic bacteria, (A) Escherichia coli and (B) Staphylococcus aureus. In Figure 5 the synthesized nanoparticles showed the antimicrobial activity of the mentioned pathogens and were found sensitive against them.

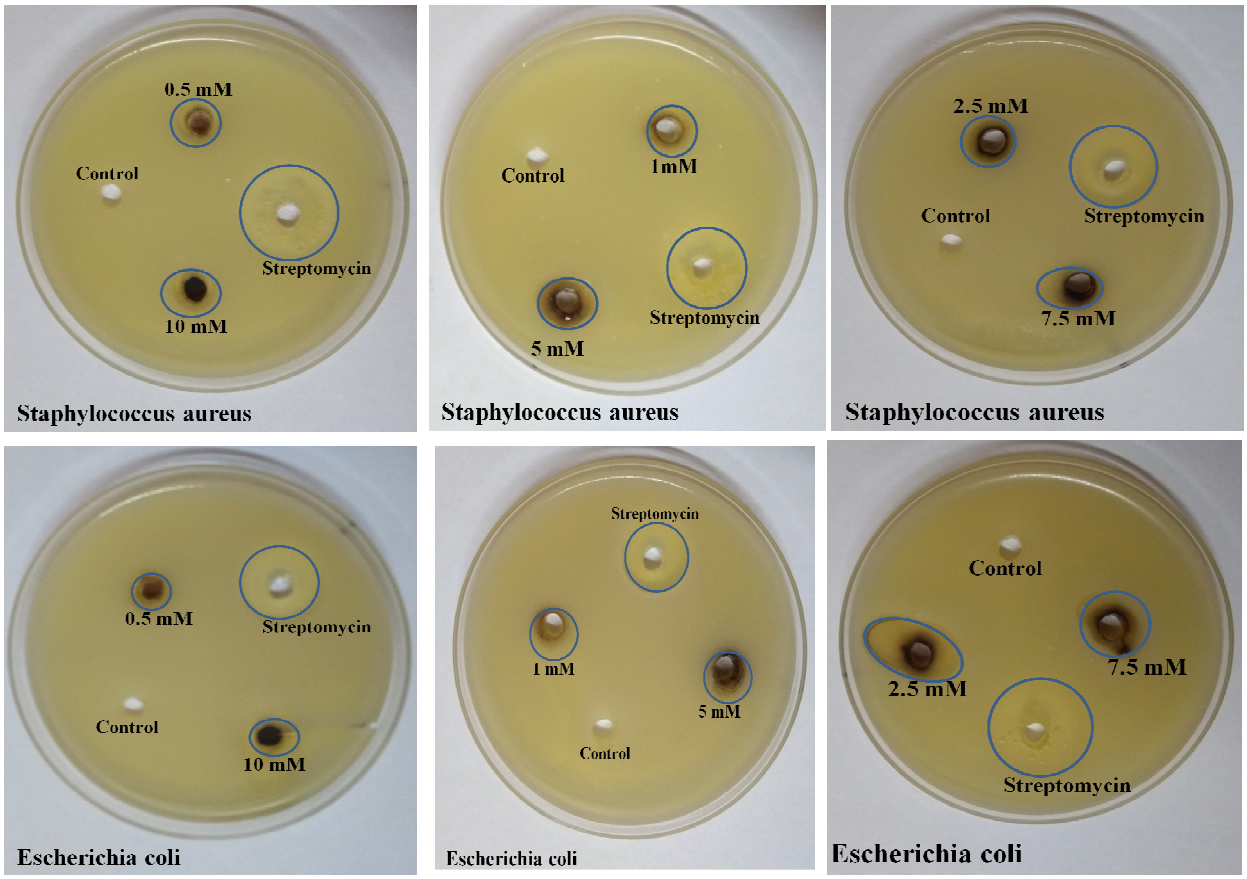

Fig. 23: Antimicrobial study of silver nanoparticles on S. aureeus and E.coli

Sl No.	Inhibition zone	Inhibition zone	Inhibition zone	Inhibition zone	Inhibition zone
	Concentrations	Antibiotic	Staphylococcus aureus	Antibiotic	Eshericha Coli
1	0.5 mM	1.27 cm	0.49 cm	0.85 cm	0.42 cm
2	1 mM	0.85 cm	0.56 cm	0.85 cm	0.56 cm
3	2.5 mM	0.78 cm	0.49 cm	1.3 cm	0.74 cm
4	5 mM	0.85 cm	0.6 cm	0.85 cm	0.71 cm
5	7.5 mM	0.78 cm	0.53 cm	1.3 cm	0.63 cm
6	10 mM	1.27 cm	0.49 cm	0.85 cm	0.49 cm

Table 3:- Inhibition Zones created by different concentrations of the Nanoparticles

Antimicrobial efficiency of green synthesized reported in this study was still remains to expurgate the accurate effect of the nanoparticle on essential cellular mechanism like DNA, RNA and protein synthesis.

- **Hemocompatibility test**

It is known that silver nanoparticle is toxic in nature but by controlling the concentration of the nanoparticle it can be used as a drug. The results of hemolysis test are given in the table below.

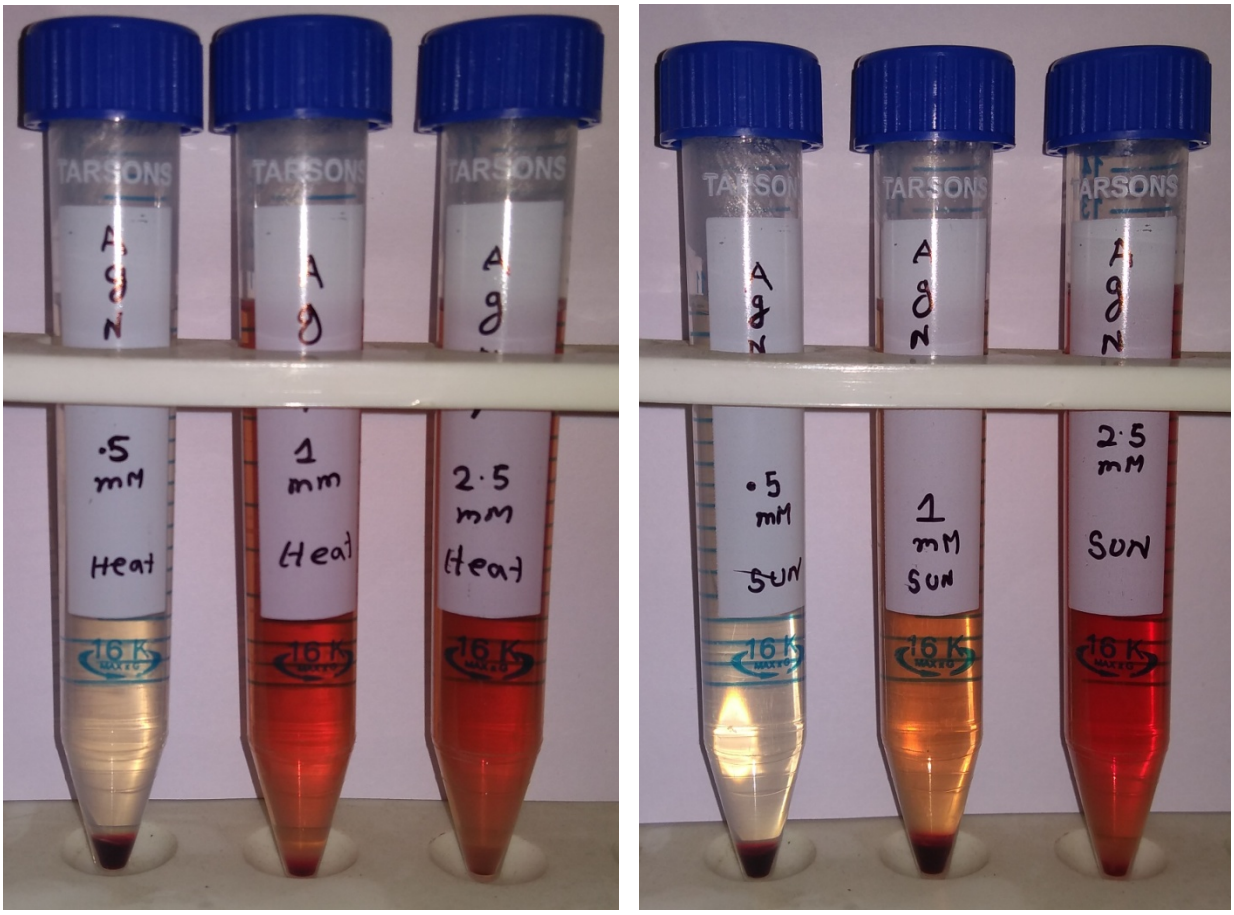

Fig. 24: Results of hemolysis test

Concentrations (mM)	% Hemolysis of heat prepared nanoparticles	% Hemolysis of sunlight exposure prepared nanoparticles
0.5	7.77	6.26
1	74.45	37.21
2.5	78.19	120.3106

Table 4:- Results of hemolysis test

The results show that 0.5mM concentration of silver nanoparticle is hemocompatible as it's hemolysis percentage lies between 5-10% as per standard norms for any means of preparation. It was found that 1mM and 2.5mM concentrations of silver nanoparticles had very high hemolysis percentage and so are not hemocompatible. It was also found that nanoparticles prepared by sunlight exposure method had better hemocompatibility than that of heat prepared nanoparticles.

- **In-vivo Study**

After 5 days of applying medicine regularly it was found that group A has shown normal growth and hair regeneration. Group B was not treated with any medicine and shows hair growth in the surrounding region of the wound and the wound has shown self recovery but no hair growth is seen in the wound. Group C was treated with silverex ointment and shows healing properties and hair regeneration in wounded region. Group D was treated with lab sample and also shows healing and very small hair regeneration.

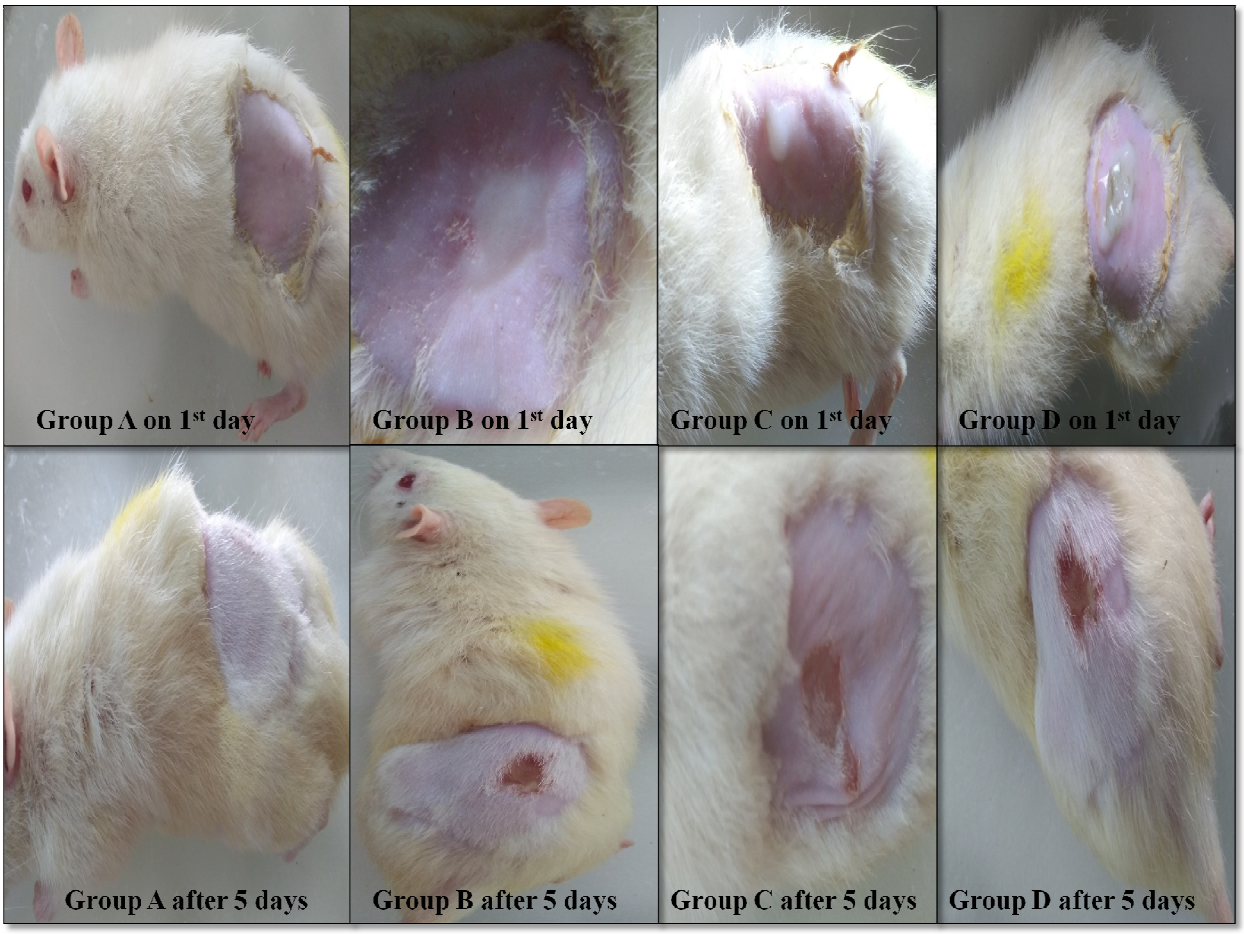

Fig. 25: Pictures of Animal study

❖ **Histopathology testing**

It was found that the cell growth for group B or the untreated group is very less. The cell growth results for both group C and group D rats were found very good and almost as good as the healthy rat tissue. The tissue growth for group D shows many cells, fibroblasts and collagen formation like the healthy tissue.

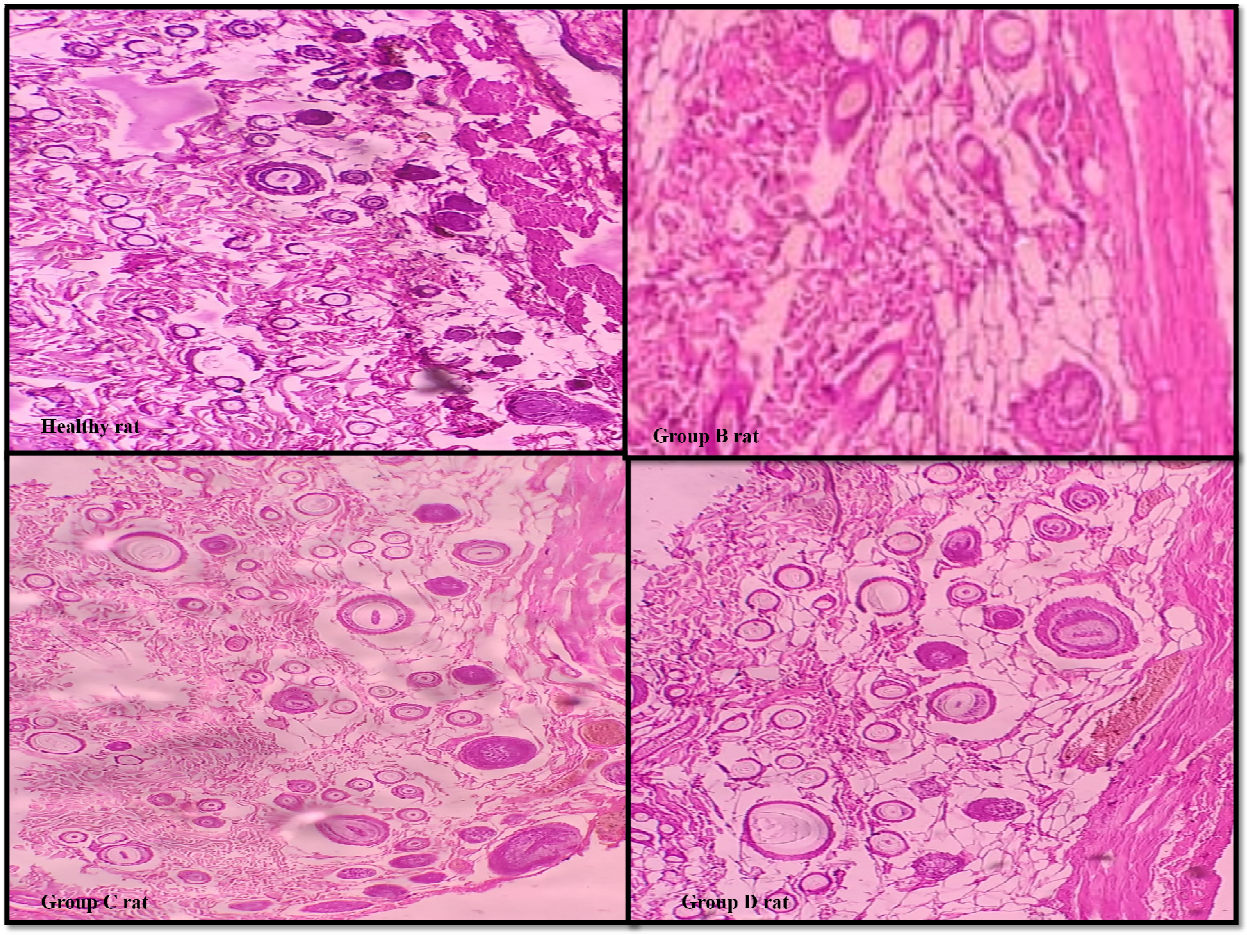

Fig. 26: Histopathological pictures of cells after treatment

Future scope of work:

- ❖ The nanoparticles can be grafted in polymer films and studied for deep tissue burn wounds.
- ❖ Detailed studies are needed to be done on specific cell lines like skin fibroblast cell line and hepatocytes cell line.

References

1. https://en.wikipedia.org/wiki/Cynodon_dactylon
2. Harborne J. Phytochemical methods, a guide to modern techniques of plant analysis,JB Harborne. *Chapman London GB*. 1973.
3. Vimalkumar CS, Hosagaudar VB, Suja SR, Vilash V, Krishnakumar NM, Latha PG. Comparative preliminary phytochemical analysis of ethanolic extracts of leaves of Olea dioica Roxb., infected with the rust fungus Zaghouania oleae (EJ Butler) Cummins and non-infected plants. *J Pharmacogn Phytochem*. 2014;3(4).
4. Evans WC. *Trease and Evans' Pharmacognosy E-Book*. Elsevier Health Sciences; 2009.
5. Edeoga HO, Okwu DE, Mbaebie BO. Phytochemical constituents of some Nigerian medicinal plants. *African J Biotechnol*. 2005;4(7):685-688.
6. Sofowora A, others. *Medicinal Plants and Traditional Medicine in Africa*. John Wiley and sons LTD; 1982.
7. Harborne JB. Phenolic compounds. In: *Phytochemical Methods*. Springer; 1973:33-88.
8. Ayoola GA, Coker HA, Adesegun SA, et al. Phytochemical screening and antioxidant activities of some selected medicinal plants used for malaria therapy in Southwestern Nigeria. *Trop J Pharm Res*. 2008;7(3):1019-1024.
9. Basak, Piyali, Pratik Das, Sheya Biswas, Narayan Chandra Biswas, and Gour Krishna Das Mahapatra. "Green Synthesis and Characterization of Gelatin-PVA Silver Nanocomposite Films for Improved Antimicrobial Activity." In *IOP Conference Series: Materials Science and Engineering*, vol. 410, no. 1, p. 012019. IOP Publishing, 2018.
10. Al-Waili, Noori S. "Mixture of honey, beeswax and olive oil inhibits growth of Staphylococcus aureus and Candida albicans." *Archives of medical research* 36, no. 1 (2005): 10-13.
11. Kaufman, T., S. N. Lusthaus, U. Sagher, and M. R. Wexler. "Deep partial skin thickness burns: a reproducible animal model to study burn wound healing." *Burns* 16, no. 1 (1990): 13-16.